Kinase Activity Reporters for Eukaryotic Signaling Pathway Study

Multiplexed-Profiling of Cellular Kinase Activities by Nuclear Magnetic Resonance Spectroscopy

Inaugural-Dissertation
to obtain the academic degree
Doctor rerum naturalium (Dr. rer. nat.)

submitted to the Department of Biology, Chemistry and Pharmacy
of Freie Universität Berlin

by

Rossukon Thongwichian

from Chonburi, Thailand

Oktober, 2012

Die vorliegende Arbeit wurde von April 2008 bis Oktober 2012 am

Leibniz-Institut für Molekulare Pharmakologie

unter der Anleitung von

Dr. Philipp Selenko

Prof. Dr. Dirk Schwarzer

angefertigt.

1. Gutachter: Prof. Dr. Christian Freund
2. Gutachter: Prof. Dr. Dirk Schwarzer

Disputation am 18.03.2013

CONTENT

ABSTRACT……..1

1. INTRODUCTION……3

1.1 Protein kinases……..3
1.2 Oocytes/eggs from *Xenopus laevis* as cellular model systems……16
1.3 Protein phosphorylation by high-resolution NMR spectroscopy……21
1.4 Objective of the Ph.D. project……...24

2. RESULTS……25

2.1 Recombinant Kinase Activity Reporters (KARs) ……25
2.2 Synthetic, peptide-based KARs……...31
2.3 KAR sequence design and optimization……42
2.4 Analyzing KAR cross-reactivity……57
2.5 Summary of KAR sequences……64
2.6 Phosphorylation and pH……64
2.7 Quantitative kinase activity profiling……67
2.8 Cellular kinase activity profiling……70
2.9 Profiling phosphatase activity..……75

3. DISCUSSION……83

3.1 Advantages/disadvantages of kinase activity profiling by NMR……...84
spectroscopy
3.2 Insights into CSF biology and extract kinase activities……..86
3.3 Insights into kinase inhibitor properties……....89
3.4 Insights into kinase/phosphatase reactions……..91

4. PERSPECTIVES……95

5. MATERIALS AND METHODS……98

5.1 Materials……98
5.2 Molecular biology methods……...102
5.3 Biochemical methods……104
5.4 Solid phase peptide synthesis……...109
5.5 NMR experiments……...112

6. REFERENCES……114

7. ABBREVIATION……129

ZUSAMMENFASSUNG……132

ACKNOWLEDGEMENTS……133

PUBLICATIONS ……134

ERKLÄRUNG……135

ABSTRACT

Protein kinases play a major role in regulating biological processes via integrated signaling networks. The cellular outcomes of such activities, including metaphase entry in cell cycle progression for example, are the result of multiple kinase and phosphatase actions. Therefore, multiplexed profiling of cellular kinase activities is of utmost importance to understand the functional correlations of these enzymes in complex signaling networks. In addition, such multiplexed kinase activity assays are essential to investigate the modes of action and specificities of kinase inhibitors, which constitute important drug targets in cancer therapy. To date, most assays fail to simultaneously quantify multiple kinase activities in parallel. Thus, new methods are needed to overcome these limitations. High-resolution nuclear magnetic resonance (NMR) spectroscopy has emerged as a powerful biophysical tool suited for the qualitative and quantitative analysis of protein phosphorylation. Since each protein residue gives rise to a characteristic NMR signal, multiple phosphorylation reactions on different residues of the same substrate protein or on different proteins can be followed simultaneously by observing the respective NMR signals of each of modified amino acid residues. NMR is non-invasive and non-disruptive, which enables direct observations of multiple phosphorylation reactions in real-time, as they proceed inside the NMR sample tube. Therefore, NMR can directly be used to simultaneously determine multiple kinase activities in integrated signaling networks.

This thesis presents a combination of time-resolved, high-resolution NMR spectroscopy with newly developed peptide-based kinase activity reporters (KARs) for multiplexed, cellular kinase activity measurements in complex environments such as cell lysates. To develop this method, I chose a well-studied model system, cytostatic factor (CSF)-arrested *Xenopus laevis* egg extracts, which contain many well-characterized, endogenous kinase activities. Central to this method is the design of ^{15}N isotope-labeled kinase activity reporters (KARs) that correspond to optimized consensus motif peptides with the highest possible phosphorylation efficiencies and substrate specificities, while exhibiting lowest degrees of cross-reactivity with off-target kinases. Using these KARs, I simultaneously quantified the activities of 8 different, cell cycle regulated serine/threonine kinases in *Xenopus* CSF extracts in a single NMR experiment.

Furthermore, I demonstrate that KARs can additionally be used to profile cellular phosphatase activities by a simple expansion of the KAR concept that entails turning KARs into phosphatase activity reporters (pKARs, i.e. pre-phosphorylated KARs). Both tools are well suited to investigate cellular signaling events that rely on the balanced action of kinases and phosphatases. Finally, NMR and KARs were employed to examine kinase inhibitor efficiencies and specificities under cellular conditions.

Overall, both methods have great potential for multiplexed-profiling approaches of cellular kinase and phosphatase activities and can be expanded to include larger number of enzymes to be assessed in parallel, as well as be applied to more complex cellular systems such as human cell lysates, or intact cells. I anticipate that both methods may become particularly useful in providing quantitative information about pathological signaling behaviors as are observed in multivariate etiology diseases such as cancer, as well as to provide novel routes for drug screening approaches.

1. INTRODUCTION

This thesis describes the development and application of a novel method for the quantification of multiple kinase activities in cellular lysates. Specifically, the aim of this Ph.D. project is to establish an approach for multiplexed-profiling of cell cycle-regulated serine/threonine kinases that are involved in *Xenopus laevis* oocyte to egg maturation.

In the following section, I will introduce the concepts of NMR-based kinase activity screening and the rationale behind peptide-based Kinase Activity Reporters (KARs). First, I will highlight the importance of protein kinases in both physiological and pathological cell states, along with a description of existing methods to analyze kinase functions and activities. I will then discuss the structural characteristics of protein kinases, which form the basis for different kinase activities and their individual substrate specificities. Information of that sort is instrumental in designing suitable KARs.

Background description of the cellular model systems, i.e. *Xenopus laevis* oocytes, mature eggs and metaphase-arrested egg extracts, which are used to test and characterize KARs will follow.

Finally, I will summarize the theory of identifying and quantifying protein phosphorylation states by time-resolved NMR spectroscopy, which constitutes the underlying rationale for the outlined approach.

1.1 Protein kinases

Protein phosphorylation, the addition of a phosphate group onto the side chains of serine, threonine and tyrosine residues, is one of the most important post-translational protein modifications in cell signal transduction[1,2]. It is a reversible modification, which regulates protein functions in many biological processes ranging from cell metabolism, growth, division, differentiation and death[3,4]. Protein phosphorylation may lead to changes in protein structures and stabilities[5,6] enzymatic activities[7,8], protein-protein interactions[9] and subcellular localization behaviors[8,10]. Therefore, the proper regulation of protein phosphorylation is one of the key aspects of human health. In turn, altered

phosphorylation behaviors are strongly associated with pathological conditions including a long list of cancers[1,8,11-13], inflammatory diseases[1], diabetes[12] and many neurodegenerative disorders[11].

As a result, cellular enzymes that mediate protein phosphorylation are at the center of explorative investigations in a large number of research laboratories. Protein kinases catalyze the transfer of phosphate moieties from adenosine-5'-triphosphate (ATP) to target substrate proteins[8]. Protein phosphatases, in contrast, remove phosphate groups from proteins and thus function in the reverse process. Both types of cellular enzymes constitute important targets in drug discovery approaches and disease therapy. In many instances, kinases themselves require reversible phosphorylation for their activation[14]. Consequently, their activities are often inferred directly from their individual phosphorylation states.

Over the last decades, our knowledge of protein phosphorylation has significantly expanded. Approximately 700,000 protein phosphorylation sites exist in eukaryotic cells, 85% of which are on serines, 15% on threonines and 2% on tyrosines[15]. Phosphorylation of other residues such as histidines, arginines, aspartatic acids, and lysines are primarily observed in prokaryotes and recently found in eukaryotes[16-20]. Protein kinases constitute 2% of the genes in the human genome and 518 human protein kinases are known to date[21]. Based on the type of amino acids that these kinases phosphorylate, they are classified to three main families;

1) Serine/threonine kinases (STK, 428 kinases) phosphorylate either serine or threonine residues.
2) Tyrosine kinases (TKs, 90 kinases) phosphorylate tyrosine residues.
3) Dual-specificity protein kinases (DSKs, 40 kinases) phosphorylate both serine/threonine and tyrosine residues.

As this Ph.D. thesis is based on developing novel kinase activity reporters, I initially selected kinases relevant to meiotic cell cycle progression during *Xenopus* oocyte to egg maturation as a model system. The selected kinases are serine/threonine kinases such as cyclin dependent kinase 1 (Cdk1), polo-like kinase 1 (Plk1), p42 mitogen activated protein

kinase (p42MAPK) and p90 ribosomal protein S6 kinase 2 (Rsk2). Therefore, these kinases will be referred to throughout the work.

1.1.1 Role of protein kinases in eukaryotic signaling pathways

Protein kinases play a key role in regulating cellular biological processes via many signaling pathways such as the MAPK signaling cascade, for example[22,23]. These pathways mostly rely on the activation of kinases by either extracellular molecules (first messengers), or metabolic molecules (second messengers), such as hormones, or cyclic adenosine monophosphate (cAMP), respectively. Activated kinases subsequently phosphorylate many downstream substrates, which are often other protein kinases. In turn, these newly activated kinases phosphorylate many of their own downstream protein substrates. These sequential phosphorylation events often converge on cellular transcription factors that eventually stimulate expression of sets of target genes[24,25] that mediate global cellular response behaviors, such as oocyte to egg maturation, as one example[26,27].

Here, I briefly illustrate the pathways that are involved in meiotic cell cycle progression during *Xenopus* oocyte to egg maturation. They involve three semi-independent signaling cascades; the phosphatidylinositol 3-kinase (PI3K) cascade, the mitogen activated protein kinase (MAPK) cascade and the cyclin-dependent kinase 1 (Cdk1) cascade[26] (**Fig. 1**). Each cascade (or pathway) involves the activities of several kinases, from which one or two have been selected as targets for the generation of KARs (they are color-coded according to the signaling cascades that they are involved in in **Fig. 1**). In each cascade, an upstream kinase phosphorylates and activates its downstream substrate (black arrows in **Fig. 1**). In addition to 'linear', or 'downstream' signaling events, some of these kinases exhibit active 'cross-talk' with other pathways (red arrows in **Fig. 1**). For example, activation of mitogen-activated kinase kinase (MAPKK or MEK1) in the MAPK cascade by Ras/Raf1 kinase from the PI3K pathway, and inhibition of the membrane-associated tyrosine and threonine specific Cdk1-inhibitory kinase 1 (Myt1) of the Cdk1 cascade by Rsk2 from the MAPK pathway[28,29]. Thus, information from cross-talk studies not only reveal specific connections between individual pathways, but also demonstrate the importance of viewing these pathways as complex, integrated signaling networks. From

this perspective, final outcomes of signaling events are a result of multiple kinase (and phosphatase) actions. By studying individual kinase activities in isolation, one is likely to fall short in understanding the multiple contributions and interconnectivities that eventually lead to a cellular response.

By extension, there is a growing interest in evaluating pharmacological compounds that modify individual kinase activities-, and that are commonly used as therapeutic agents in many human disease-, in 'network medicine' type of approaches. Therein, multiple cellular signaling pathways are monitored simultaneously and several kinase activities are quantitatively studied in parallel[30,31]. Novel tools to investigate different cellular kinase activities in a multiplexed fashion are sought after, which also led to the development of the approach reported here.

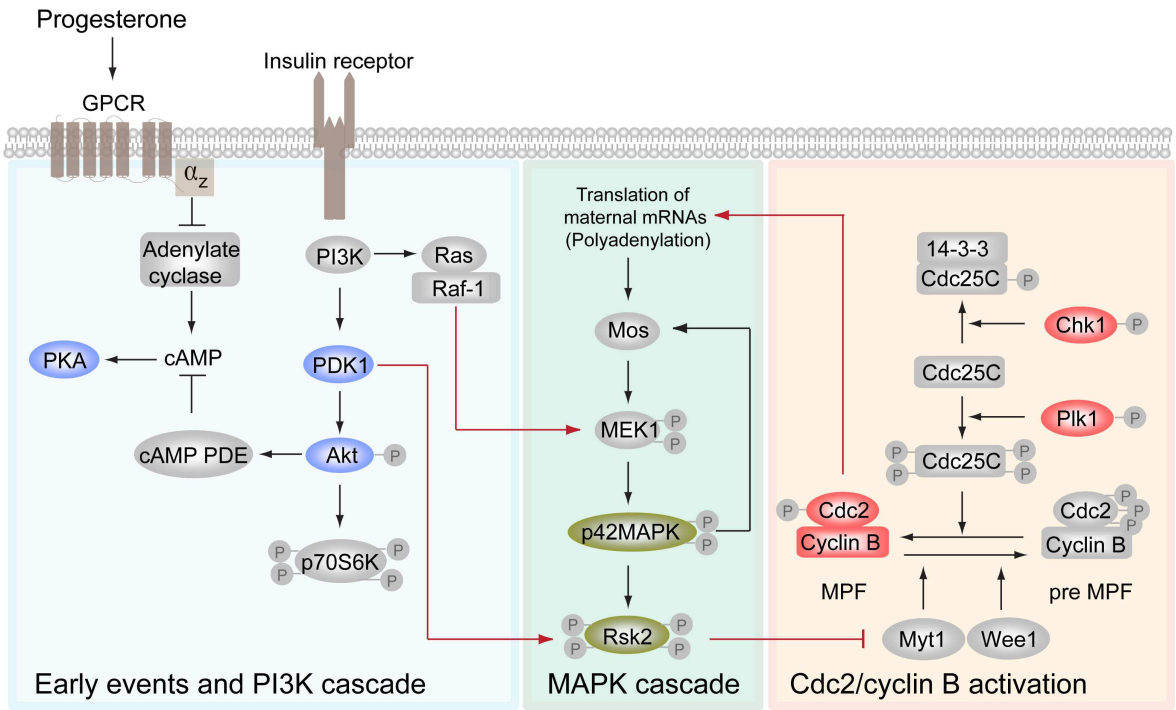

Figure 1. Integrated signaling networks of protein kinases involved in meiotic cell cycle progression during *Xenopus* oocyte to egg maturation (upon progesterone induction).

1.1.2 Current methods for kinase activity profiling

Because protein kinases regulate several cellular processes, pathological changes in their individual activities are causally implicated in a large number of several human diseases[8,11-13] and several methods have been developed for their characterization. In general, most of these techniques focus on either mapping protein phosphorylation sites, or on directly quantifying kinase activities. As this Ph.D. work focuses on the development of a novel method to directly determine the activities of kinase in cellular environments, it is important to firstly discuss concepts and limits of existing phospho-detection techniques.

To date, there are two main approaches to quantify cellular kinase activities: either by indirectly deducing enzymatic activities via the identification of the respective phosphorylation states of 'activated' kinase, or by assessing the phosphorylation states of known downstream kinase target substrates. Because many protein kinases are themselves 'activated' by reversible phosphorylation, immunodetection of modified kinase residues with phospho-specific antibodies is amongst the most common method for inferring kinase activities in cell lysates. This indirect method has high sensitivity but is limited by the requirement for available antibodies against 'activating' phospho-sites on the respective kinases. These antibodies are not always easy to generate and often poorly discriminate between similar phospho-activation sequences in different kinases, or between differentially activated kinase isoforms[32].

More direct measurement of kinase activities can be performed by means of peptide array assays[33]. In these assays, conversion of kinase peptide substrates into phosphorylated entities is typically monitored in multi-reaction formats, either by colorimetric reactions[34] or via [γ-^{32}P] ATP-radionucleotide incorporation experiments[35-37]. Assays of that kind are equally applicable to determine kinase consensus motifs[38] and are often used in kinase inhibitor screening approaches[39]. Despite being highly sensitive, they harbor some disadvantages. Individual kinase activities are measured in separate, non-continuous reaction setups and absolute amounts of modified versus unmodified substrates are not usually determined, which makes it difficult to comparatively assess multiple kinase activities. Besides, experiments that require handling of radioactive isotopes necessitate a dedicated experimental environment. In many instances, these peptide-based assays are

often developed for a single kinase only and are not suitable to comparatively analyze multiple kinase reaction in parallel.

Most recently, an alternative method for kinase activity screening has been reported that relies on quantitative mass spectrometry (MS). This assay, called Kinase ActivitY Assay for Kinome profiling (KAYAK), has the distinct advantage of being able to report the phosphorylation states of up to 90 kinase peptide reporters in parallel, which translates into 30 kinase activity measurements in single reaction setup[40,41]. KAYAK is based on MS signal intensity measurements of phospho-peptide products obtained directly in cell-lysate reactions, with known internal standards of defined concentrations. KAYAK thereby enables phospho-reporter quantification, which directly relates to the cellular activities of individual kinases, although for a single time point of cell extract exposure only.

The above methods share common limitations that they do not directly observe protein phosphorylation in the course of the actual modification reactions. Samples are quenched at individual time-points in order to stop the reactions and to process the samples for analysis. Therefore, both methods do not allow monitoring of modification reactions in a continuous manner. To obtain time-resolved modification readouts, the phosphorylation states of the different reporter peptides or substrate proteins have to be determined at different time points, for which multiple samples and highly parallelized processing routines are needed.

In response to such drawbacks, I set out to develop an approach to enable multiplexed-profiling of cellular kinase activities in real-time by using kinase-specific peptide reporters and time-resolved, high-resolution NMR spectroscopy. The design of such a method is based on several key requirements: protein phosphorylation should be detectable in a continuous manner and the kinase substrate peptides should be highly specific and stable for several hours in a large variety of different cellular environments.

In order to achieve this goal, knowledge about protein kinases, especially their structural properties with regard to substrate binding and recognition (**1.1.3**), their catalytic mechanisms (**1.1.4**), means of regulation (**1.1.5**) and their substrate specificities via

kinase consensus sequence elements (**1.1.6**) and distal docking sites (**1.1.7**) has to be properly integrated into the process of designing these reporters.

1.1.3 Protein kinase structures

The 3-dimensional (3D) structures of catalytic protein kinase domains are very similar[42,43]. Briefly, they typically comprise two protein domains that are connected by a short, flexible peptide linker. The linker region regulates two main conformations of the catalytic kinase domain that we refer to as the 'open' and 'closed' state of the enzyme[43] (**Fig. 2**).

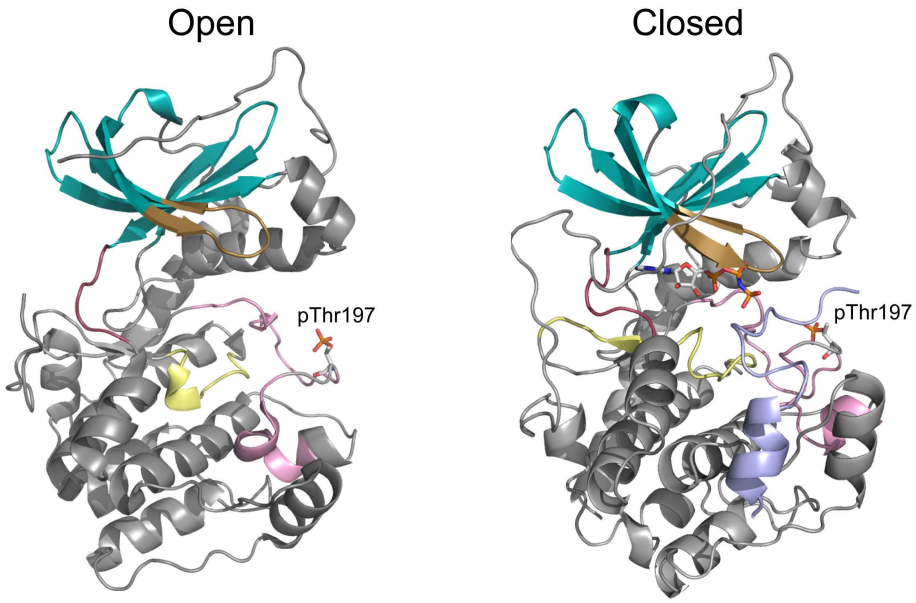

Figure 2. Catalytic kinase domain structure of PKA: open and closed conformations (PDB codes 1J3H and 1CDK, respectively); cyan=β-sheet of the N-terminal lobe, gray=α-helix, red=peptide linker, brown=P-loop, yellow=C-loop, pink=A-loop. ATP analogue and phosphorylated Thr197 (pThr197) in the A-loop are shown as sticks. The protein kinase A inhibitor peptide (TTYADFIASGRTGRRNAIHD, blue) incorporates mutation of Ser17 to Ala of a standard PKA substrate peptide.

In more detail, the N-terminal part or lobe of the catalytic kinase domain harbors a globular, β-sheet conformation, while the C-terminal kinase lobe is comprised of α-helices. The active site of the kinase is located in between the two lobes and contains the ATP binding pocket (**Fig. 2**). ATP serves as the ubiquitous phosphate donor in all phosphorylation reactions. The adenosine moiety of ATP is buried in a hydrophobic cleft and the γ-phosphate moiety interacts with the phosphate-binding loop or P-loop. The C-terminal lobe regulates kinase activation. It contains the activating loop, or A-loop, and

phosphorylation of a key threonine in most serine/threonine kinases (STKs), or of a tyrosine in tyrosine kinases (TKs) in the A-loop 'activates' the respective kinases[43,44]. The presence of phosphate groups at these key sites of the A-loop neutralizes the overall positive electrostatic properties of the A-loop region and of other conserved, basic residues in the catalytic loop, or C-loop segment. Activating phosphorylation events of that sort lead to a defined structural rearrangement of the whole kinase domain, which eventually mediates proper binding of the respective substrate molecule.

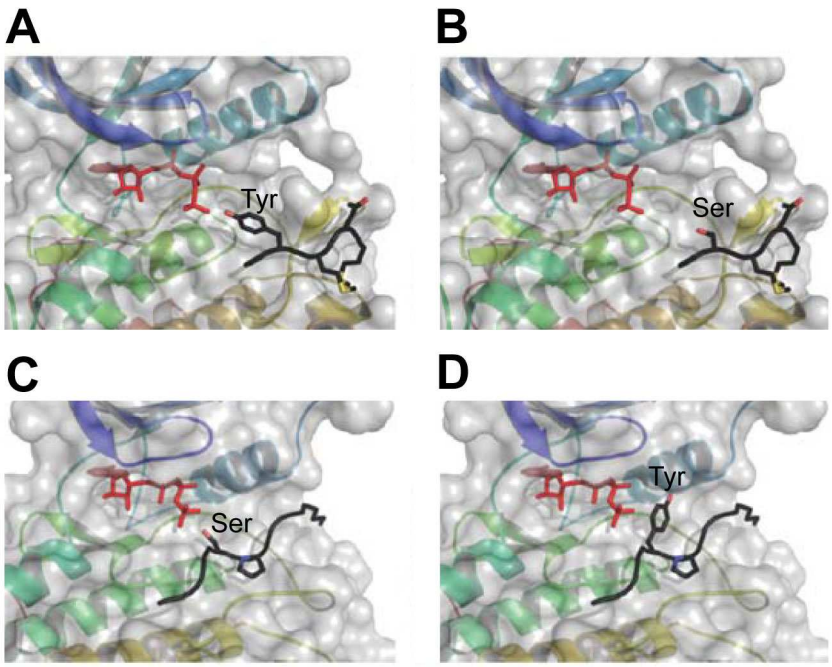

Figure 3. Catalytic clefts of STKs and TKs. A) Structure of the TK catalytic domain from insulin receptor bound to a tyrosine substrate peptide (PDB code 1IR3), red ATP, black protein substrate. B) Model of a STK substrate peptide. C) The structure of Cdk2 bound to a serine substrate peptide (PDB code 1QMZ). D) Model of TK substrate peptide. The figure is modified from Ubersax *et al* [2].

The structure of cAMP-dependent protein kinase, or protein kinase A (PKA), is commonly used to illustrate the different kinase conformations (**Fig. 2**). In addition, its catalytic kinase domain structure was the first to be determined at atomic resolution[45,46]. Later on, a similar overall architecture was determined for the cyclin-dependent protein kinase 2 (Cdk2)[47]. Availability of the first kinase domain structure of a tyrosine kinase, the insulin receptor kinase (IRK) led to investigations about substrate specificity determinants of STKs and TKs[2,48]. Substrate binding clefts of TKs are deeper than those of STKs and only allow binding of tyrosine side-chains that are close enough for γ-phosphate transfer (**Fig. 3A)**. In

contrast, side chains of serine/threonine residues are too 'short' for TK binding pockets and cannot access the γ phosphate of ATP (**Fig. 3B**). Consistently, tyrosine side chains are too large to enter the active sites of STKs (**Fig. 3C, D**). Dual-specificity protein kinases (DSKs) contradict this cleft depth hypothesis as the sole determinant for amino acid residue selectivity[49]. DSKs most likely alternate between multiple conformations that allow them to accommodate the different incoming substrates.

Knowledge about kinase structures, in combination with mutational studies paved the way for understanding the universal kinase phosphate transfer mechanism, as outlined in section **1.1.4** below.

1.1.4 Protein kinases, phosphate transfer mechanism and kinase inhibitors

Protein phosphorylation reactions catalyzed by cellular kinases require ATP as the universal phosphate source and a divalent metal ion (commonly Mg^{2+}) as the enzyme cofactor. Most kinases have similar phosphoryl transfer mechanisms including conserved residues in their ATP-binding clefts, which I outline here in an exemplary fashion for PKA. The catalytic cleft of PKA is surrounded by a glycine-rich loop and three highly conserved amino acid residues; Asp184, Lys72 and Asp166[50]. The side chain of Asp184 interacts with Mg^{2+} and positions the γ phosphate moiety for the transfer reaction[50] (**Fig. 4A**). The side chain of Lys72 stabilizes the α and β phosphates of ATP[50], while the carboxyl group of the last invariant active site residue Asp166 forms a hydrogen bond with the hydroxyl group of the phosphorylatable amino acid of the substrate. This bond promotes the nucleophilic attack on the γ phosphate. Besides these conserved residues, there are two further amino acids that facilitate the phospho-transfer reaction. In PKA, Thr201 forms a hydrogen bond with the side chain of Asp166 but only in the presence of a peptide substrate in its binding site[50]. This interaction functions as an activating 'signal' that initiates the catalytic reaction. The ε-amino group of Lys168 simultaneously interacts with the γ phosphate oxygen of ATP and with the hydroxyl oxygen of the phosphorylatable residue (**Fig. 4B**) and thereby links phosphate transfer from ATP to the substrate (**Fig. 4B, C**).

Knowledge about the interactions of ATP and the respective kinase ATP-binding pockets provides important information for the design of ATP-competitive kinase inhibitors[51,52]. These compounds constitute the predominant types of kinase inhibitors. They contain heterocyclic ring systems that typically function in occupying the purine binding sites. On average, they additionally form between one and three specific hydrogen bonds with residues of the ATP-binding cleft and thereby mimic generic hydrogen bond networks that are also formed with adenine moiety of ATP. In consequence, most kinase inhibitors compete with cellular ATP for binding to the kinase ATP site. By doing so they directly antagonize kinase function. In this Ph.D. thesis, I will also extend the application of KARs and NMR to evaluate the efficiency and specificity of the ATP-competitive kinase inhibitors.

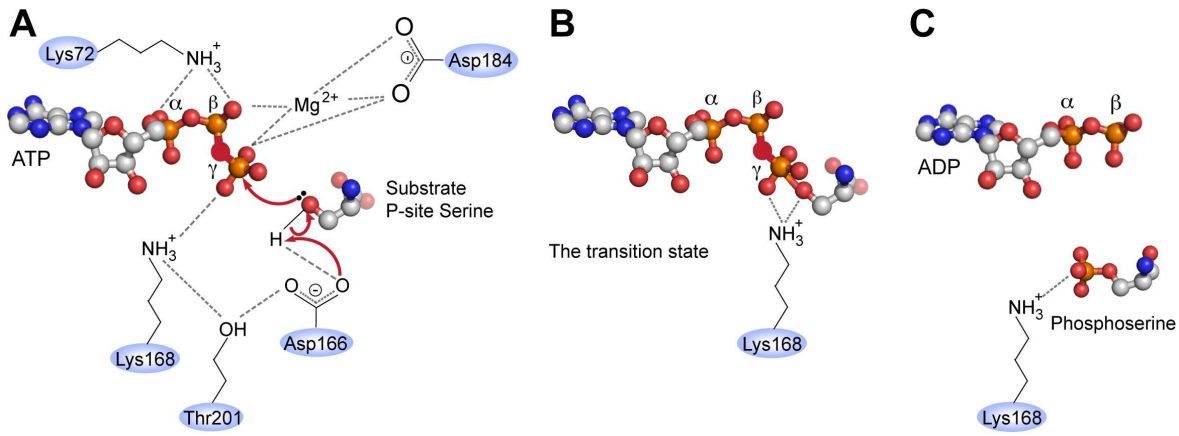

Figure 4. Schematic depiction of the PKA phosphoryl transfer mechanism. A) Conserved amino acid residues of the kinase catalytic site involved in the phospho-transfer reaction are outlined. Dashed lines represent interactions between atoms of conserved kinase residues with ATP, Mg^{2+} and the protein substrate. Red arrows indicate the nucleophilic attack. B) Role of Lys168 in the transition state of the phosphoryl transfer reaction. C) Final products: phosphoserine and adenosine diphosphate (ADP).

Although protein kinases have similar catalytic mechanisms, their functions are often further regulated by specific cofactors, or kinase regulatory subunits, which I will describe in the next section. Information about additional regulatory mechanisms is essential to understand diverse kinase functions under physiological conditions, which particularly influence kinase activity reporter design. This information is also useful for individual phosphorylation reaction set up, especially with regard to what cofactors are needed for optimal kinase function.

1.1.5 Cofactors and regulatory subunits

Some kinases require cofactors (besides Mg^{2+}) or regulatory subunits that modulate their activities or affect their cellular localization. For instance, in its inactive form, the PKA holoenzyme contains two catalytic domains and two regulatory subunits[53]. Binding of cAMP on the regulatory subunits induces dissociation of the catalytic and regulatory domains. This leads to PKA activation. Therefore, the concentration of cellular cAMP modulates the activity of PKA. Another example is the regulation of Polo-like kinase 1 (Plk1). Plk1 contains a catalytic domain and a regulatory domain[54]. The regulatory Polo box domain (PBD) at the C-terminus regulates Plk1 activation[54]. In the absence of kinase substrates, PBD binds to the catalytic domain and inhibits Plk1 activity. In the presence of substrates, PBD binds to substrate phospho-motifs (S-pS/pT-P/X), which releases kinase domain inhibition and simultaneously stimulates Plk1 activity to phosphorylate substrates[55]. In many instances, protein substrates are first phosphorylated by priming kinases, such as Cdks and MAPKs[55,56]. Subsequently, Plk1 phosphorylates additional substrate sites. High concentrations of protein substrates also induce dissociation of the catalytic domain from the PBD, regardless of the phosphorylation states of other substrate sites. In addition, the PBD domain critically influences Plk1 localization[57]. Mutations of some PBD residues lead to Plk1 mislocalization to cellular regions that are void of Plk1 substrates[58].

Despite the notion that most protein kinases have similar kinase domain architectures and similar phosphoryl transfer mechanisms, they have vastly different substrate specificities. Differences in substrate specificity are primarily regulated by variations in the amino acid composition of kinase-substrate binding site regions, which contain specific residues for optimal kinase binding[2]. In the following section, I will introduce the concept of kinase consensus sequences, which universally regulate kinase-substrate specificities.

1.1.6 Kinase consensus sequences

Firstly, I will introduce the common nomenclature for kinase substrate phosphorylation sites, which will be used throughout the thesis. Conventionally, we refer to the phosphorylatable residue of the substrate protein as the phosphorylation site or the P-site[2]. Residues N-terminal of the P-site are designated P-1, P-2, P-3 etc. Residues C-terminal of the P-site are referred to P+1, P+2, P+3 etc. Although a kinase only

phosphorylates the P-site residue, amino acids N- and C-terminal of the P-site (usually P-4 to P+4) are critical determinants for kinase-substrate recognition[59]. In most instances, amino acids between P-4 and P+4 are 'complementary' to those of the kinase substrate-binding site. Here, complementary means that specific interactions between kinases and substrates are established via sequence-specific electrostatic interactions, hydrogen bond networks, or selective hydrophobic contacts. As a result, kinase/substrate binding is usually tight and mediated by short peptide stretches only.

In the following section, I will provide two examples of complementary substrate/kinase sequences that enable specific kinase-substrate binding events. The first example is PKA and its peptide substrate Kemptide (LRRASLG)[60]. Arginine residues at position P-3 and P-2 in the substrate peptide are essential for interaction with PKA because they bind to side chains of Glu127 and Glu230 within the kinase substrate-binding site[61]. The binding pocket of PKA also comprises two hydrophobic residues, Leu198 and Leu205 that target the preference for a sequence that contains a hydrophobic residue at the P+1 position. In other words, PKA phosphorylates substrates that contain the consensus sequence motif R-R-X-S/T-θ; where X is any amino acid and θ is a hydrophobic residue. The second example is proline-directed protein kinases, which mainly constitute members of the Cdk and MAPK families. These enzymes strictly require substrates with a proline residue at the P+1 position[62,63]. Because prolines do not contain amide hydrogens in their peptide backbones, they do not form hydrogen bonds. This unique property is selectively exploited in proline-directed protein kinases. Their minimal consensus sequence is S/T-P.

Kinase consensus sequences have been studied over many years and by different approaches. Optimized peptide-based kinase substrates often exhibit higher phosphorylation efficiencies than physiological protein substrates. The V_{max} of casein kinase 1 (CK1) and a substrate peptide (RRKDLHDDEEDEAMSITA), for example, is 6 times higher than that of the casein protein itself[64]. The sequences of KARs in this project are derived from published kinase consensus sequences. However, since additional contacts of some kinases with substrate residues outside the consensus motifs play a major role in kinase-substrate recognition events, my KAR design process also had to incorporate information of that sort in order to maximize kinase/susbtrate specificity and to reflect the most physiological 'docking sites' for each of the kinases to be reported.

Understanding the molecular details of kinase docking sites is therefore critical in the development of kinase activity reporters.

1.1.7 Additional kinase docking sites

Besides kinase consensus sequences, kinase-substrate specificity is often achieved via additional interactions with distal kinase motifs (not the active site) and substrate docking sites other than the P-site region[65]. For instance, p42MAPK substrates contain two additional kinase interaction surfaces, the D- and DEF-domains[66]. D domains are located 50-100 residues away from the substrate P-site and always contain the conserved R/K_2-X_{2-6}-L/I-X-L/I motif that binds to conserved acidic and hydrophobic patches on p42MAPK. c-Jun N-terminal kinase and p38MAPK substrates also contain D domains[67,68]. DEF-domains contain the F/Y-X-F/Y-P motif and are located between 6 and 20 residues downstream of P-sites[66]. DEF-domains interact with hydrophobic pockets in close proximities to the MAPK active sites. Mutation of the first Phe to Asp of the DEF-domain motif decreases overall phosphorylation of MAPK substrates 15 times[66]. Other additional docking site examples are substrates of the 3-phosphoinositide-dependent protein kinase 1 (PDK1). In this case, they are called PDK1-interacting fragments (PIFs) and contain the conserved F-X-X-F motif. PIFs specifically interact with hydrophobic pockets of PDK1, which results in a 100-fold increase in phosphorylation efficiency[65].

Knowledge of kinase consensus sequences, together with information about additional docking sites, is essential for generating suitable KARs that get efficiently phosphorylated by their respective kinases. Once KAR design is completed, the reporters have to be tested both *in vitro* and in cellular contexts. In the following section, I will outline the cellular model system, *Xenopus* oocyte and egg extracts, that I employed to test these KARs.

1.2 Oocytes/eggs from *Xenopus laevis* as cellular model systems

Oocytes from the African clawed frog *Xenopus laevis* are a well-studied model system for cellular signaling events. Immature oocytes develop into fertilizable eggs via two consecutive rounds of meiosis in a process called oocyte maturation, which, under physiological conditions, is triggered by action of female-specific steroid hormones[69]. Oocyte to egg maturation involves the activation of different signaling pathways and several cellular kinases. Cell cycle regulated kinases that participate in oocyte maturation have been studied over the past decades and are very well characterized[26,69]. Additionally, oocytes, as well as fertilizable eggs, are naturally synchronized and arrested at defined stages of the cell cycle (see below). Signaling events can be triggered exogenously and studied in individual cells, or in pools of cells, because they mostly occur in a synchronous fashion in all the cells[70]. Cell cycle competent cell extracts can easily be prepared from oocytes and eggs and these retain the synchronous behavior of intact cells also under *ex vivo* conditions. Extracts can be produced in large quantities, owing to the large cell sizes of oocytes and eggs (~1 mm in diameter)[71], and can be stored safely for long periods of time.

1.2.1 Overview of *Xenopus* meiotic signaling during oocyte to egg maturation

The meiotic cell cycle consists of two consecutive M-phases, meiosis I and meiosis II, in the absence of DNA replication (S phase)[69,72,73]. Immature *Xenopus* oocytes also called stage VI oocytes are arrested in prophase of the G2/M transition of meiosis I[26,69] (**Fig. 5**). Steroid hormones, such as progesterone (PG), stimulate stage VI oocytes to enter/resume meiosis I, which leads to nuclear envelope (also called germinal vesicle) breakdown (GVBD), chromosome condensation and spindle formation (~6 h after PG treatment)[26]. In turn, oocytes enter meiosis II and become mature eggs[74]. Fertilizable eggs, also called cytostatic factor (CSF) arrested eggs, halt at this stage of the cell cycle to await fertilization. The fertilization results in the completion of the second round of meiosis II and the onset of embryogenesis[74]. During oocyte maturation, three major signaling cascades participate in meiotic cell cycle progression; the PI3K cascade (section **1.2.2**), the MAPK cascade (section **1.2.3**) and Cdc2/cyclin B activation[26] (section **1.2.4**).

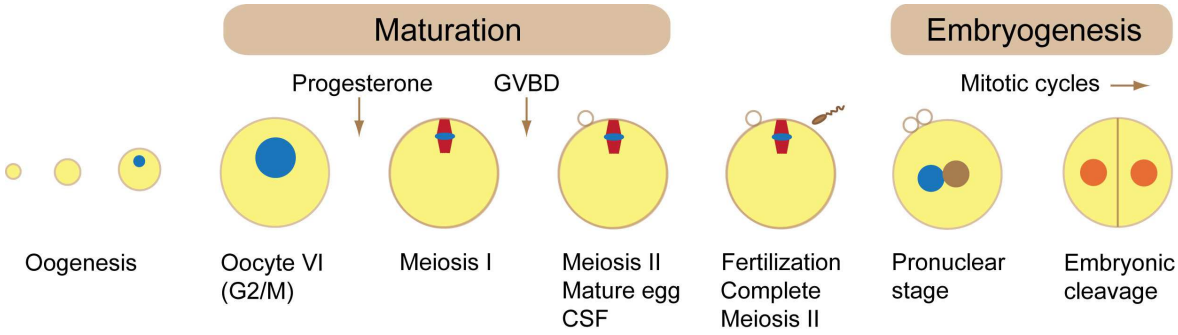

Figure 5. Schematic representation of meiotic signaling events during *Xenopus* oocyte to egg maturation and embryogenesis upon PG stimulation.

1.2.2 Early events and the PI3K signaling cascade

One of the earliest events in frog, mouse, rat and fish oocyte maturation (~1-2 h after PG treatment) is a sharp decrease in cytosolic cAMP, probably via inhibition of adenylate cyclase, which mediates cellular cAMP synthesis[75] (**Fig. 1**). As a result, the activities of cAMP dependent protein kinases, such as PKA drop drastically. This decline in PKA activity is essential for oocyte maturation. For instance, microinjection of catalytically active PKA subunits blocks PG-induced oocyte maturation. In contrast, microinjection of PKA inhibitors leads to oocyte to egg maturation in the absence of PG stimulation[76]. These early events further involve activation of the phosphatidylinositol 3-kinase (PI3K) signaling cascade. This pathway is activated upon PG treatment via a yet uncharacterized steroid hormone receptor. PI3K activity increases approximately two-folds in PG treated oocytes[28]. Active PI3K potentiates oocyte maturation by promoting Ras and Akt/protein kinase B (PKB) activation via PDK1, which phosphoryates Akt/PKB at Thr308[77,78]. Active Akt/PKB further promotes oocyte maturation by stimulating type 3-cAMP phosphodiesterase (cAMP-PDE), which inhibits cAMP production[79]. Downstream kinases in this cascade include p70 ribosomal protein S6 kinase (p70S6K), which is eventually switched on, but its activity does not appear to be essential for PG-induced maturation[80].

1.2.3 The MAPK cascade

During oocyte to egg maturation, the rate of translation of maternal mRNAs increases[81]. This also correlates with increased mRNA polyadenylation, which indicates elevated levels of protein synthesis[82]. One of the most important proteins actively made at this

stage is the Mos oncoprotein, also termed mitogen-activated protein kinase kinase kinase (MAPKKK)[83]. Accumulation of cellular Mos depends on its synthesis and degradation rates, and is crucial for oocyte maturation as the addition of Mos antisense oligonucleotides blocks maturation[83]. Mos phosphorylates downstream mitogen-activated protein kinase kinase (MAPKK) or MEK1 at Ser218 and Ser222[84]. Via cross talk from the PI3K pathway, Ras/Raf1 also phosphorylates MEK1 in the same manner[28] (**Fig. 1**). MEK1 is a dual-specificity protein kinase that phosphorylates the activation loop of p42MAPK at Thr183 and Tyr185[85]. p42MAPK is also called extracellular related protein kinase 2 (Erk2). Active p42MAPK provides a positive feedback loop via phosphorylating Mos at Ser3[86]. Phosphorylation of Mos at Ser3 inhibits its degradation[87]. In addition, p42MAPK activates p90 ribosomal protein S6 kinase 2 (Rsk2) via phosphorylation at Rsk2 activation loop[88-90]. As a result, Rsk2 is active and auto-phosphorylates itself at Ser383[88]. The phosphorylated Ser383 of Rsk2 functions as a PDK1 docking site and PDK1 eventually phosphorylates Rsk2 at Ser224[88]. Activities of kinases in this cascade are detected 30-60 min before GVBD. Rsk2 plays a pivotal role in oocyte to egg maturation. The kinase phosphorylates and inhibits Myt1[29]. Inactivation of Myt1 leads to the activation of Cdc2/cyclin B, or Cdk1[27,69], which constitutes the Cdc2/cyclin B pathway/cascade outlined in section **1.2.4** below.

1.2.4 Cdc2/cyclin B activation

Meiotic M phase entry of immature oocytes critically requires activation of Cdc2 in complex with its regulatory subunit cyclin B[91]. Cdc2/cyclin B is alternatively designated cyclin-dependent kinase 1 (Cdk1). Initially, Cdc2 is present in G1 phase and its T-loop is phosphorylated at Thr161 by Cdk1 activating kinase[92]. Newly synthesized cyclin B binds to phosphorylated Cdc2 in S phase[93]. This Cdc2/cyclin B complex is still inactive due to inhibitory phosphorylation at Thr14 and Tyr15 by Myt1 and Wee1[94-96] (**Fig. 1**). At the G2/M transition, active Plk1 phosphorylates and activates Cdc25c[97], a dual-specificity phosphatase. Activation of Cdc25c causes dephosphorylation of Thr14 and Tyr15 of Cdc2/cyclin B and eventually activates Cdk1[26]. Cdk1 activity increases sharply before GVBD, which is around the same time that MAPK activity is highest. Active Cdk1 provides a positive feedback loop by phosphorylating and inhibiting Myt1. Moreover, Cdk1 activation possibly promotes Mos translation or prevents Mos degradation[26].

Cyclin B contains a cytoplasmic retention signal (CRS) which consists of 42 amino acids at its N-terminus[98]. Interaction of the CRS with the nuclear export protein 1 (Exportin1) maintains cyclin B in the cytoplasm[99]. During oocyte maturation, five phosphorylation sites in cyclin B become modified. Four out of those five sites are located within the nuclear localization sequence (NLS) and phosphorylation promotes nuclear entry of cyclin B[98]. Nuclear entry is crucial for Cdk1 activation, because the Cdc2/cyclin B complex requires dephosphorylation by Cdc25c, which is highly abundant in the nucleus.

In late metaphase, Cdk1 activity declines (after ~6 h PG treatment) due to degradation of cyclin B by the anaphase promoting complex/cyclosome (APC/C) of the ubiquitin-mediated destruction pathway. Cyclin B contains a destruction box motif, Arg-Thr-Ala-Leu-Gly-Asp-Ile-Gly-Asn, which is targeted by a destruction box recognition protein (DBRP)[100]. The complex of cyclin B and DBRP is susceptible to proteolysis at the exit of metaphase. Deleting the destruction box in mutant cyclin B Δ90 improves cyclin B stability and maintains Cdk1 activity[101].

1.2.5 Cytostatic factor (CSF)

The cytoplasm of mature *Xenopus* eggs comprises two distinct biochemical activities that provide different effects when injected into oocytes/embryos[102]. The first one induces maturation in immature oocytes in the absence of PG treatment (**Fig. 6**). Therefore, this activity is called the maturation-promoting factor, or MPF. MPF is presently known as Cdc2/cyclin B, which catalyzes entry into M-phase, meiosis I and II in all eukaryotic cells[91]. The second one causes cell cycle arrest in metaphase when injected into a mitotically dividing embryo[102] (**Fig. 6**). This activity is referred to as cytostatic factor, or CSF. CSF arrests mature oocytes in meiosis II and its activity disappears upon fertilization[102].

There are several proteins proposed to constitute CSF components[103,104]. First, cleavage arrest of *Xenopus* embryos upon microinjection of Mos RNA indicates that Mos may participate in CSF functions[103]. Second, Mos downstream kinases such as MEK1, p42MAPK and Rsk2 have been characterized and annotated as components involved in CSF arrest[104-107]. CSF components are believed to inhibit APC/C and to maintain meiosis II arrest. Activation of the MAPK cascade inhibits APC/C by activating budding uninhibited by benzimidazoles 1 (Bub1), which is a subset component of spindle assembly checkpoint

that prevents anaphase entry under normal growth conditions[108]. Finally, members of the exported repeated protein family (Emi/Erp) have been reported to act as CSF components. Immunodepletion of Emi1 from CSF-arrested *Xenopus* egg extracts causes APC/C activation[109,110]. Excess Emi1 prevents the release of extracts from CSF arrest upon fertilization-mimicking conditions upon Ca^{2+} treatment.

Based on this information, in a mature egg, or a CSF-arrested egg, the kinases involved in either MPF- or CSF-activities are predicted to be active. These kinases mainly belong to the MAPK and Cdk1 activation pathways (**Fig 1**).

In conclusion, well-characterized cell cycle-dependent kinases in the *Xenopus* system offer an ideal model scenario for the testing individual KARs. In addition, regulation of these kinases is strictly preserved in other eukaryotic systems, including mammalian cells. Therefore, developing KARs with CSF-arrested *Xenopus* egg extracts enables functional extrapolation to other cellular systems, most importantly mammalian cell environments, which may constitute more pharmacologically relevant disease models.

Now that the concept of KAR design and the cellular model system for testing KARs have been introduced, I will outline the key rationale behind using time-resolved, high-resolution NMR spectroscopy for monitoring protein phosphorylation events in native, cellular environments.

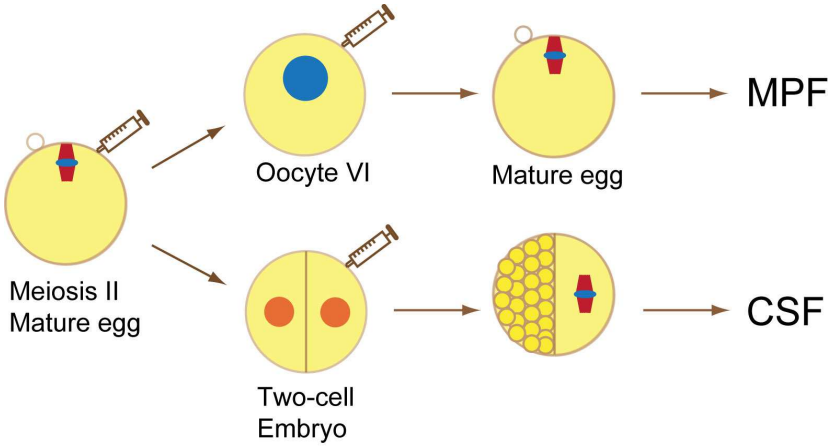

Figure 6. Schematic representation of microinjection studies revealing the functional identities of MPF and CSF.

1.3 Protein phosphorylation by high-resolution NMR spectroscopy

Most biomolecular NMR applications rely on the selective observation of ^{1}H, ^{13}C and ^{15}N nuclei in proteins and other biomolecules. These nuclei possess nuclear spin properties that make them suitable for detection by NMR spectroscopy. However, the natural abundance of ^{13}C and ^{15}N is only 1.1% and 0.37%, respectively[111]. The most abundant isotopes of these nuclei are ^{12}C and ^{14}N, which are not suitable for NMR detection[112]. Therefore, ^{13}C - and/or ^{15}N -labeling of proteins is commonly employed to turn these biological molecules into NMR-observable entities. This is achieved by recombinant protein expression in growth media that are supplemented with ^{13}C-carbohydrates, mostly glucose, and $^{15}NH_4Cl$ as the sole sources of carbon and nitrogen, respectively[113,114] (**Fig. 8A, upper panel**). Recombinant protein expression and purification from isotope-labeled bacterial cultures yields NMR-active biomolecules that can be studied by multi-dimensional NMR methods.

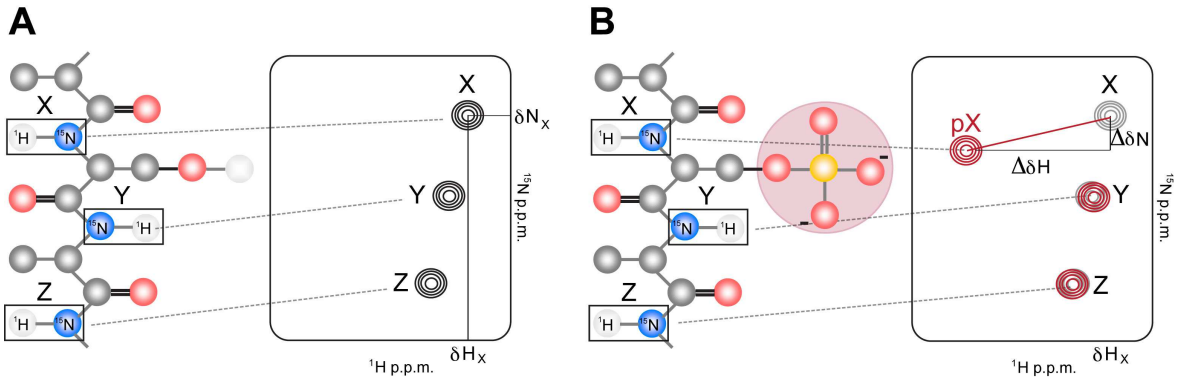

Figure 7. Schematic representation of 2D ^{1}H-^{15}N edited NMR spectra; carbon, oxygen, hydrogen and nitrogen atoms are shown in grey, red, white and blue, respectively. A) NMR cross-peaks of backbone amide spin-pairs (^{1}H-^{15}N) exhibit characteristic NMR resonance frequencies. The chemical shift of each NMR resonance reports the individual chemical environment of the detected spin-pair. B) Phosphorylation induces large chemical shift changes (Δδ) of phosphorylated protein residues (pX). In contrast, phosphorylation does not affect the chemical environments of other protein residues and their chemical shift values, resonance frequencies, or NMR peak positions remain unchanged.

The chemical environments of NMR-active nuclei in proteins directly translate into characteristic NMR resonance frequencies, or chemical shift (δ) values. Alterations in these chemical environments induce site-selective changes in the resonance frequencies of individual protein residues. In case of protein phosphorylation, the covalent addition of

a phosphate moiety onto serine or threonine residue results in a backbone amide chemical shift change (Δδ) of the modified amino acid in the range of ~0.5-1.5 p.p.m., which is readily detected in ^{1}H-^{15}N backbone amide correlation NMR spectra[115] (**Fig. 7**). Phosphorylation induces changes in serine/threonine chemical environments by causing intra-residue hydrogen bonds between amide protons and the phosphate moieties of the respectively modified protein residues[116,117].

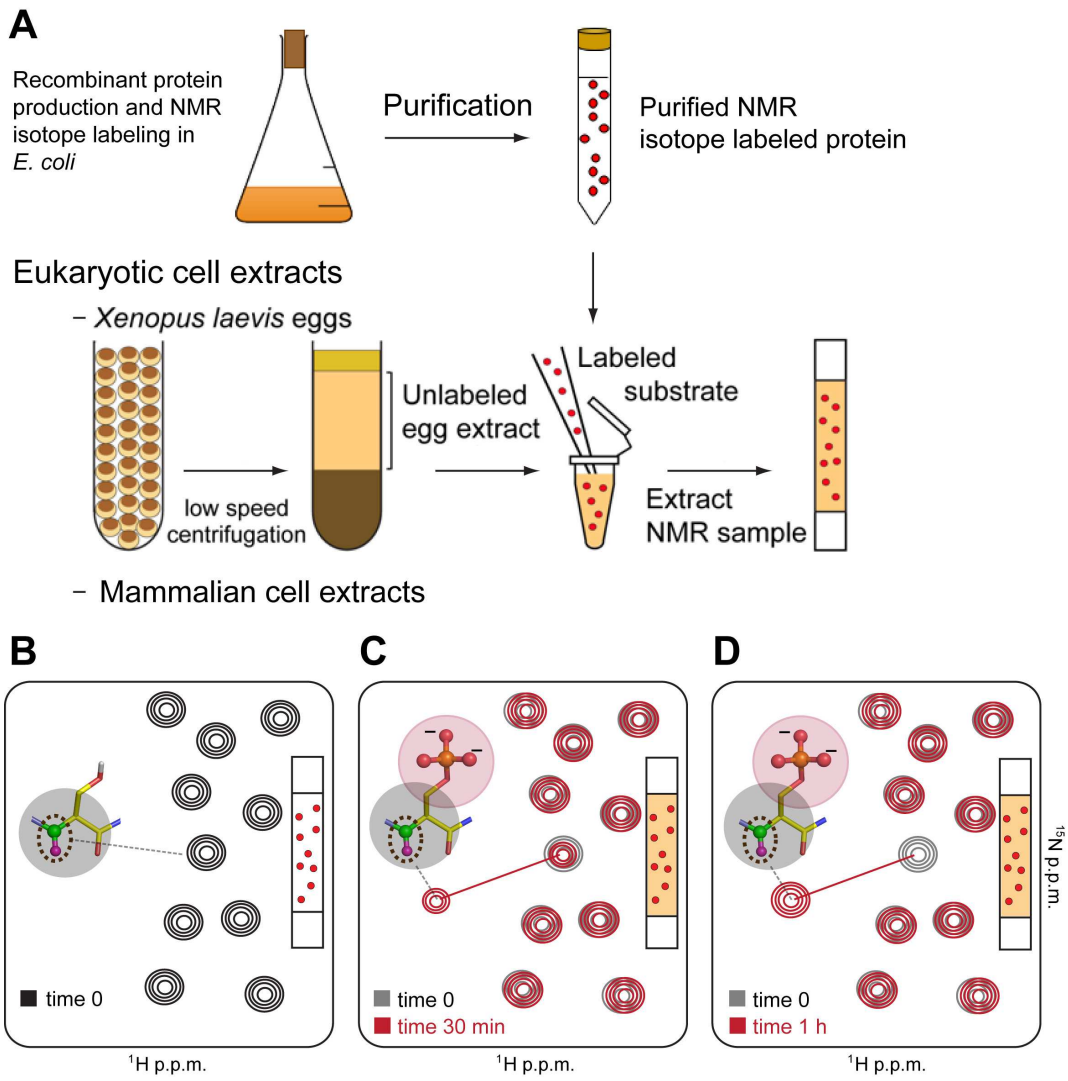

Figure 8. Protein phosphorylation study by NMR spectroscopy. A) Schematic representation of a uniformly ^{15}N labeled NMR sample preparation for *in extract* phosphorylation studies. B) Schematic representation of time-resolved *in extract* detection of protein phosphorylation events by NMR spectroscopy. 2D ^{1}H-^{15}N edited NMR spectrum of a uniformly ^{15}N-labeled protein substrate (XXXXXS/TXXXXX). C) Overlay of 2D ^{1}H-^{15}N NMR spectra at time points t=0 (gray), t=30 min (red) in cell extract. D) Overlay of 2D ^{1}H-^{15}N NMR spectra at t=0 (grey), t=1 h (red) in cell extract. Absence of NMR signals of the non-phosphorylated protein species indicates completion of the modification reaction (complete substrate turnover).

Several features of solution-state NMR spectroscopy make it particularly advantageous for protein phospho-detection and phospho-site mapping studies. First of all, NMR is an atomic resolution method, which means that individual protein residues are directly detected in either unmodified or respectively modified states. It is a non-invasive and non-disruptive analytical tool, which enables monitoring of continuous phosphorylation reactions in real-time as they proceed inside the NMR sample tube by recording consecutive sets of time-resolved NMR experiments (**Fig. 8B, C, D**). NMR spectroscopy is inherently quantitative, which means that NMR signal intensities directly reflect the absolute concentrations of NMR-active nuclei in the studied mixtures. Since NMR signals of phosphorylated and unphosphorylated species are detected side-by-side within the same NMR experiment, NMR signal-integration of both species directly deduces the absolute concentrations of modified versus unmodified substrate molecules. Thus, quantitative reaction trajectories of the respective phosphorylation events can be obtained. Isotope labeling can also be exploited as a selective visualization filter in the sense that NMR-active proteins or peptides can be selectively detected-, and hence studied-, in any type of environment that is not isotope-labeled (**Fig. 8A**). Therefore,

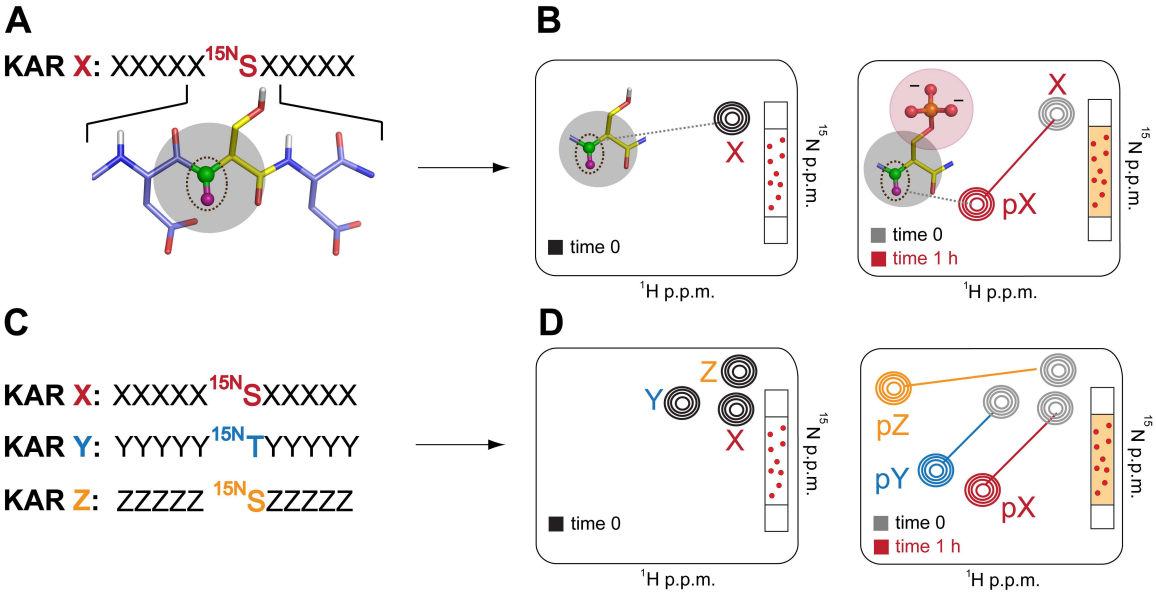

Figure 9. Schematic representation of *in extract* phosphorylation of multiple peptide-based kinase activity reporters (KARs). A) A site specifically ^{15}N-labeled reporter peptide for kinase X or KAR X. B) 2D ^{1}H-^{15}N edited NMR spectrum of the peptide KAR X at time point t=0 (left panel) provides only a single NMR signal. Right panel, overlay of 2D ^{1}H-^{15}N NMR spectra at time points t=0 (gray), t=1 h (red) upon in cell extract phosphorylation. C) Peptide-based KARs for reporting kinases X, Y and Z, individually. D) 2D ^{1}H-^{15}N edited NMR spectrum of a mixture of KAR X, Y and Z (left panel). Right panel, overlay of 2D ^{1}H-^{15}N NMR spectra at time points t=0 (gray), t=1 h upon in cell extract. The NMR signals of the phosphorylated residues are colored differently according to the kinase which each KARs reports its activity.

phosphorylation reactions in cell lysates with added isotope-labeled proteins/peptides as targets of cellular kinases can directly be analyzed by NMR.

Following this rationale, the goal of my thesis project was to generate peptide-based kinase activity reporters by solid-phase peptide synthesis (SPPS), in which only the phosphorylatable peptide residues are ^{15}N isotope-labeled. In combination, each of these reporters will give rise to unique sets of NMR signals that correspond to unmodified and modified phosphorylation states of the reporter. Added to eukaryotic cell lysates or CSF arrested *Xenopus* egg extracts, they will enable multiplexed NMR readouts of endogenous kinase activities in a time-resolved fashion (**Fig. 9**).

1.4 Objective of the Ph.D. project

Protein kinases regulate protein functions that control many biological processes. In turn, abnormalities in these functions and/or the regulation of kinase activities are causally involved in a large number of human diseases. Although several methods to examine cellular kinase activities have been developed, most of them fail to monitor multiple kinase activities in parallel. High-resolution NMR spectroscopy has recently emerged as a novel tool to directly observe protein phosphorylation events in a time-resolved and quantitative manner. The goal of this Ph.D. project, therefore, was to develop a multiplexed kinase activity profiling approach based on high-resolution NMR spectroscopy and peptide-based kinase activity reporters. Cytostatic factor (CSF) arrested *Xenopus* egg extracts and cell cycle-regulated protein kinases were chosen as an initial cellular model system to develop the assay and to assess the overall functionality and suitability of the outlined approach. Kinase activity reporters were designed and engineered with specific features in mind: Firstly, to be able to measure cellular kinase activities with high accuracy and a great degree of reproducibility. Secondly, to monitor cellular kinase activities with high specificity, for which extended cross-reactivity testing routines had to be employed. Thirdly, to develop protocols for the generation of stable reporters which resist cellular degradation by endogenous proteases and enable time-resolved NMR measurements over extended periods of time. Forth, to design peptide-base kinase activity reporters that can be employed in multiplexed manners, without detrimental effects on readout specificity and reporting accuracy.

2. RESULTS

2.1 Recombinant Kinase Activity Reporters (KARs)

In the initial stage of this project, KARs were generated by recombinant approach, which was useful to quickly construct KARs and test their phosphorylation. This chapter presents the overall rationale behind this design and production process and describes KAR testing routines by time-resolved NMR spectroscopy.

2.1.1 Recombinant KAR-GB1 design

The design of KAR sequences was based on known kinase consensus motifs (**1.1.6**). These motifs contain short amino-acid sequences that were extended at their N- and C-termini to resemble peptides that have previously been used in kinase activity measurement assays (**Table 2**). Peptide sequences were added to the N-termini of *Streptococcal* protein G B1 domains (GB1) by recombinant cloning techniques, to generate so called 'reporter-GB1', or 'GB1-fusion' versions of the reporters (**Fig. 10**). The GB1 domain was chosen based on its property as a solubility-enhancement tag and high over-expression levels[118]. The presence of the GB1 domain in the initial reporter constructs also enabled facile protein identification and quantification by protein electrophoresis and UV-absorbance measurements at 280 nm, during expression and purification steps. If KARs were to be expressed as peptides only, monitoring of purification steps and quantitative measurements of peptide concentrations would be

Figure 10. Recombinant KAR design. CK2-GB1 fusion construct: the CK2 reporter sequence (RRRADDSDDDDD) added to the N-terminus of the GB1 domain (residue 1-57). The CK2 reporter contains the phosphorylatable serine residue indicated in red.

difficult due to the exceedingly small size of the reporters and lack of aromatic residues in most of the reporter sequences.

In order to obtain GB1-fusion reporters, I initially expressed double-GB1 constructs that contained the KAR-GB1 sequences with an additional GB1 moiety at their N-termini (**Fig. 11**). As a result, the KAR sequences were 'protected' from possible proteolytic degradation events at both their N- and C-termini during recombinant protein expression in *E. coli*. The N-terminal GB1 moiety was eventually separated from the KAR-GB1 sequence by Tobacco Etch Virus (TEV) protease cleavage via the engineered TEV recognition sequence (ENLYFQ*G, cleavage site indicated by an asterisk). Therefore, the glycine residue of the TEV site remains as the N-terminal residue in the released KAR-GB1 fusion protein. Additionally, a N-terminal 6 His-tag was included in the double GB1 constructs for purification purpose via a Nickel-affinity chromatography. *E.coli* were transformed with these plasmids and fusion proteins were expressed in ^{15}N-labeled bacterial cultures as described below.

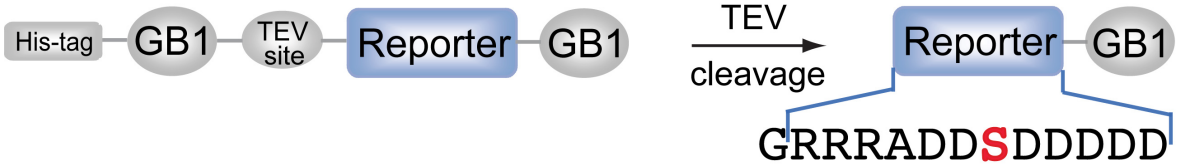

Figure 11. Outline of CK2 double-GB1 reporter construct: 6 His-tag (grey square) followed by first GB1 domain grey circle), TEV recognition site (grey circle), KAR sequence (blue square) and second GB1 domain (grey circle). TEV cleavage releases the reporter-GB1 construct.

2.1.2 Optimizing KAR-GB1 expression conditions

To screen for optimal yields of recombinant KAR-GB1 constructs, initial expression tests of CK2 double-GB1 fusion were performed in *E.coli* cells grown under different supplement conditions to M9 minimal media (**Fig. 12A** and section **5.1.6**). Uniform expression levels were detected in all growth media. Expression was also tested in different *E. coli* strains. BL21 (DE3), BL21 (DE3) Express and BL21 STAR provided comparable yields of soluble, recombinant double-fusion proteins (**Fig. 12B)**. In contrast, the pLysS strain gave no over-expression protein. Based on these experiments, *E. coli*

BL21 (DE3)- Express strains were chosen for all further expressions and M9 media were supplemented with trace elements solutions for optimal expression levels.

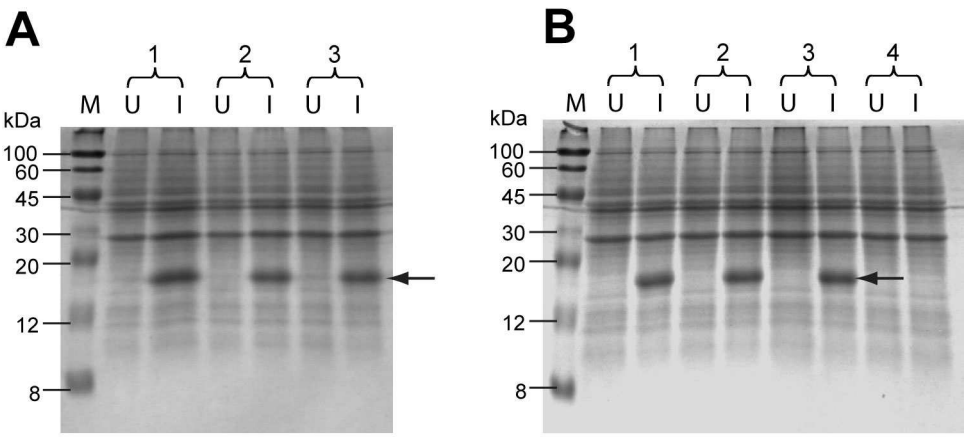

Figure 12. Over-expression tests in 100 mL bacterial cultures. A) 18% SDS-PAGE of total *E.coli* lysates of CK2 double-GB1 fusion over-expression in different M9 media at 37°C, M= protein marker, U=no IPTG induction, I=IPTG induction (0.4 mM for 4 h). 1=M9 + Trace elements, 2=M9 + O solution, 3=M9 + S and O solutions, plus vitamin mix. Double-GB1 fusion constructs (16.5 kDa) marked by arrow. B) Screening different *E. coli* strains. 18% SDS-PAGE of total *E.coli* lysates of CK2 double-GB1 fusion over-expression. M=protein marker, U=no IPTG induction, I=IPTG induction (0.4 mM for 4 h), 1=*E.coli* BL21 (DE3), 2= *E.coli* BL21 (DE3) Express, 3=*E.coli* BL21 STAR, 4=*E.coli* pLysS.

2.1.3 KAR-GB1 purification routines

Next, double-GB1 over-expression was performed in 500 mL of M9 cultures. Under the selected conditions (**2.1.2**), similar expression levels for different KAR constructs were detected (**Fig. 13A**). Bacterial cultures were harvested, lysed and soluble fractions were further purified (**Fig. 13B**). Purification routines involved two affinity-chromatography runs and one size-exclusion chromatography step. Nickel affinity purification resulted in 90% purity of the corresponding fusion proteins (**Fig. 13B**). Release of KAR-GB1 fusion moieties after TEV cleavage was checked by SDS-PAGE (**Fig. 13C**). A second Nickel affinity chromatography step resulted in the removal of the N-terminal His tag-GB1-containing fragment, while the KAR-GB1 fragment was retained in the flow-through. Further purification by size-exclusion chromatography yielded pure and monomeric KAR-GB1 (**Fig. 13D**). Correct size of purified KAR-GB1 was confirmed by MALDI-TOF mass

spectrometry (MS) (**Fig. 13E**). These expression and purification routines resulted in reproducible yields of ~4-6 mg of uniformly ^{15}N-labeled KAR-GB1 proteins for the different KAR sequences that I generated.

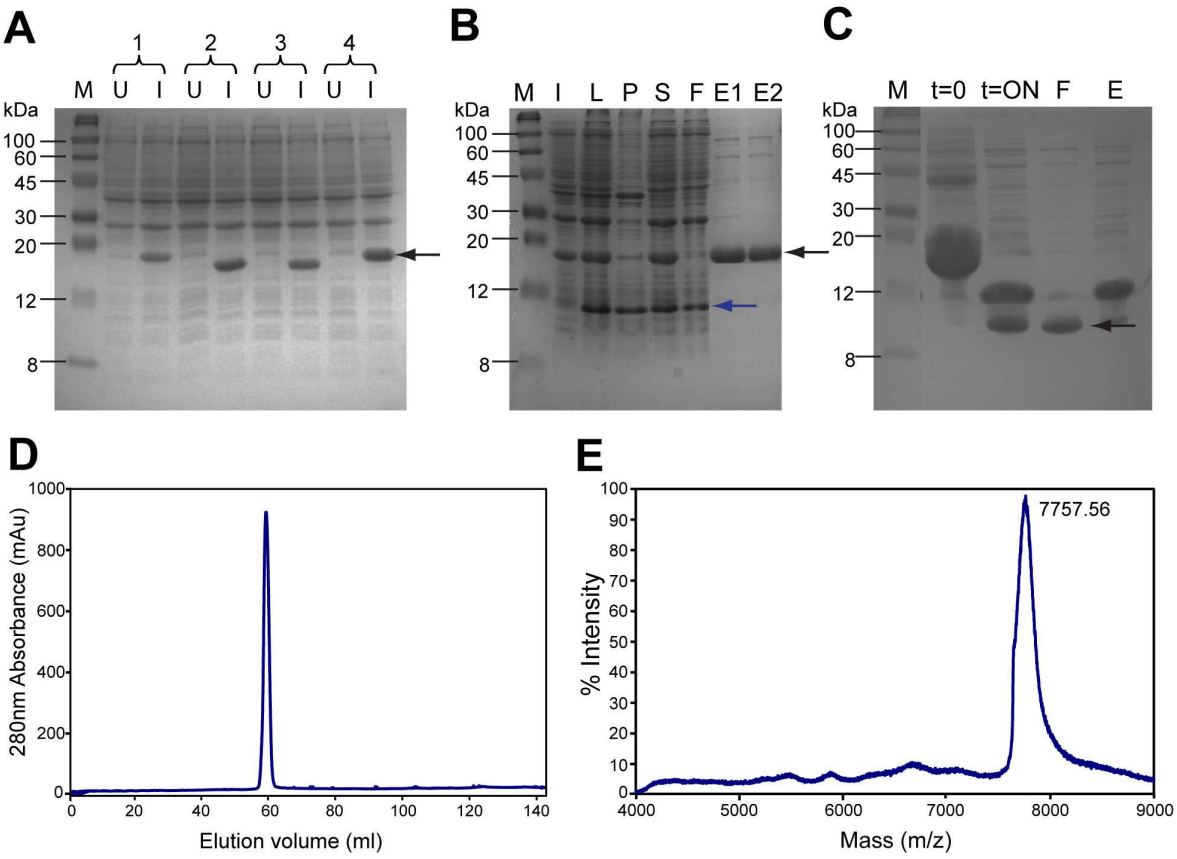

Figure 13. Recombinant KAR-GB1 production. A) 18% SDS-PAGE: overexpression of Plk1-, Chk1-, CK2- and p42MAPK-reporter double-GB1 fusions in ^{15}N isotope-labeled M9 growth media with 1x trace elements (1, 2, 3, 4, respectively). M=protein marker, U=no IPTG induction, I=IPTG induction (0.4 mM for 4 h). B) 18% SDS-PAGE of the double-GB1 CK2 reporter purification scheme. First Nickel affinity chromatography purification step, M= protein marker, I=IPTG induction (0.4 mM for 4 h), L=total cell lysate, P=cell pellet (insoluble fraction), S=soluble fraction, F=Nickel column flow-through, E1=first eluted fraction elution (2 mL), E2=second eluted fraction (2 mL). The double-GB1 CK2 reporter and lysozyme protein bands are indicated by black and blue arrows, respectively. C) 18% SDS-PAGE of double-GB1 fusion (CK2 reporter) and TEV cleavage and purification, followed by second Nickel column purification. t=0 input construct, t=ON overnight TEV cleavage reaction (upper band is the N-terminal GB1 fragment (9.19 kDa), lower band is the KAR-GB1 (7.76 kDa). F=flow-through after TEV cleavage second Nickel column, E=elution from second Nickel column. The purified KAR GB1 product is indicated by an arrow. D) Size-exclusion chromatography profile of KAR-GB1 (CK2 reporter example). E) MALDI-TOF-MS KAR-GB1 (CK2 reporter example); expected mass 7.76 kDa, observed mass 7.76 kDa.

2.1.4 Phosphorylation of recombinant KAR-GB1

Prior to setting up phosphorylation reactions, I recorded reference 2D ^{1}H-^{15}N spectra of KAR-GB1 proteins (50 µM, 300 µL), as illustrated for the CK2 KAR-GB1. In uniformly ^{15}N-labeled proteins, every HN amide group gives rise to a NMR resonance signal in 2D ^{1}H-^{15}N hetero-nuclear correlation experiments. Overlay of KAR-GB1 spectra with that of the original GB1 domain enables me to quickly identify NMR resonance signals that correspond to KAR residues (**Fig. 14A**). Notably, most NMR signals of GB1 domain remain unchanged in KAR-GB1 constructs and new resonance cross peaks correspond to KAR amino acids. Phosphorylation of KAR-GB1 proteins was initially tested with 500 units (U) of the respective kinases *in vitro,* for example CK2 (**Fig. 14B**). Phosphorylation consistently produced large downfield chemical shift changes of KAR backbone amide resonances of the respectively modified amino acids.

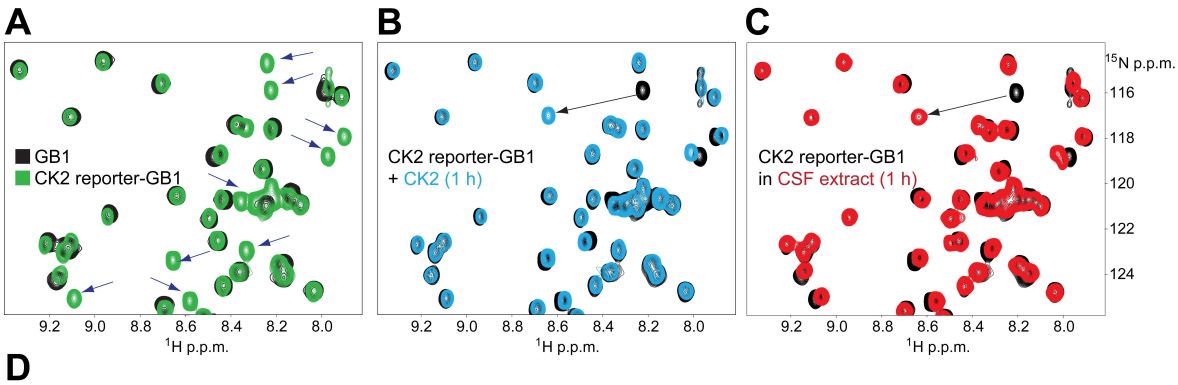

Figure 14. Phosphorylation of recombinant KAR-GB1 (CK2 reporter for example, GRRRADDSDDDDD-GB1). A) Overlay of 2D ^{1}H-^{15}N NMR spectra (selected region) of the protein domain GB1 (black) and recombinant CK2 KAR-GB1 (green). NMR signals of amino acid residues corresponding to the KAR peptide sequence (dark blue arrows) are well set apart from those of the folded GB1 domain. B) Overlay of 2D ^{1}H-^{15}N NMR spectra of CK2 KAR-GB1 before (black) and after *in-vitro* phosphorylation with 500 U of CK2 (blue). The arrow indicates the characteristic downfield chemical shift change (Δδ) of the Ser resonance cross peak of the phosphorylated KAR residue. C) Overlay of 2D ^{1}H-^{15}N NMR spectra of CK2 KAR-GB1 reference (black) and in the CSF extract (red). All reactions were performed at identical KAR-GB1 concentrations of 50 µM at pH 7.5, 25°C. D) Amino acid sequence of the GB1 domain residues (1-57).

Because CK2 reporter contains only one phosphorylatable serine, the serine assignment of the CK2 reporter is easily accomplished via the modification in the CK2 *in vitro* reaction (**Fig. 14B**). Further, I ensured that KAR-GB1 proteins conveyed cellular kinase activities by adding them to CSF extracts that were known to contain active amounts of the kinases to be tested. Identical NMR chemical shift displacements in CSF extracts were employed to confirm the suitability of the KAR peptide sequence in reporting endogenous kinase activities (**Fig. 14C**). Although the GB1 domain contains ten threonine residues (**Fig. 14D,** blue letters), no phosphorylation of GB1 by endogenous kinases in CSF extracts/recombinant kinases was observed (**Fig. 14B, C**). Therefore, the GB1 moiety did not interfere with identifying cellular kinase activities via the outlined approach. The same strategy was employed to test phosphorylation of every other KAR-GB1 protein *in vitro* and in CSF extracts. Results are shown in section **2.3** and **2.6**.

2.1.5 Drawbacks of uniformly ^{15}N isotope-labeled KAR-GB1 proteins

The main goal of this Ph.D. project was to quantify multiple kinase activities in parallel. To achieve this goal, I intended to perform experiments with multiple reporters in single phosphorylation reactions. By using multiple, uniformly ^{15}N isotope-labeled KAR-GB1 proteins in the same reaction, substantial signal overlap of GB1 and KAR resonances would severely obstruct the respective readout schemes and render identifications of individual KAR reactions difficult. In a next step, the number of NMR signals and therefore the overall spectral complexity had to be reduced. This was achieved by transforming recombinant KAR-GB1 proteins into peptide-based KARs that would only contain the minimal kinase consensus sequence necessary for targeting the actual kinase activity, including the phosphorylatable substrate residue. In addition, I employed solid-phase-peptide synthesis (SPPS) to generate individual versions of peptide-based KARs and to isotope label only the phosphorylatable amino acids in each of them. This procedure enabled me to obtain single-site isotope-labeled KARs, which I outline in the next section.

2.2 Synthetic, peptide–based KARs

I used information previously gathered from KAR-GB1 constructs (**Table 2**) to generate peptide-based KARs by solid-phase peptide synthesis (SPPS). In this section, I describe the production, phosphorylation and evaluation of cellular stability of synthetic KARs.

2.2.1 Peptide KAR design and production

Peptide-based KARs only contain the KAR portion of KAR-GB1 proteins described in the previous section (**2.1**). Therefore, the peptide-based KARs are much smaller than KAR-GB1 proteins. KARs were produced by Fmoc-based SPPS, which permitted the site-selective introduction of ^{15}N isotope-labeled amino acid precursors at the respective phosphorylation sites (**5.4**). For instance, the serine of the CK2 reporter sequence was incorporated as a ^{15}N-labeled amino acid, while all other residues were synthesized in their unlabeled forms (**Fig. 15A**). Initially, only the N-termini of the synthetic KARs were protected by acetylation[119]. After detachment from TentaGel RRAM-resins, crude KARs were ether precipitated. On average, 40 mg of crude peptides was initially obtained. This crude was further purified by preparative reverse-phase (RP) high-performance liquid chromatography (HPLC) using C18 columns. KARs were confirmed by MALDI-TOF MS (**Fig. 15B**). KAR purity was further verified by analytical RP-HPLC (>90%) (**Fig. 15C**). 3-5 mg of purified peptide KARs was usually obtained from 25 µmol synthesis scale.

Table 1. KAR sequences: Original and modified sequences

KAR	Original sequence	Modified sequence
Plk1	Ac-GHLGESSFSSDWDDESLG	Ac-GALGESSFSSDWDDESLG
Cdk1	Ac-GQHSTPPKKKRKV	Ac-GQASTPPKKKRKV
Akt/PKB	Ac-GSQRQRSTSTPNVH	Ac-GSQRQRSTSTPNVA

Phosphorylatable amino acids are shown in red, mutated histidines are indicated in blue.

Notably, histidine and cysteine residues can undergo racemization during Fmoc-based SPPS[120,121]. Therefore, histidines that were originally present in different KAR sequences were replaced by alanines, as was the case for the Plk1-, Cdk1- and Akt/PKB- reporters (**Table 1**). Alanine mutations of those histidines did not influence their kinase-substrate

specificities because the residues belong to none of these kinase consensus sequences[122-126].

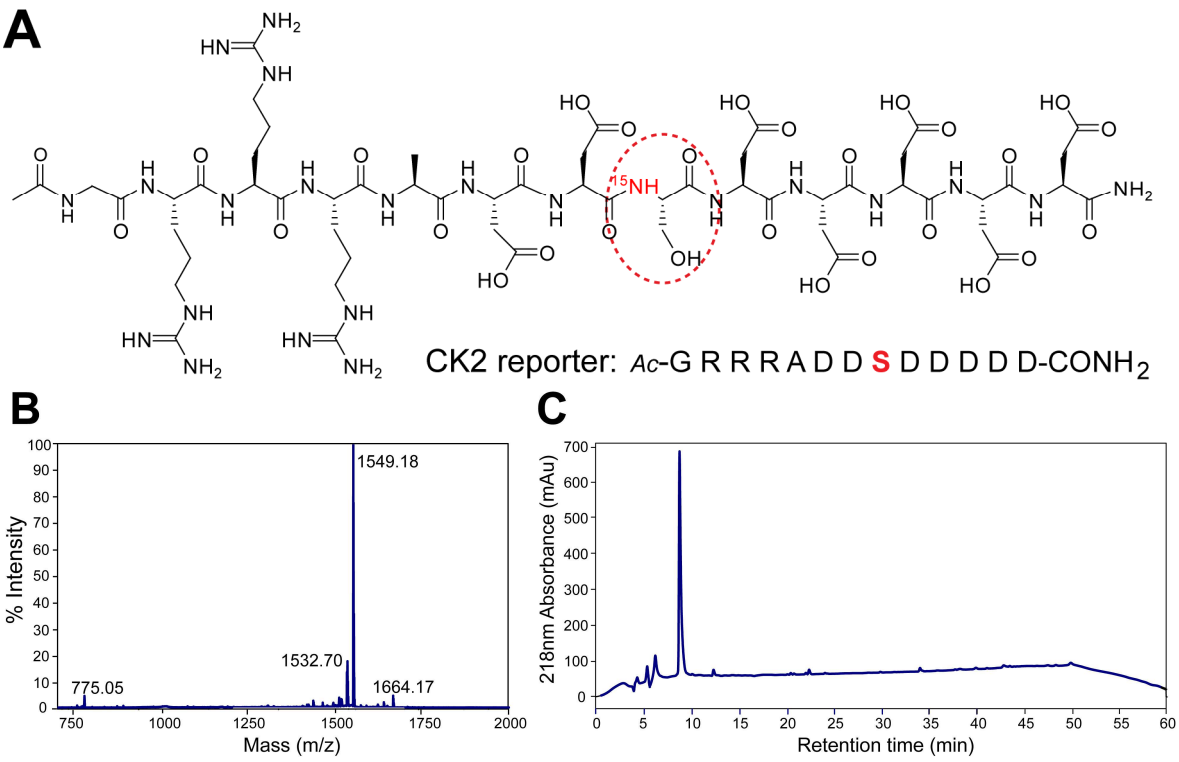

Figure 15. Schematic outline of peptide-based CK2 reporter production. A) Sequence and chemical structure of ^{15}N-serine CK2 reporter. B) MALDI-TOF MS spectrum of the purified CK2 reporter. Expected mass 1548.44 g/mol, detected mass 1549.18 g/mol. C) Analytical RP-HPLC chromatogram of the CK2 reporter peptide. A single peptide (>90% purity) was eluted with a retention time (t_r) of 8.8 min.

2.2.2. Phosphorylation of peptide KARs

In contrast to uniformly ^{15}N isotope-labeled KAR-GB1 proteins, site-selective ^{15}N-labeled KARs give rise to single NMR cross peaks in 1D and 2D ^{15}N-edited NMR spectra. KAR phosphorylation of single reporter reactions can therefore be studied by time-resolved, consecutive 1D NMR experiments (**Fig. 16A**). Using 500 U of CK2, progressive KAR modification was monitored during the reaction time course (**Fig. 16B**). While the NMR resonance signal of the unmodified substrate species decreased over time, the signal corresponding to phosphorylated species increased. After normalizing the signal intensities of both states, a quantitative reaction profile could be obtained (**Fig. 16C**). Reaction rates were fitted to exponential build-up (phospho-species) and decay curves (unmodified species, see also **5.5.4**). Both curves intersected at a substrate/product ratio

of 1, i.e. when 50% of KAR molecules were present in either phosphorylated, or unphosphorylated forms. For each reporter/enzyme combination at fixed enzyme (500 U) and substrate concentrations (50 µM), the intersection of both curves yielded the specific reaction half-time, or T_{50} value that I later used to assess the individual kinase reactions (**Fig. 16C**).

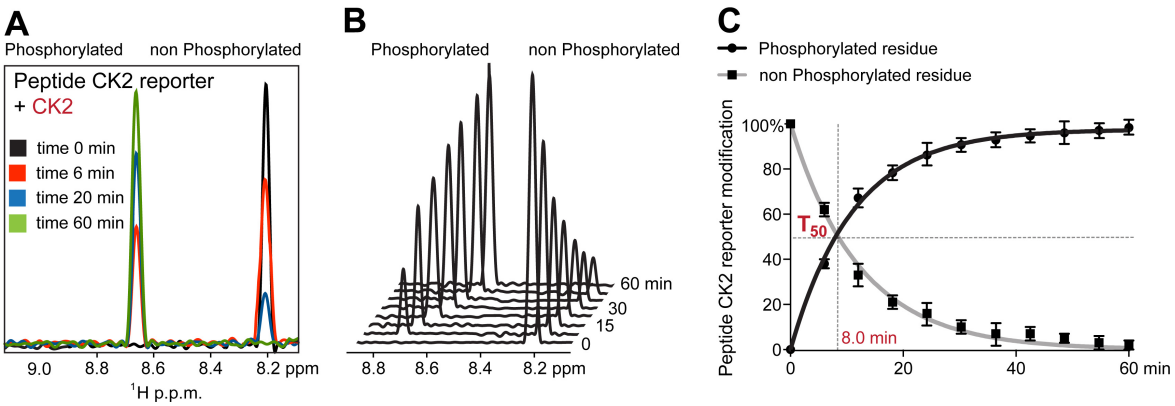

Figure 16. *In vitro* phosphorylation of the peptide-based CK2 KAR. A) Overlay of 1D ^{15}N-edited ^{1}H NMR spectra at t=0 (black) and after addition of 500 U CK2 at t=6 min (red), t=20 min (blue), t=60 min (green). The single NMR signal of ^{15}N Ser-labeled CK2 KAR is detected at δ(^{1}H)=8.20 p.p.m.. Phosphorylation creates a phospho-serine resonance signal at δ(^{1}H)=8.65 p.p.m.. B) Time-resolved staggered plot of the CK2 phosphorylation reaction. C) Modification curves of the same reaction. Peak intensities of phosphorylated and unphosphorylated species were quantified and translated into % of phosphorylation, plotted against time. Exponential build-up and decay curves are colored in black and grey, respectively.

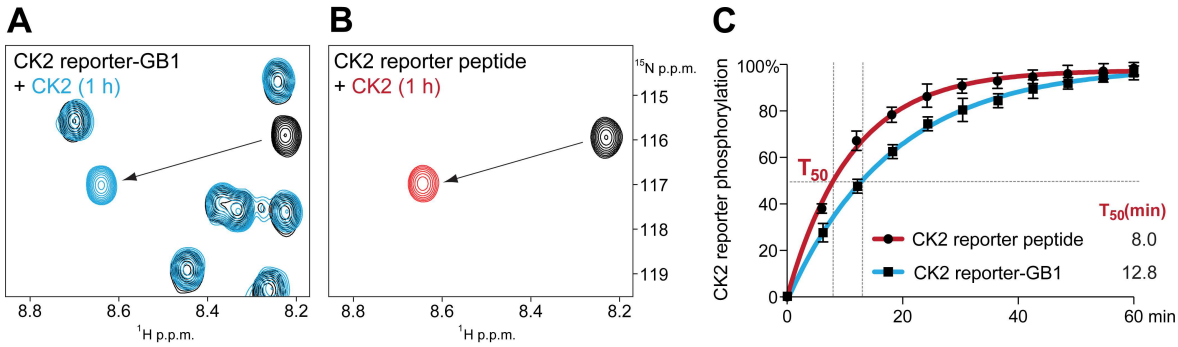

Figure 17. Reduction of spectral complexity by selective ^{15}N isotope labeling. A) Overlay of 2D ^{1}H-^{15}N NMR spectra of uniformly ^{15}N isotope-labeled CK2 KAR-GB1 at t=0 (black) and upon reaction with 500 U of CK2 at t=1 h (blue). B) Overlay of 2D ^{1}H-^{15}N NMR spectra of site-selective ^{15}N isotope-labeled CK2 KAR at t=0 (black) and upon reaction with 500 U CK2 at t=1 h (red). C) Modification curves of synthetic CK2 KAR (red) and CK2 KAR-GB1 (blue). All *in vitro* reactions were performed with CK2 reporter concentrations of 50 µM in 300 µL at pH 7.5, 25°C.

By generating site-selective, ^{15}N-labeled KAR peptides, the complexities of the resulting NMR spectra are greatly reduced. In essence, each KAR gives rise to a single ^{1}H-^{15}N resonance signal, as shown for the CK2 KAR example (**Fig. 17A, B**). In the following, I also determined that the folded GB1 moiety often decreased overall KAR phosphorylation efficiency, as evidently displayed by the *in vitro* 500 U CK2 modification trajectories of CK2 KAR-GB1 (T_{50}=12.8 min) and peptide CK2 KAR (T_{50}=8.0 min) (**Fig. 17C**). These results suggested that individual GB1 domains at the C-termini of reporter sequences hindered kinase accessibility and partially reduced phosphorylation efficiency.

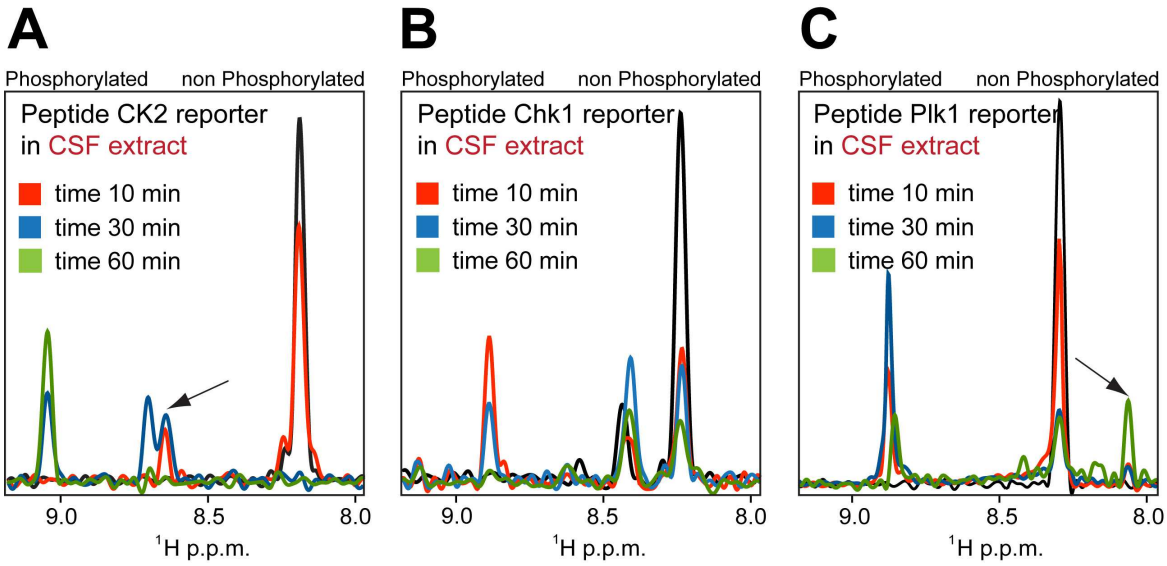

Figure 18. Degradation of synthetic KARs in CSF extracts. A) Overlay of 1D ^{1}H NMR spectra of the peptide-based CK2 reporter in CSF extracts at t=0 (black), t=10 min (red), at t=30 min (blue), at t=60 min (green). The arrow indicates the phosphorylated serine residue. B) Overlay of 1D ^{1}H NMR spectra of the Chk1 reporter (Ac-GRLYRSPSMPEKLDR). The NMR signal at δ=8.43 p.p.m. arises from an impurity. C) Overlay of 1D ^{1}H NMR spectra of the Plk1 reporter (Ac-GALGESSFSSDWDDESLG). An additional NMR signal appears at δ= 8.08 p.p.m., which indicates degradation of the reporter (black arrow). All reactions were performed with reporter peptide concentrations of 50 µM in 300 µL at pH 7.5, 25°C.

Although the presence of the GB1 domain induced slight reductions in KAR-GB1 phosphorylation efficiencies, GB1-tagging also considerably improved the cellular stability of KARs. When synthetic, peptide-based KARs were tested in CSF extracts, rapid proteolytic degradation was often observed (**Fig. 18**). In every case, peptide KARs were moderately phosphorylated at the beginning of the time course (10-30 min), but NMR signals of proteolytic fragments rapidly appeared and most resonance signals eventually

disappeared altogether. Obviously, KARs consisting of 10-20 amino acids were highly prone to proteolytic degradation regardless of the actual reporter sequences. Supplementing CSF extracts with protease inhibitors during the extract preparation (**5.3.7**) did not abolish these effects. As CSF extracts (total protein concentration >100 mg/mL) closely mimic the conditions of intact cells, KAR degradation was also expected to occur in intact cells. Because the ultimate goal of developing the reporters is to employ KARs in living cells, it was important to investigate the degradation behavior of peptide KARs in more detail.

I initially investigated the degree of KAR degradation by comparing the reaction profiles of different KARs in undiluted and 10-fold diluted CSF extracts. Peptide KARs were found to be more stable in diluted CSF extracts (**Fig. 19**). Cellular degradation of peptide KARs was thus dependent on extract concentration. In order to identify a suitable strategy to improve KAR stability in cellular environments, I initially performed a series of experiments to narrow down the nature of the degradation process, as described in the next section.

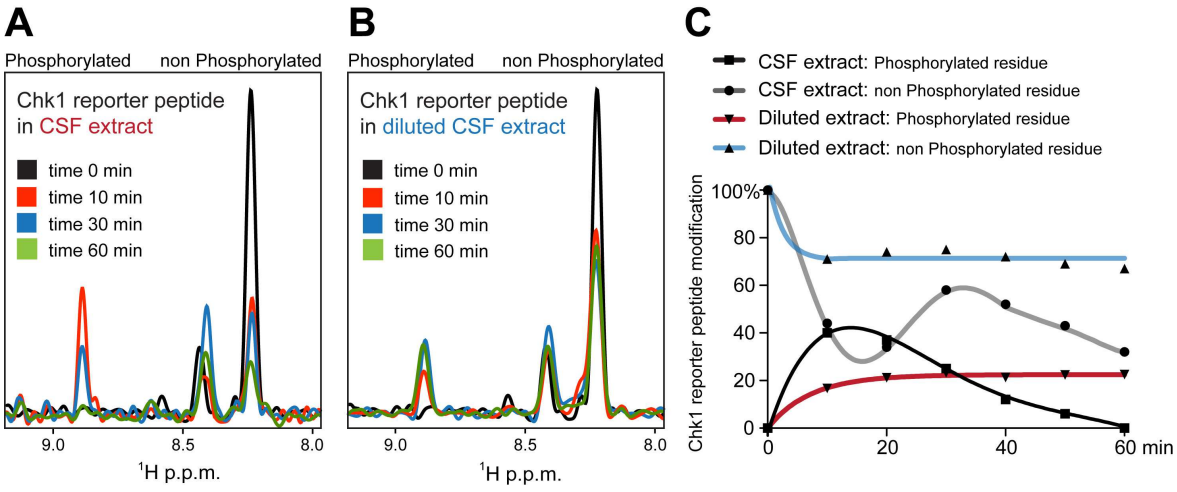

Figure 19. Cellular degradation tests on the Chk1 reporter (Ac-GRLYRSPSMPEKLDR). A) Overlay of 1D ^{1}H NMR spectra of the Chk1 reporter in CSF extracts at t=0 (black), at t=10 min (red), t=30 min (blue), t=60 min (green). B) Overlay of 1D ^{1}H NMR spectra of the Chk1 KAR in 10-fold diluted CSF. The NMR signal at δ(^{1}H)=8.43 p.p.m. arises from the same impurity. C) Chk1 KAR modification curves. Black and grey curves are from phosphorylated and non-phosphorylated residues, respectively, in CSF extract. Red and blue curves indicate phosphorylated and non-phosphorylated residues in diluted extracts. All reactions were performed with initial reporter concentrations of 50 µM at pH 7.5, 25°C.

2.2.3 KAR degradation site mapping

To gain insight into the nature of the degradation events, I set out to more closely analyze the sites of KAR degradation by recombinantly expressing uniformly ^{15}N isotope-labeled peptide KARs. For this purpose, I selected a peptide fragment of the viral SV40 large T antigen, 121-AMGEEMP^{111}S^{112}SDDEATADQHS^{124}TPPKKKRKV-132^{126}. After 1 h of CSF extract incubation, proteolytic degradation was evidently detected in 1D ^{1}H NMR spectra (**Fig. 20A,** upper panel). To compare the in CSF extract results with the SV40 reference 2D ^{1}H-^{15}N NMR spectrum, I had to increase the amplitude of the SV40 peptide (in CSF extract) spectrum by a factor 10. With this process, I could detect few NMR signals with

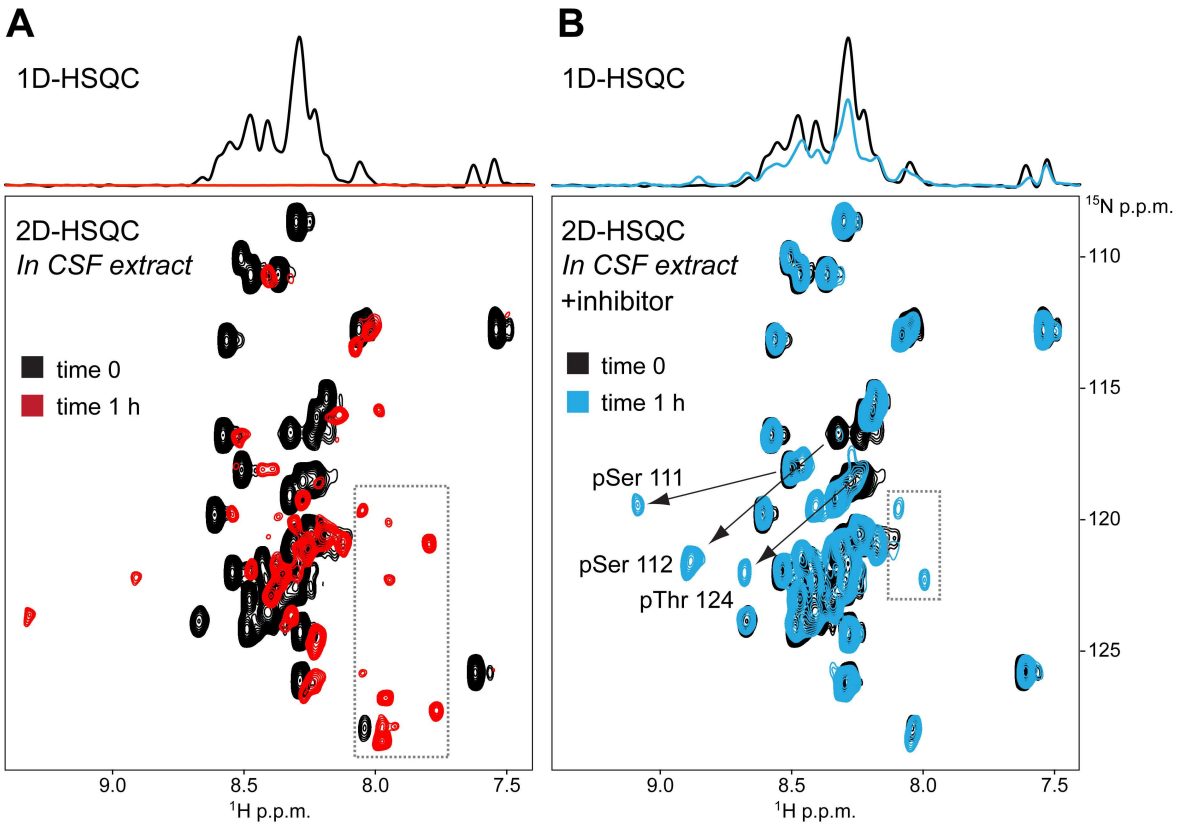

Figure 20. Identification degradation sites using uniformly ^{15}N isotope-labeled SV40 peptide. A) Overlay of 1D (upper panel) and 2D (lower panel) ^{1}H-^{15}N NMR spectra of the SV40 peptide in CSF extracts at t=0 (black) and at t=1 h (red). Characteristic NMR cross peaks of the 2D NMR spectrum (lower panel) indicate peptide degradation (dashed square). B) Addition of carboxypeptidase inhibitors reduces extract degradation. Overlay of 2D ^{1}H-^{15}N NMR spectra of the SV40 peptide in CSF extract at t=0 (black) and supplemented with inhibitors at t=1 h (blue). Arrows indicate phosphorylation of Ser111 and Ser112 by cellular CK2 and Thr124 by cellular Cdk1. Blue NMR signals in the dashed square (lower panel) indicate residual degradation activity. All reactions were performed with peptide concentrations of 50 µM in 300 µL at pH 7.5, 25°C. CSF extracts were incubated with the inhibitor mixture 15 min. prior to the addition of the SV40 peptide.

similar chemical shifts as those of the reference SV40 peptide (**Fig. 20A, lower panel**). I observed additional NMR signals that indicated KAR degradation (the red cross peak signals in a dashed square).

Because KAR-GB1 fusions were much less susceptible to degradation, I reasoned that the degradation process might initiate at the C-terminus of the peptide KAR sequence. Thus, I incubated CSF extracts with carboxy-peptidase inhibitors 15 min prior the SV40 addition. These inhibitors slowed down cellular degradation of the SV40 peptide to a significant extent (**Fig. 20B**). Because the cellular stability of the peptide was improved under those conditions, phosphorylation of three substrate sites by cellular enzymes was readily detected[126] (**2.3.1** and **Fig. 20B**). Nevertheless, additional NMR signals indicative of partial degradation were still present (**Fig. 20B,** dashed square). Based on these results, I concluded that KAR degradation primarily initiated at the C-termini of the peptide reporters.

In a next step, I set out to employ different strategies for C-terminal KAR protection (described in section **2.2.4**) as addition of protease inhibitors to intact cells was not a viable option for studying cellular kinase activities under native conditions.

2.2.4 Stabilization of peptide KARs

This section outlines two rationales that I followed to improve the cellular stability of peptide-based KARs. Along the first rationale, I replaced KAR amino acids that did not consitute kinase consensus residues with analogous D-amino acids. In the second approach I conjugated polyethylene-glycol (PEG) to KARs in order to establish a bulky protective entity at their C-termini. Phosphorylation efficiencies and cellular stability were comparatively analyzed as described below.

2.2.4.1 Replacing L-amino acids with a D-amino acids

The substitution of L-amino acids with D-amino acids is a well-known approach to protect peptides from cellular degradation[127-130]. Because D-amino acids are not natural amino acids, cellular peptidases fail to recognize and degrade D-amino acid peptides. I replaced

non-kinase consensus residues at the C-termini of KARs with D-amino acids, as shown for the Plk1 KAR example (Ac-GALGESSFSSDWD^{D}D^{D}E^{D}S^{D}L^{D}G). Under identical experimental conditions in CSF extracts, phosphorylation of the D-amino acid substituted KAR was significantly slower than for the L-amino acid version (38% versus 58% at 30 min, **Fig. 21A, B, C**). However, NMR signals of the D-amino acid reporter also decreased after 30 min of extract exposure and proteolytic degradation was eventually observed (**Fig. 21B, C**). In summary, replacement of L- with D-amino acids decreased overall kinase activity, but did not result in higher KAR stability in CSF extracts.

To circumvent the degradation problem, I also transformed linear KAR peptides into cyclic peptides. These peptides lack free N- and C termini, and are thus expected to be less prone to proteolytic degradation[131]. However, I encountered difficulties in the generation of these cyclic peptides by the native chemical ligation approach (data not shown). Using cyclic KARs for conveying kinase activity, I had to consider the conformational strain affecting the backbone geometry, which might lead to poor interaction between the reporters and the respective kinases. Therefore, I employed other methods such as C-terminal PEGylation of peptide KARs to improve their stability, as described in detail in the following section.

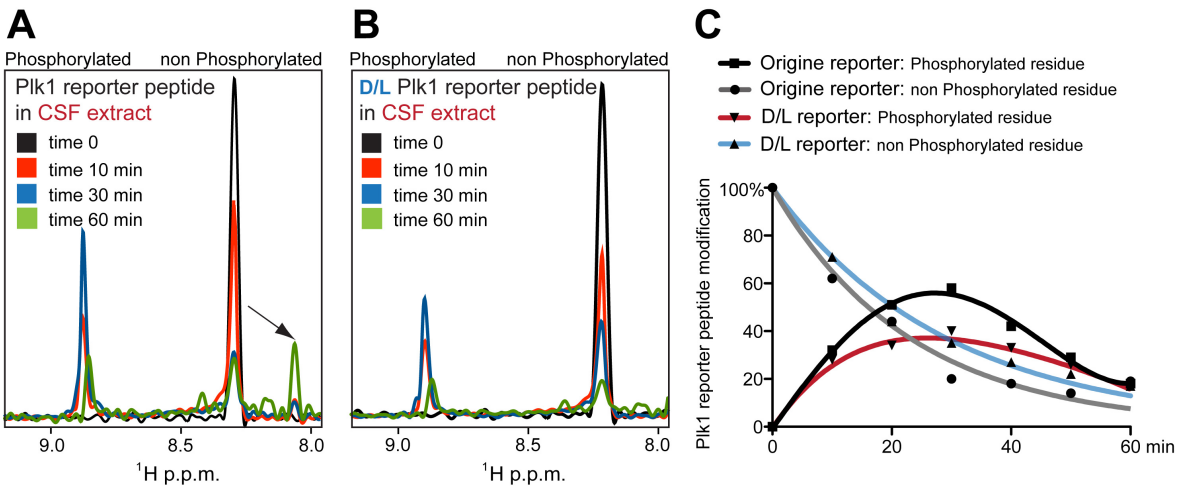

Figure 21. D-amino acid KAR stability tests. A) Overlay of 1D ^{1}H NMR spectra of L-amino acid Plk1 reporter peptide in CSF extracts at t=0 (black) and t=10 min (red), t=30 min (blue), t=60 min (green). B) Overlay of 1D ^{1}H-^{15}N edited NMR spectra of the Plk1 reporter peptide with C-terminal residues changed to D-amino acids in CSF extracts at t=0 (black), t=10 min (red), t=30 min (blue), t=60 min (green). C) Modification curves of the peptide Plk1 KAR. Black and grey curves are from phosphorylated and non-phosphorylated residues of the L-amino acid Plk1 KAR, respectively. Red and blue curves are from the phosphorylated and the non-phosphorylated residues of the D-amino acid Plk1 KAR, respectively. All reactions were performed with peptide concentrations of 50 µM in 300 µL at pH 7.5, 25°C.

2.2.4.2 Polyethylene glycol (PEG) coupling

PEG is extensively used in biomedical applications[132-134]. A unique property of PEG is its high solubility in aqueous solutions and organic solvents. PEG characteristically binds two to three water molecules per ethylene oxide unit, which greatly increases the molecular weights of hydrated PEG moieties[135]. Therefore, PEG functions similarly to a folded protein entity in terms of bulkiness and hydration behavior, and can confer inhibitory properties against proteolytic degradation[133].

Three different versions (structure and length) of PEG were initially tested for their abilities to stabilize KARs in cellular environments and were analyzed their effects on the reporting capacities of the conjugated KARs. I coupled different units of PEG onto the C-termini of peptide CK2 KARs using PEG-modified resins in the SPPS steps (**Fig. 22**). Adding more PEG units to the CK2 KARs progressively enhanced the solubilities of the reporters. Purity and molecular weights of PEGylated KARs were confirmed by RP-HPLC and MALDI-TOF MS (**Fig. 23**). Increasing numbers of PEG units also affected their retention times (t_r). t_r =12.54 min for 2 PEG units, t_r=14.32 min for 10 PEG units and t_r=22.30 min for TentaGel-PEG (**Fig. 23A, C, E**). The final masses of the PEGylated CK2 reporters were 2,318.22 (with 2 PEG units), 3,878.68 (with 10 PEG units), and 4,682.11 (with TentaGel-PEG) g/mol, respectively.

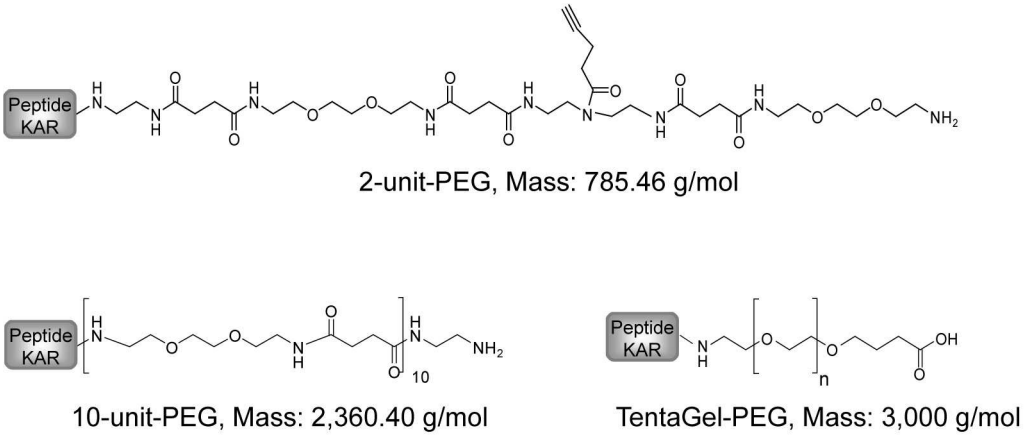

Figure 22. Chemical structures of PEGylated KARs. Calculated mass of the corresponding PEG moieties are shown.

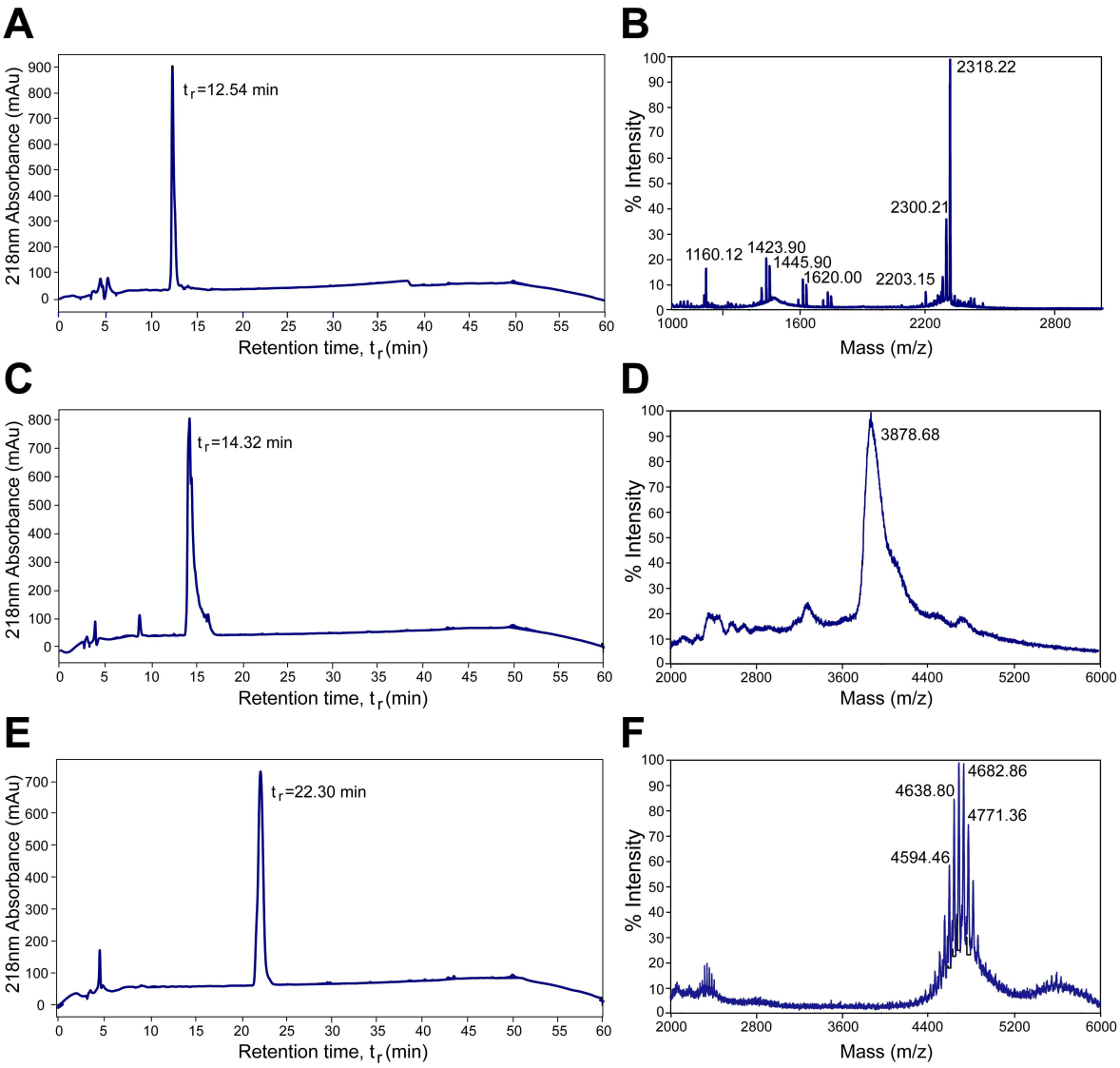

Figure 23. PEGylated CK2 KARs. RP-HPLC chromatograms and MS data of (A, B) 2-unit PEGylated CK2 reporter (C, D) 10-unit-PEGylated CK2 reporter (E, F) and Tentagel-PEGylated CK2 reporter.

Having synthesized PEGylated reporters, I comparatively analyzed their *in vitro* phosphorylation behaviors using recombinant CK2 (500 U) (**Fig. 24A**). Whereas the non-protected (linear CK2 peptide) and the low PEG unit number reporters displayed very similar phosphorylation rates (T_{50}=8.0 min for the non PEGylated reporter, T_{50}=8.2 min for the 2 PEG unit-modified reporter and T_{50}=9.5 min for the 10 PEG unit-modified reporter), TentaGel-PEGylated and GB1-fusion reporters exhibited comparably lower phosphorylation rates (T_{50}=14.4 min for the TentaGel-PEG KAR and T_{50}=12.8 min for the GB1-reporter).

All of the 'fast', PEGylated KARs were readily degraded in CSF extracts (**Fig. 24B, C**), while the multiple-unit PEGylated KAR was highly stable (**Fig. 24D**). Degradation of PEGylated 'fast' reporters may arise from the presence of repeating amide bonds in the PEG subunits (**Fig. 22**), which are likely to be cleaved by cellular proteases[136]. CSF extract phosphorylation revealed similar phosphorylation rates of the TentaGel-PEGylated

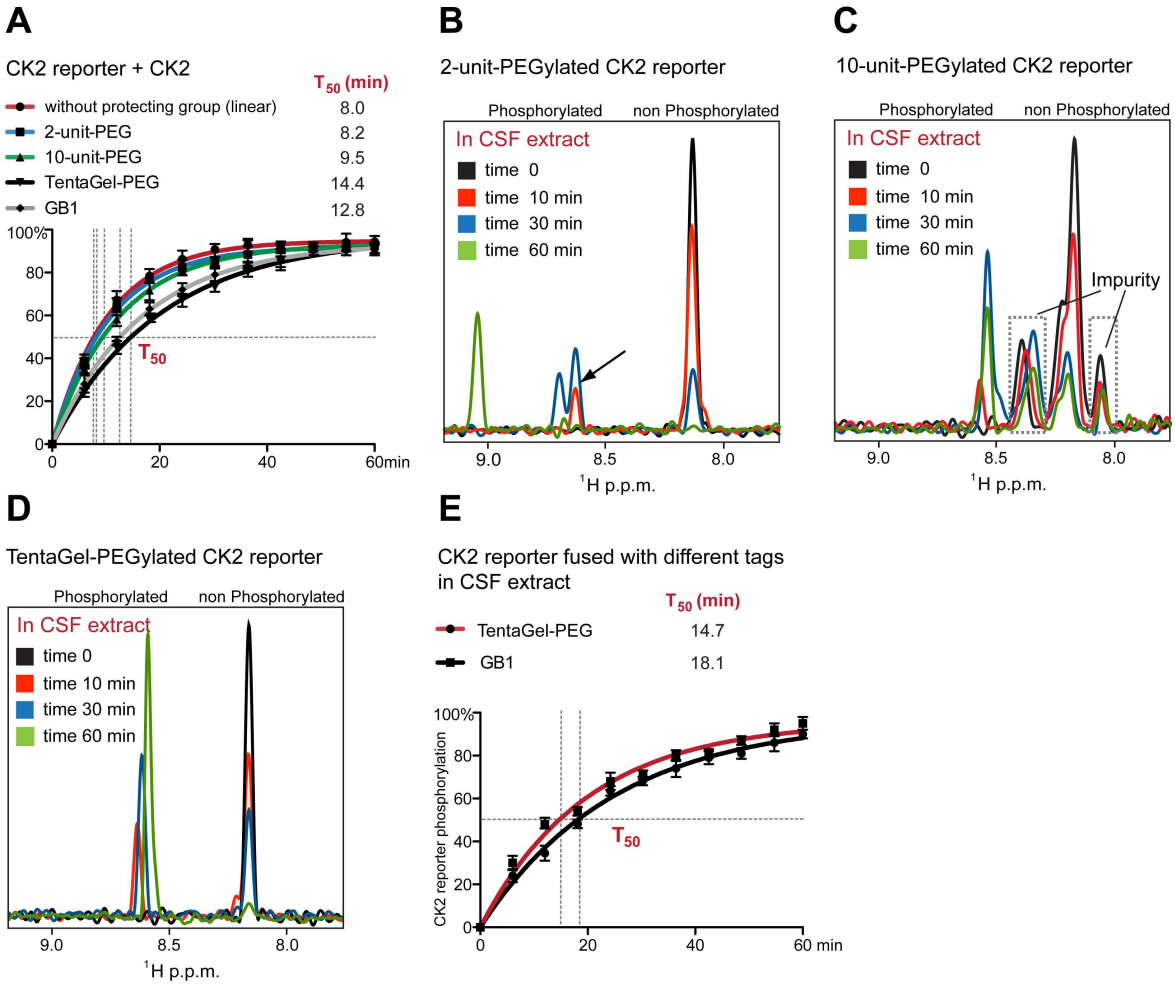

Figure 24. Phosphorylation and stability of PEGylated CK2 reporters. A) *In vitro* phosphorylation of CK2 KARs with different C-terminal protecting groups. Reactions were set up with 500 U of CK2. B) Overlay of 1D ^{15}N-edited NMR spectra of the 2-unit PEGylated CK2 reporter in CSF extract at t=0 (black), t=10 min (red), t=30 min (blue) and t=60 min (green). The degradation pattern is similar to that of the linear CK2 KAR (Fig. 18A). C) Degradation of the 10-unit PEGylated CK2 reporter in CSF extracts by 1D ^{15}N-edited NMR experiments at t=0 (black), t=10 min (red), t=30 min (blue) and t=60 min (green). D) Improved stability of the TentaGel-PEGylated CK2 reporter in CSF extract at t=0 (black), t=10 min (red), t=30 min (blue) and t=60 min (green). E) Comparison of phosphorylation efficiencies of the TentaGel-PEGylated and GB1-KAR CK2 reporters in CSF extarcts. All reactions were performed with peptide concentrations of 50 µM in 300 µL at pH 7.5, 25°C.

(T_{50}=14.7 min) and GB1-fusion reporters (T_{50}=18.1 min) (**Fig. 24E**). These results indicated that bulky protection groups, or C-terminal protein tags slightly reduced the phosphorylation efficiencies of the different KARs, but significantly improved their cellular stabilities. Multiple PEGylation via the TentaGel approach was finally chosen for peptide-based KAR synthesis.

2.3 KAR sequence design and optimization

Having established a suitable KAR production strategy, I further developed protocols to assess phosphorylation efficiencies of different KARs by NMR spectroscopy. For most kinases, different databases, or literature sources provided good starting point for the design of kinase substrate sequences. In the following, these sequences had to be further developed into optimized motifs for maximal phosphorylation efficiency and lowest inter-kinase cross-reactivity.

2.3.1 CK2 and Cdk1 KAR design

CK2 and Cdk1 consensus sequences were originally derived from the viral SV40 large T antigen, 104-AMGEEMP^{111}S^{112}SDDEATADQHS^{124}TPPKKKRKV-132^{126}. In this sequence, Ser111 and Ser112 are phosphorylated by CK2, while Thr124 is phosphorylated by Cdk1[126]. I divided the SV40 sequence into two parts for creating the individual CK2 and Cdk1 reporters. In addition, I optimized and simplified the CK2 reporter sequence to contain only one phosphorylation site. For the CK2 consensus motif S/T-X-X-D/E, it is known that the kinase prefers aspartic acid at P+3 over glutamic acid[137]. Hence, the CK2 sequence was changed to RRRADDSDDDDD. The phosphorylation efficiency of this KAR was comparable to that of the original SV40-derived substrate *in vitro* and in CSF extracts (**Fig. 25A, B, C**). Thus, I used this new CK2 sequence, which has the advantage of possessing only one single phosphorylation site.

Similarly, the original Cdk1 motif QHS^{124}TPPKKKRKV containing the S/T-P-X-R/K consensus sequence, where the proline residue at P+1 is minimally required for this

proline-directed kinase and arginine/lysine residues at P+3 are essential for Cdk1 recognition[123], was changed to QHRTPPKKKRKV because arginine/lysine residues at the P-1 site are known to significantly enhance kinase-substrate specificity. The new Cdk1 reporter performed better than the original SV40-derived peptide *in vitro* (**Fig. 25D, E, F**). The new Cdk1 reporter was also proved that it showed no cross-reactivity with other active proline-directed kinases in CSF extract such as p42MAPK (see **2.4.1, Fig. 36**). As a result, this reporter is a substrate of cellular Cdk1 in CSF extract.

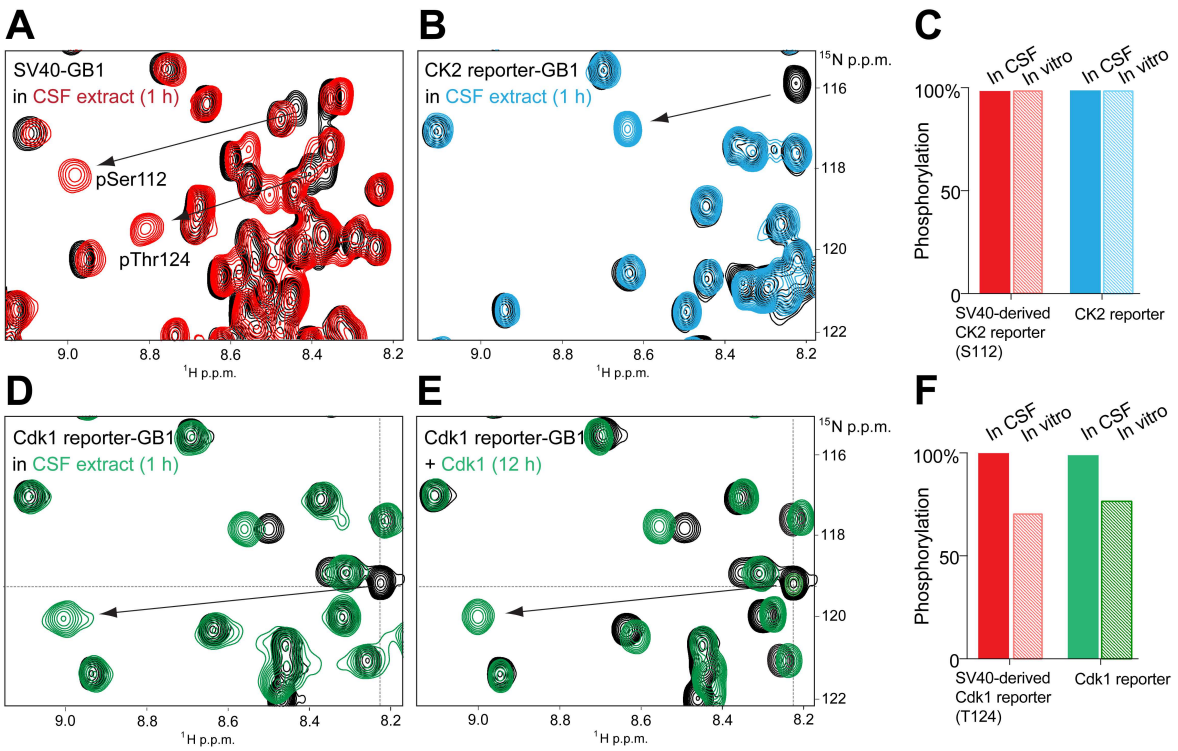

Figure 25. Sequence optimization of CK2 and Cdk1 KARs. A) Overlay of 2D ^{1}H-^{15}N NMR spectra of uniformly ^{15}N isotope-labeled, recombinant SV40-GB1 in CSF extracts at t=0 (black) and at t=1 h (red). B) Overlay of 2D ^{1}H-^{15}N NMR spectra of uniformly ^{15}N isotope-labeled, modified CK2 reporter-GB1 in CSF extracts at t=0 (black) and at t=1 h (blue). C) Bar graphs of phosphorylation levels of SV40-GB1 (red) and modified CK2 reporter-GB1 (blue) *in vitro* and in CSF extracts. Peak volumes of phosphorylated residues were integrated and plotted as % of phosphorylation after 1 h. *In vitro* phosphorylation reactions were performed with 500 U CK2. D) Overlay of 2D ^{1}H-^{15}N NMR spectra of uniformly ^{15}N isotope-labeled, modified Cdk1 reporter-GB1 in CSF extracts at t=0 (black) and at t=1 h (green). E) Overlay of 2D ^{1}H-^{15}N NMR spectra of uniformly ^{15}N isotope-labeled, modified Cdk1 reporter-GB1 with 50 U of Cdk1 at t=12 h (green). F) Bar graphs of phosphorylation levels of SV40-GB1 (red) and modified Cdk1 KAR-GB1 (green) *in vitro* and in CSF extracts. All reactions were performed with KAR-GB1 concentrations of 50 µM in 300 µL at pH 7.5, 25°C.

After obtaining optimized reporter sequences for CK2 and Cdk1, I synthesized TentaGel-PEGylated versions of these KARs. Site-selective incorporation of ^{15}N isotopes at the respective serine/threonine phosorylation sites enabled NMR recordings of 1D and 2D ^{1}H-^{15}N NMR spectra each containing single NMR cross peaks (shown for the Cdk1 reporter in **Fig. 26A, B**). *In vitro* and in CSF extracts, phosphorylation yielded identical chemical shift changes in uniformly ^{15}N isotope-labeled Cdk1 reporter-GB1 and site-selective ^{15}N isotope-labeled Cdk1 reporter (compare NMR spectra in **Fig. 25D, E** and in **Fig. 26A, B**). Furthermore, the TentaGel-PEGylated Cdk1 reporter and the GB1-tagged Cdk1 reporter were phosphorylated with comparable rates *in vitro* and in CSF extracts (**Fig. 26C, D**). Similar results were obtained for the CK2 KAR (**Fig. 24A, E**).

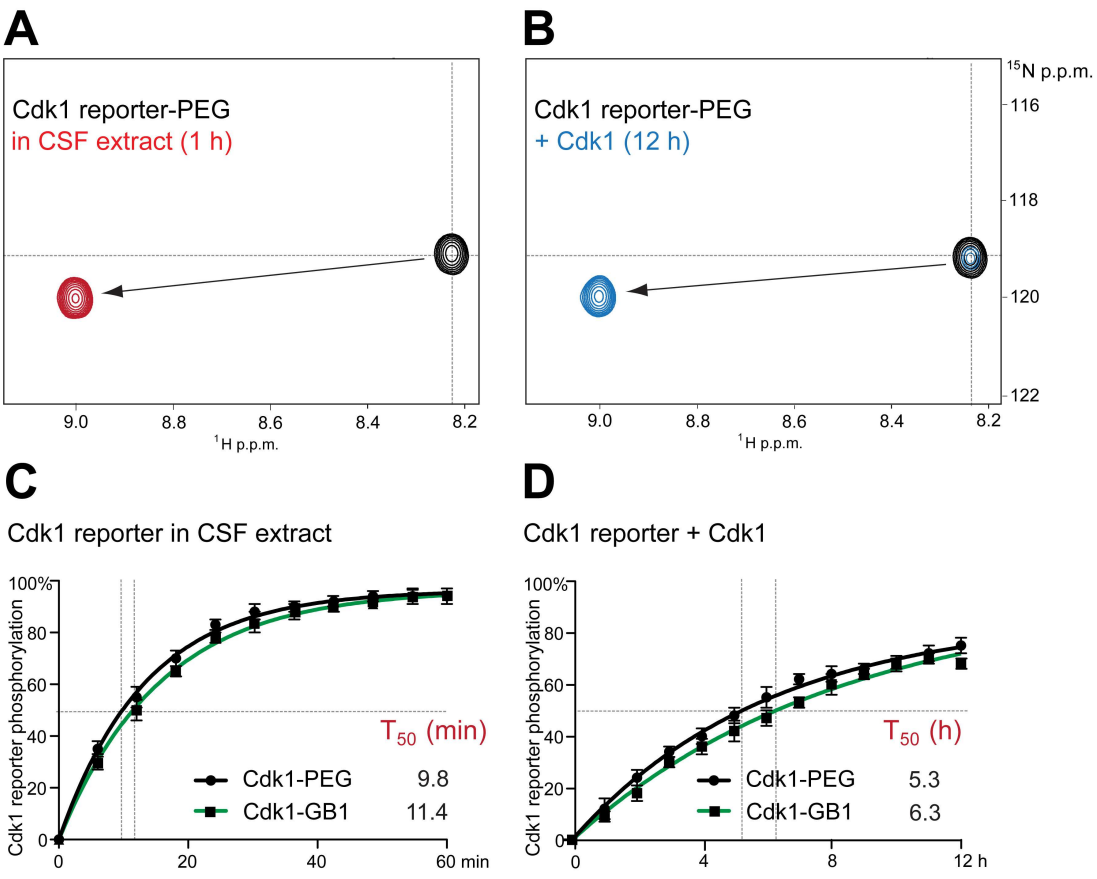

Figure 26. 2D ^{1}H-^{15}N NMR signals and phosphorylation efficiencies of the Cdk1 reporter. A) Overlay of 2D ^{1}H-^{15}N NMR spectra of the TentaGel-PEGylated Cdk1 reporter in CSF extracts at t=0 (black) and at t=1 h (red). B) Overlay of 2D ^{1}H-^{15}N NMR spectra of the TentaGel-PEGylated Cdk1 reporter with 50 U of Cdk1 at t=0 (black) and at t=12 h (blue). C) Modification curves of the TentaGel-PEGylated Cdk1 reporter (black) and Cdk1 reporter-GB1 (green) in CSF extracts. D) Modification curves of the TentaGel-PEGylated Cdk1 reporter (black) and Cdk1 reporter-GB1 (green) with 50 U of Cdk1. All reactions were performed with reporter concentrations of 50 µM in 300 µL at pH 7.5, 25°C.

2.3.2 PKA KAR design

The original protein kinase A (PKA) reporter sequence was derived based on the known kinase consensus motif R-R-X-S/T-θ (**1.1.6**) as LRRASLG, the so-called Kemptide according to previous study[60]. Another study suggested a different peptide substrate sequence, referred to PKAtide (RTGRRNSIG)[138]. I initially compared the phosphorylation efficiencies of both substrate species, which I cloned as recombinant GB1-fusion proteins. In addition, a poly-glycine linker was introduced in between the 'reporter' sequence and the GB1 moiety in order to reduce steric repulsion between the folded GB1 domain and the incoming kinase (i.e. LRRASLGGGGG-GB1 and RTGRRNSIGGGGG-GB1).

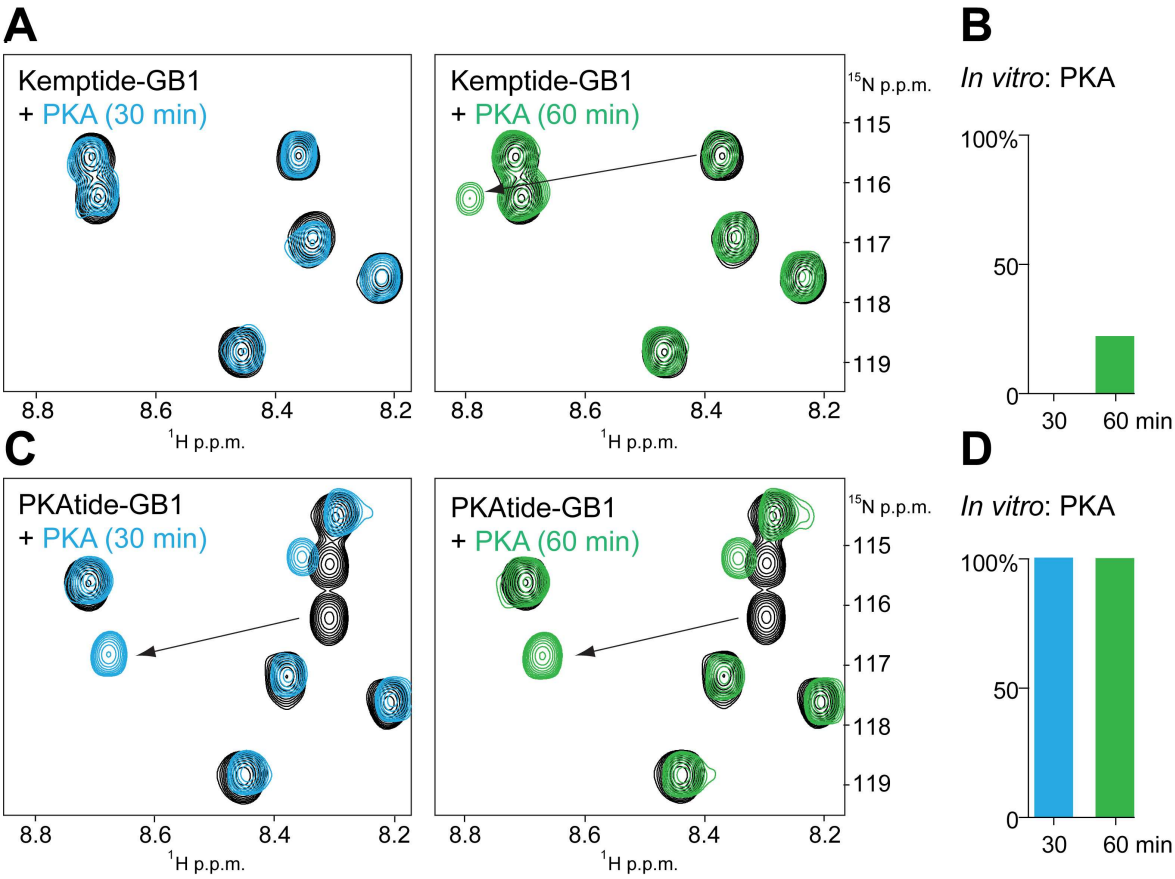

Figure 27. *In vitro* Phosphorylation efficiency tests using Kemptide-GB1 and PKAtide-GB1 constructs (500 U of PKA). A) Overlay of 2D ^{1}H-^{15}N NMR spectra of uniformly ^{15}N isotope-labeled Kemptide-GB1 *in vitro* at t=0 (black), at t=30 min (blue) and at t=60 min (green). B) Bar graphs of Kemptide-GB1 phosphorylation efficiencies. C) Overlay of 2D ^{1}H-^{15}N NMR spectra of PKAtide-GB1 *in vitro* at t=0 (black), at t=30 min (blue) and at t=60 min (green). D) Bar graphs of PKAtide-GB1 phosphorylation efficiencies. All reactions were performed with reporter-GB1 concentrations of 50 µM in 300 µL at pH 6.4, 25°C.

In vitro phosphorylation of Kemptide-GB1 using 500 U of PKA was low (**Fig. 27A, B**). In contrast, under the same experimental conditions, phosphorylation of PKAtide-GB1 was efficiently complete within 30 min (**Fig. 27C, D**). Therefore, I chose the PKAtide sequence as the optimal PKA reporter.

PKA is a holoenzyme that is composed of two inhibitory subunits and two catalytic subunits (**1.1.5**). Cellular cAMP is required for kinase activation via binding to the regulatory subunits. cAMP binding results in the dissociation of the regulatory and catalytic subunits, which constitutes the kinase activation process. Commercial PKA contains only the catalytic subunits so that activation of the kinase does not require cAMP *in vitro*[53]. However, cellular PKA is regulated by the inhibitory regulatory subunits and kinase activation depends on cellular pools of cAMP[26]. Upon progesterone stimulation during oocyte to egg maturation, adenylate cyclase activity is downregulated, which leads to a decrease in cAMP production. As a result, cellular PKA is inactive in metaphase-arrested CSF extracts[139]. To assess the cellular phosphorylation efficiencies of Kemptide-GB1 and PKAtide-GB1, CSF extracts were supplemented with 3 mM of exogenous cAMP prior to performing NMR measurements. Phosphorylation of the Kemptide-GB1 (54 %) and PKAtide-GB1 (100 %) was observed under these conditions in CSF extracts (**Fig. 28A, B, C**). These results further confirmed that the PKAtide sequence constituted

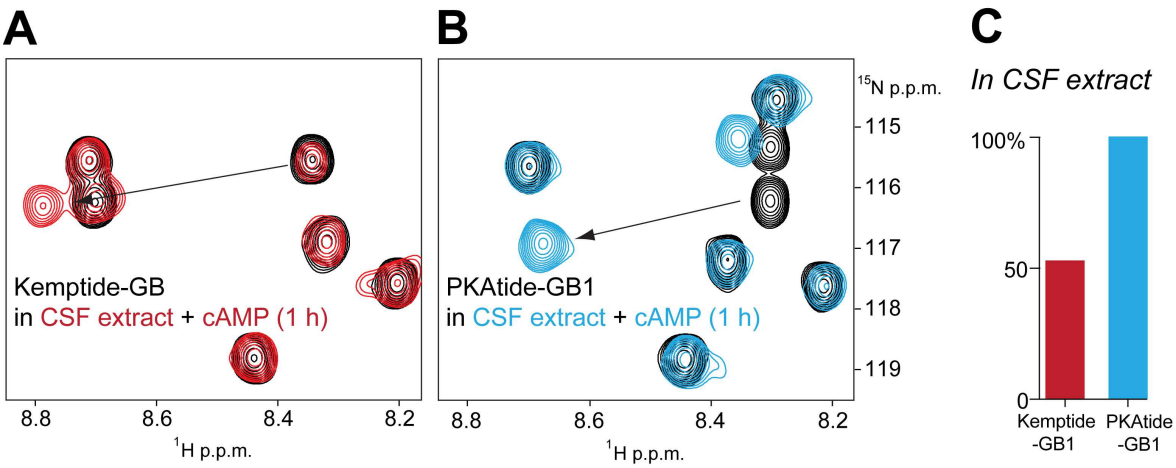

Figure 28. Phosphorylation efficiency tests of Kemptide-GB1 and PKAtide-GB1 constructs in CSF extracts. A) Overlay of 2D ^{1}H-^{15}N NMR spectra of Kemptide-GB1 in CSF extracts (3 mM cAMP) at t=0 (black) and at t=1 h (red). B) Overlay of 2D ^{1}H-^{15}N NMR spectra of PKAtide-GB1 in CSF extracts (3 mM cAMP) at t=0 (black) and at t=1 h (blue). C) Bar graphs of Kemptide-GB1 (red) and PKAtide-GB1 (blue) phosphorylation efficiencies after 1 h of CSF extract incubation. All reactions were performed with reporter-GB1 concentrations of 50 µM in 300 µL at pH 6.4, 25°C.

preferred substrate motif for cellular kinase (s). Furthermore, I conducted control reactions of in CSF extract experiments in the absence of exogenous cAMP and checked cross-reactivity of the PKA reporter with other kinases, which I will demonstrate the experimental details in section **2.4.2.1**.

2.3.3 PDK1 KAR design

3-Phosphoinositide-dependent kinase (PDK1) is the master kinase of the Protein kinase A, protein kinase G and protein kinase C (AGC) kinase family, because it phosphorylates and, thus, activates a large number of other kinases including Akt, PKA, and Rsk[14]. PDK1 was reported to phosphorylate a peptide substrate termed Aktide (i.e. KDGATMKTFCGTPEY); this sequence was derived from residues 301-315 of human Akt[140,141]. In a first step, I generated recombinant Aktide-GB1 and tested its modification *in vitro* and in CSF extract (**Fig. 29A, B**). No phosphorylation was detected in both reactions. Also a C-terminally extended version of Aktide (i.e. KDGATMKT FCGTPEYLAPE) failed to report phosphorylation by PDK1 (**Fig. 29C, D**).

By studying remote sequence homologies between different PDK1 protein substrates, a C-terminal PDK1-interacting fragment (PIF) was discovered[65]. PIF represents a conserved FXXF motif that is required for PDK1 docking and plays a key role in PDK1-substrate recognition. The phosphorylation rate of a PIF-containing version of Aktide, called PDKtide, is 100-fold higher than that of original peptide[65]. PDKtide consists of 20 amino acids of human Akt, 301-KDGATMKTFCGTPEYLAPEV-321, and 24 residues of protein kinase C-related kinase 2 (PRK2), 962-REPRILSEEEQEMFRDFDYIADWC-984. I generated a GB1-fused version of PDKtide and tested its phosphorylation efficiency *in vitro* and in CSF extracts. PDKtide-GB1 was efficiently phosphorylated with 500 U of PDK1 *in vitro* (**Fig. 29E**). Additionally, PDKtide-GB1 was ~40% phosphorylated by endogenous kinase(s) in CSF extracts (**Fig. 29F**).

The PDKtide sequence, 1- KDGATMK^{8}TFCG^{12}TPEYLAPEVRREPRIL^{28}SEEEQEMFR DFDYIADWC-39, contains more than one phosphorylation site. Other sites may therefore be phosphorylated by other kinases in cellular mixtures. Thr12 of PDKtide contains a proline residue at the P+1 position, which may serve as a consensus motif for proline-directed protein kinases such as Cdk1 (**1.1.6**). I found out that Thr12 did not get modified by Cdk1 *in vitro* (**Fig. 30A**). Ser28 of PDKtide could further function as a CK2

phosphorylation site, in agreement with previous knowledge about CK2 consensus motifs bearing the invariant S/T-X-X-E/D sequence[137] (**2.3.1**). However, PDKtide-GB1 was not phosphorylated by recombinant CK2 *in vitro* (**Fig. 30B**). Furthermore, no reports implicate Thr8 phosphorylation of human Akt by a kinase other than PDK1[140-143]. Together, these results suggested that the PDKtide sequence motif was highly specific for PDK1 and phosphorylation of this sequence in CSF extracts implied that cellular PDK1 was present and active.

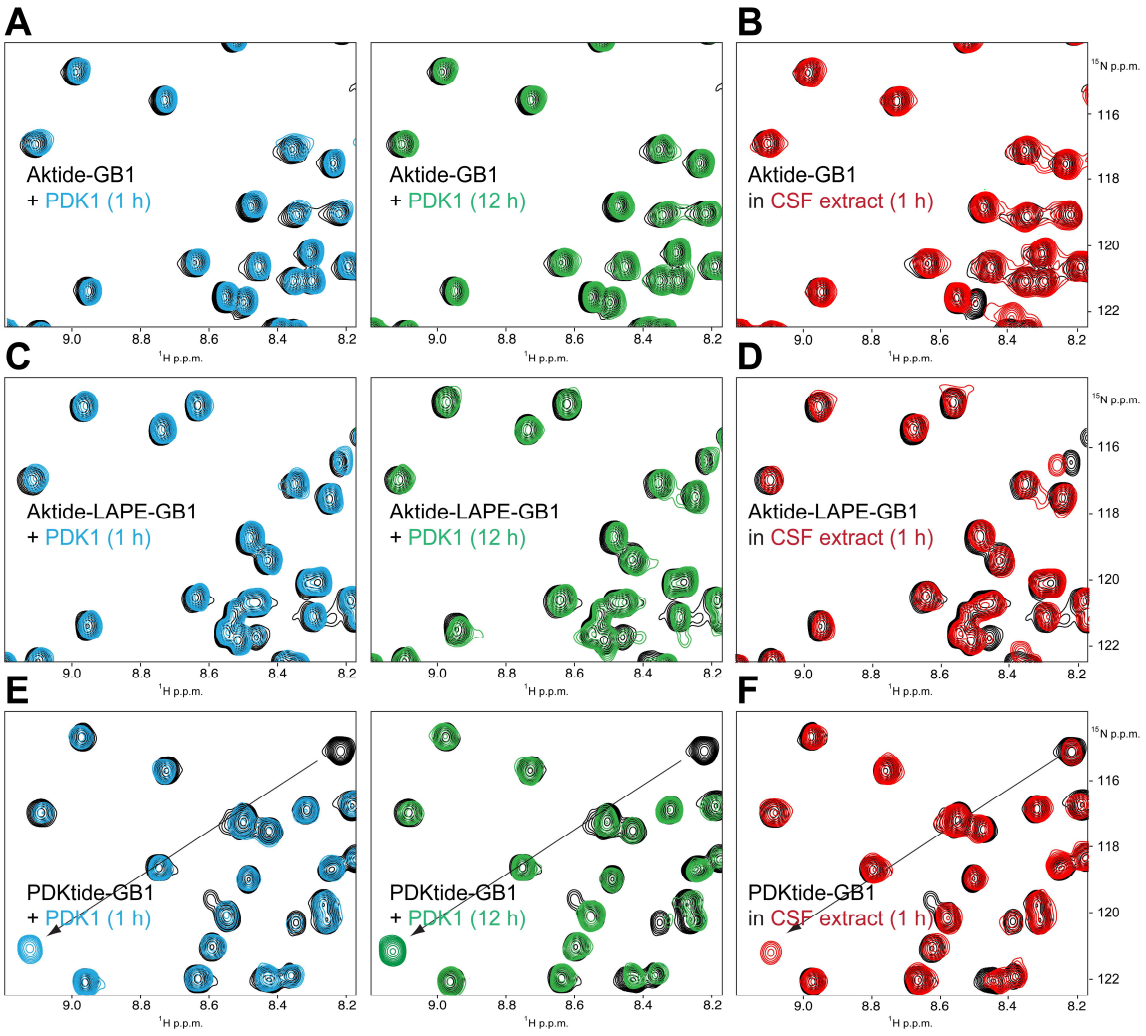

Figure 29. Optimization of PDK1 KAR sequences. A) *In vitro* phosphorylation of Aktide-GB1 with 500 U of PDK1 and its cofactor at t=0 (black), t=1 h (blue) and t=12 h (green). B) Phosphorylation of Aktide-GB1 in CSF extract at t=0 (black) and at 1 h (red). C) *In vitro* phosphorylation of recombinant Aktide-LAPE-GB1 with 500 U of PDK1 and its cofactor at t=0 (black), t=1 h (blue) and t=12 h (green). D) Phosphorylation of Aktide-LAPE-GB1 in CSF extract at t=0 (black) and at t=1 h (red). E) *In vitro* phosphorylation of recombinant PDKtide-GB1 with 500 U of PDK1 and its cofactor at t=0 (black), t=1 h (blue) and t=12 h (green). F) Phosphorylation of PDKtide-GB1 (black) in CSF extract at t=1 h (red). All reactions were performed with reporter concentrations of 50 µM in 300 µL, at pH 6.4, 25°C.

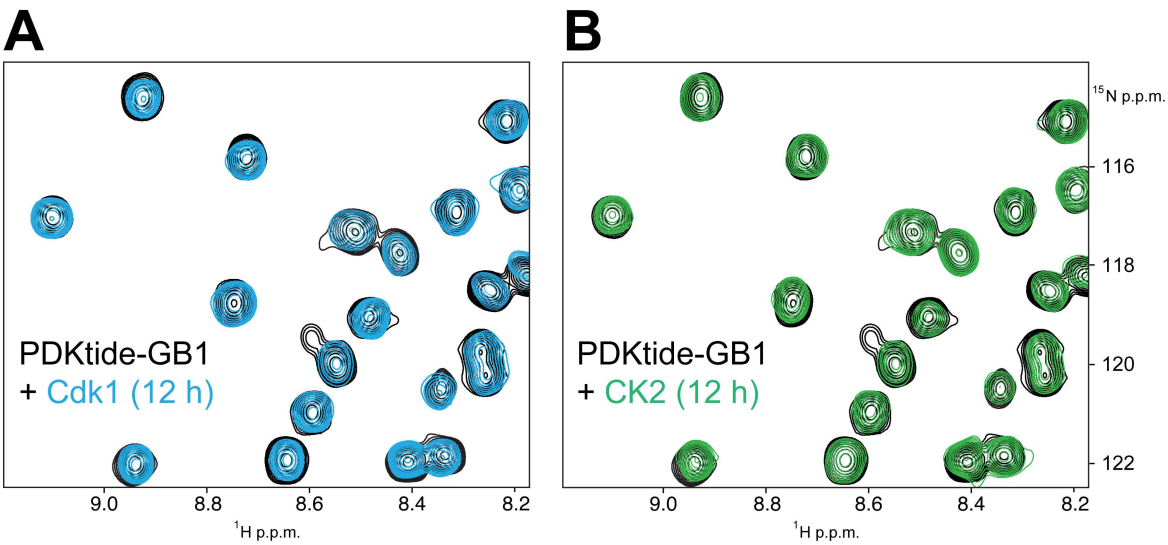

Figure 30. Cross-reactivity tests of the PDKtide-GB1 reporter. A) Overlay of 2D ^{1}H-^{15}N NMR spectra of recombinant PDKtide-GB1 with 50 U of Cdk1 at t=0 (black) and t=12 h (blue). B) Overlay of 2D ^{1}H-^{15}N NMR spectra of recombinant PDKtide-GB1 with 500 U of CK2 at t=0 (black) and t=12 h (green). All reactions were performed with reporter-GB1 concentrations of 50 µM in 300 µL at pH 6.4, 25°C.

2.3.4 CK1 KAR design

The first determined substrate sequence for casein kinase 1 (CK1) was the casein protein itself[144]. However, casein turned out to be a poor CK1 substrate[64] and is therefore not generally used in CK1 activity assays. Many studies have attempted to optimize the CK1 substrate sequence in terms of increasing kinase specificity. I initially chose three known CK1 substrate motifs and compared their phosphorylation efficiencies by CK1. The first sequence, RRKDLHDDEEDEAMSITA, was selected based on an acidic cluster N-terminal to the phosphorylation site, which is known to act as a CK1 specificity determinant[64]. The CK1 consensus sequence is D/E-D/E-D/E-D/E-X-X-S/T. This CK1 peptide was determined to exhibit a V_{max} that is 6-times higher than that of the casein protein[64]. The second sequence, DDDDVASLPGLRRR was chosen because it also contained a cluster of aspartatic acid residues N-terminal to the canonical phosphorylation site, and has been previously characterized as a CK1 substrate[145]. The third sequence, KRRRAIpSVASLPGL has been derived from the N-terminal part of rabbit muscle glycogen synthase (1-PLSRTLp^{7}SVS^{10}SLPGL-14)[146], in which pSer7 presents a priming

phospho-site that is required for CK1 phosphorylation at Ser10. This sequence contains the alternative CK1 consensus motif, pS/pT-X-X-S/T[145,146].

Uniformly ^{15}N isotope-labeled CK1 reporter-GB1 proteins were expressed in *E. coli* and purified. The CK1 reporter-GB1 from the first CK1 substrate sequence was called CK1 reporter-GB1 (A), whereas sequence 2 reporter-GB1 was referred to as CK1 reporter-GB1 (B). The phospho-primed version of the CK1 KAR was not obtained by recombinant protein expression, but synthesized by SPPS using Fmoc-Ser(PO(OBZL)OH)-OH

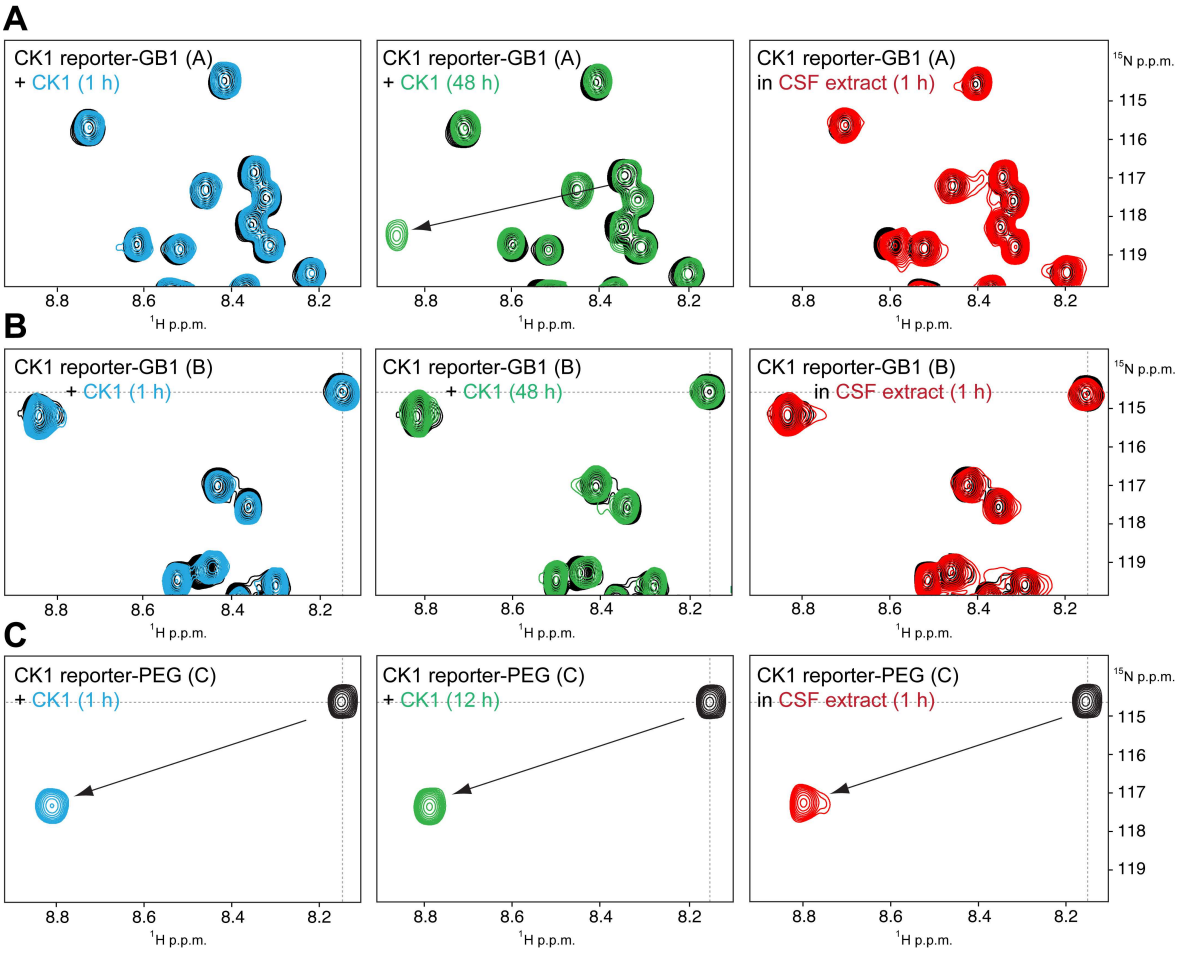

Figure 31. Phosphorylation efficiencies of the three different CK1 substrates. A) Phosphorylation of recombinant CK1 reporter-GB1 (A) at t=0 (black), at t=1 h (*in vitro,* blue) and at t=48 h (*in vitro*, green) and in CSF extract at t=1 h (red). B) Phosphorylation of recombinant CK1 reporter-GB1 (B) at t=0 (black), at t=1 h (*in vitro*, blue) and at t=48 h (*in vitro*, green) and in CSF extracts at t=1 h (red*). C) Phosphorylation of the synthetic CK1 reporter-PEG (C) at t=0 (black), at t=1 h (*in vitro*, blue) and at t=48 h (*in vitro*, green) and in CSF extracts at t=1 h (red*). All reactions were performed with concentrations of the reporters of 50 µM at pH 7.5, 25°C. The *in vitro* phosphorylation setups were with 500 U of CK1.

(Novabiochem) as the starting building-block for Ser7 incorporation and named CK1 reporter-PEG (C).

CK1 reporter-GB1 (A) showed no phosphorylation when reacted with 500 U of CK1 (**Fig. 31A**). After 48 h, only 30% of CK1 reporter-GB1 was phosphorylated *in vitro*. No phosphorylation was observed in CSF extracts. CK1 reporter-GB1 (B) was not phosphorylated *in vitro,* or in CSF extract under the same experimental conditions (**Fig. 31B**). Partial phosphorylation of CK1 reporter-GB1 (A) suggested that acidic amino acids N-terminal to the phosphorylation site were important for CK1 activity. Notably, CK1 reporter-PEG (C) was fully phosphorylated within 1 h in the *in vitro* reaction and also efficiently phosphorylated in CSF extract (**Fig. 31C**). Thus, the CK1 reporter-PEG (C) construct was the best CK1 substrate amongst all the tested reporters. These results are in agreement with Flotow *et al* work, which described the requirement for a phosphoserine at the P-3 position as the preferred recognition site for CK1[145]. Since the motif pS/pT-X-X-S/T motif is unique for CK1, I assumed that this reporter would not exhibit cross-reactivity with any other kinase.

2.3.5 Plk1 KAR design

The Plk1 reporter sequence was derived from a fragment of the membrane-associated tyrosine- and threonine-specific cdc2-inhibitory kinase (Myt), i.e. residues 419-HLGES[424]SFSSDWDDESLG-435[124]. Plk1 phosphorylates Ser424 according to its consensus motif D/E-X-S/T-θ-X_{1-2}-D/E[124]. Whereas the serine resonances of uniformly ^{15}N isotope-labeled Plk1 reporter-GB1 are overlapped in the corresponding 2D ^{1}H-^{15}N NMR spectra, only one NMR signal displayed the characteristic chemical shift change upon Plk1 phosphorylation *in vitro* and in CSF extract (**Fig. 32A, B**). This indicated that only one serine was phosphorylated. When the peptide-based reporter was synthesized and Ser424 was incorporated in a site-selective ^{15}N isotope-labeled manner, phosphorylation by Plk1 *in vitro* and also in CSF extract confirmed the canonical Plk1 substrate site (**Fig. 32A, C, D** dashed lines). Because the Plk1 consensus motif is unique amongst other kinases (**Table 2**), modification of Ser424 indicated cellular Plk1 activity. Although recent work has considerably broadened the consensus sequence for Plk1 site (i.e. L/θ-E/N/D-X-S/T-L/θ)[147], the tested Plk1 reporter is still practical for evaluating cellular Plk1 activity..

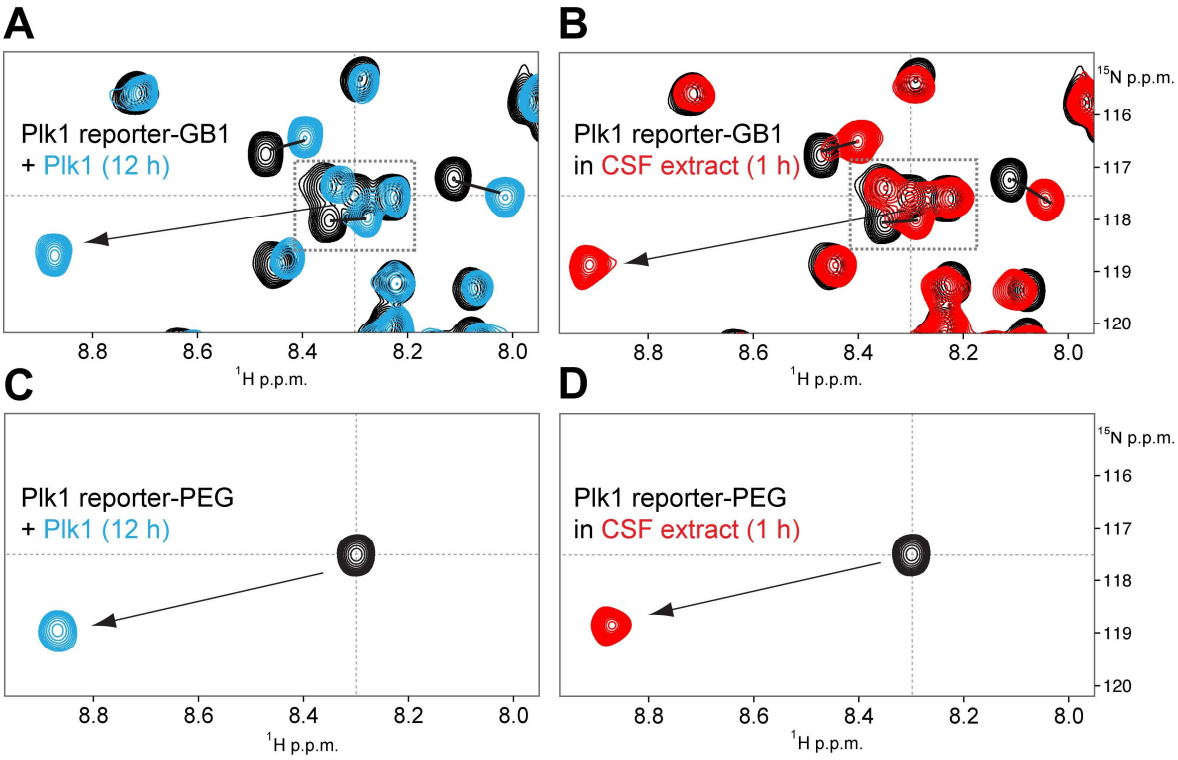

Figure 32. Phosphorylation of the Plk1 reporter. A) *In vitro* phosphorylation of uniformly ^{15}N isotope-labeled Plk1 reporter-GB1 at t=0 (black) and at t=12 h (blue). B) Phosphorylation in CSF extract at t=0 (black) and at t=1 h (red). C) *In vitro* phosphorylation and residue-specific assignment of ^{15}N isotope-labeled Plk1 peptide reporter at t=0 (black) and at t=12 h (blue). D) Phosphorylation of peptide Plk reporter in CSF extract at t=0 (black) and at t=1 h (red). All reactions were performed with reporter concentrations of 50 µM at pH 7.5, 25°C. *In vitro* phosphorylation setups were with 50 U of Plk1.

2.3.6 Rsk2 KAR design

The p90 ribosomal protein S6 kinase 2 (Rsk2) reporter was designed based on the C-terminal portion of the human 40S ribosomal protein S6 (rS6). This region of the protein (i.e. 228-IAKRRRL^{235}S^{236}SLRA^{240}STSK^{244}SES^{247}SQK-249) contains several substrate sites for the Rsk family of kinases[148,149]. Rsk kinases play important roles in meiotic cell cycle progression, especially also during *Xenopus* oocyte to egg maturation[29]. Two isoforms of Rsk, Rsk1 and Rsk2, are present in metaphase-arrested CSF extracts and Rsk2 is highly abundant[104]. Because Ser236 and Ser235 of rS6 are potential Rsk2 phosphorylation sites[148,150], I initially designed a Rsk2 reporter that only contained these two phosphorylatable serine residues (228-IAKRRRL^{235}S^{236}SLRA-239)[151].

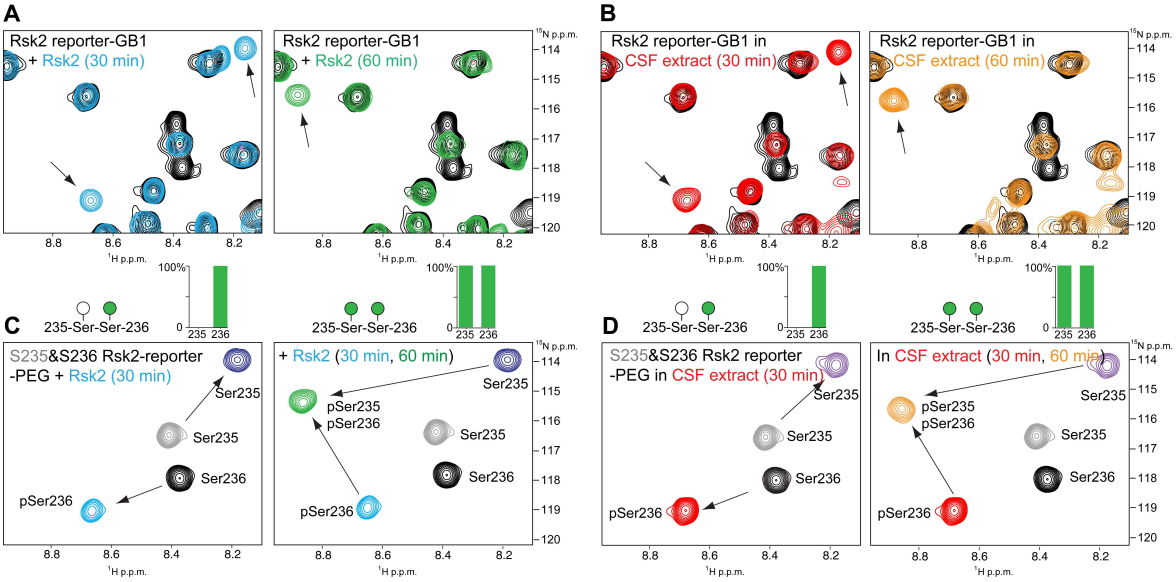

Figure 33. Step-wise phosphorylation of the Rsk2 reporter. A) *In vitro* phosphorylation of uniformly ^{15}N isotope-labeled Rsk2 reporter-GB1 at t=0 min (black), at t=30 min (blue) and at t=60 min (green). B) Phosphorylation in CSF extract at t=0 min (black), at t=30 min (red) and at t=60 min (orange). C) *In vitro* phosphorylation of S235-Rsk2 reporter-PEG and S236-Rsk2 reporter-PEG. 2D ^{1}H-^{15}N NMR spectra of S235-Rsk2 reporter-PEG are shown in grey, dark blue and green and correspond to t=0 min, t=30 min and t=60 min, respectively. NMR spectra of S236-Rsk2 reporter-PEG are superimposed and shown in black, blue and green, corresponding to t=0 min, t=30 min and t=60 min, respectively. D) Phosphorylation in CSF extract of S235- and S236-Rsk2 reporter-PEG. 2D ^{1}H-^{15}N NMR spectra of S235-Rsk2 reporter-PEG are shown in grey, violet and orange, corresponding to t=0 min, t=30 min and t=60 min, respectively. Spectra of S236-Rsk2 reporter-PEG are shown in black, red and orange, corresponding to t=0 min, t=30 min and t=60 min, respectively. All reactions were performed with reporter concentrations of 50 µM at pH 7.5, 25°C. *In vitro* reaction setups were with 500 U of Rsk2.

Uniformly ^{15}N isotope-labeled Rsk2 KAR-GB1 was expressed, purified and tested in an *in vitro* reaction with 500 U of Rsk2 (**Fig. 33A**). I observed the disappearance of two NMR signals from the non-phosphorylated serine region of the 2D ^{1}H-^{15}N NMR spectrum (**Fig. 33A**, left panel). At the same time, two new NMR signals were detected (**Fig. 33A**, left panel, black arrows). Whereas one NMR signal resonated in the characteristic phospho-serine region of the spectrum (δ (^{1}H/^{15}N)=8.69/119.1 p.p.m.) and the position of the other one did not indicate a phosphorylation event (δ (^{1}H/^{15}N)=8.18/114.0 p.p.m.). After 1 h, both new NMR signals disappeared and a single new NMR resonance cross peak was detected (δ (^{1}H/^{15}N)=8.91/115.7 p.p.m.) (**Fig. 33A**, right panel, black arrow). The same phosphorylation behavior was observed in CSF extracts (**Fig. 33B**). Altogether, the

observations indicated a stepwise modification cascade that affected Ser235 and Ser236 in a sequential fashion. To resolve the underlying nature of this behavior, I synthesized two Rsk2 reporter peptides. One was individually ^{15}N isotope-labeled at Ser 235, termed S235-Rsk2 reporter-PEG, the other one at Ser236, called S236-Rsk2 reporter-PEG. Monitoring the individual NMR signals of S235- and S236-Rsk2 reporter-PEG peptides in *in vitro* reactions with recombinant Rsk2 revealed a step-wise phosphorylation behavior (**Fig 33C**). Rsk2 phosphorylated Ser236 first (**Fig. 33C**, left panel). This modification also induced a chemical shift change of neighboring Ser235. Once Rsk2 phosphorylated all substrate molecules at Ser236, the kinase modified Ser235, which gave rise to the single, new NMR signal. Thus, the results implied that the two phosphorylated serine residues pSer235 and pSer236, once present on the same substrate molecule, resonated at exactly the same resonance frequency (**Fig. 33C**, right panel). This step-wise phosphorylation behavior of Ser236 and Ser235 of Rsk2 reporter was similarly detected in CSF extracts (**Fig. 33D**).

Rsk2 belongs to arginine/lysine directed family of protein kinases and shares a common consensus motif with other members of the family. Hence, extended cross-reactivity tests were performed, the results of which are outlined in section **2.4.2.2**.

2.3.7 PKB/Akt KAR design

The first PKB/Akt reporter was directly derived from human Raf-1 (250-SQRQRST^{257}STPNVH-262), in which Ser257 constitutes the canonical PKB/Akt phosphorylation site[122,125]. This reporter sequence also corresponds to the Akt consensus motif R-X-R-X-X-S/T-θ. The uniformly ^{15}N isotope-labeled recombinant Akt reporter-GB1 was expressed and purified. Its phosphorylation was detected in CSF extracts, but not *in vitro* using 500 U of recombinant Akt kinase (**Fig. 34A**). This discrepancy may be explained by the fact that Akt required physiological settings to modify its substrate site, or that one of the five serines and threonines of the reporter, i.e. Ser250, Ser255, Thr256, Ser257, or Thr258 was phosphorylated by other cellular kinase(s) in the CSF extracts.

To properly interpret these results, I synthesized the Akt reporter-PEG reporter specifically ^{15}N isotope-labeled at position Ser257. Superposition of 2D ^{1}H-^{15}N NMR spectra of recombinant, uniformly labeled Akt reporter-GB1 and Akt reporter-PEG revealed that the phosphorylated amino acid was not Ser257 (**Fig. 34B**). Upon in CSF extract phosphorylation, the NMR signal of Akt reporter-GB1 at δ (^{1}H/^{15}N)=8.52/117.4 p.p.m. disappeared, which is in the serine region of the spectrum. Altogether, the results suggested that one of the remaining serines, Ser250 or Ser255 could be targeted by endogenous kinases in CSF extracts. The reporter sequence also contained a partial Rsk2 consensus motif (R/K-X-R-X-X-S/T-θ)[59] and so phosphorylation of Ser255 by Rsk2 could be a possible explanation for the observed modification behavior. *In vitro* phosphorylation of the Akt KAR-GB1 construct with 500 U of Rsk2 confirmed this hypothesis (**Fig. 34C**).

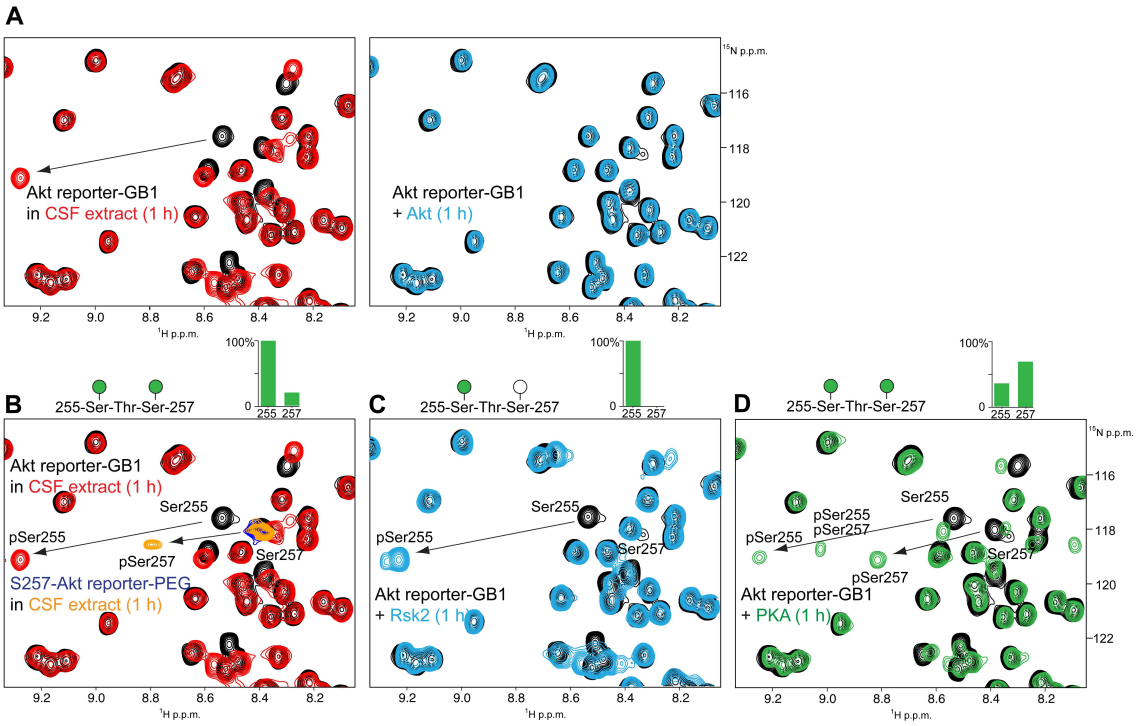

Figure 34. Phosphorylation of the proposed Akt reporter. A) Overlay of 2D ^{1}H-^{15}N NMR spectra of uniformly ^{15}N isotope-labeled Akt reporter-GB1 in CSF extract at t=0 (black), at t=1 h (red) (left panel) and *in vitro* with 500 U of Akt at t=0 (black) and at t=1 h (blue). B) Phosphorylation of Akt reporters in CSF extracts. Overlay of 2D ^{1}H-^{15}N NMR spectra of uniformly ^{15}N isotope-labeled Akt KAR-GB1 at t=0 (black), at t=1 h (red) and site-selective ^{15}N-labeled Ser257-KAR-PEG at t=0 (blue) and at t=1 h (orange). C) Phosphorylation of recombinant Akt reporter-GB1 at Ser255 with 500 U of Rsk2 at t=0 (black) and at t=1 h (blue). D) Phosphorylation of recombinant Akt reporter-GB1 at Ser255 and Ser257 with 500 U of PKA at t=0 (black) and at t=1 (green). All reactions were performed at reporter concentrations of 50 µM, 300 µL at pH 7.5, 25°C.

I also reacted Akt reporter-GB1 with 500 U of PKA, whose consensus motif R-R-X-S/T-θ is rather similar to the one of Rsk2 and Akt. 40% of Ser255 and 70% of Ser257 were efficiently phosphorylated by PKA *in vitro* (**Fig. 34D**). Together, this indicated that substantial cross-reactivity of the Akt reporter with Rsk2 and PKA existed. All of these results suggested that the original Akt reporter was not suitable for selectively studying cellular Akt activity.

Amongst the many Akt substrate studies[152-157], one set out to identify Akt substrate specificity determinants[152]. The peptide sequence RPRAATF was reported to exhibit the lowest Rsk2 cross-reactivity[152]. Whereas the serine to threonine mutation was reported to improve Akt specificity, it slightly decreased overall phosphorylation efficiency[152]. I generated a new recombinant Akt reporter-GB1 construct that I tested for Akt phosphorylation *in vitro* and in CSF extract. However, this reporter was not phosphorylated under any of the tested conditions (**Fig. 35**). Since Akt shares consensus sequence with Rsk2 and PKA and generating highly specific Akt reporter was not successful, I decided to stop investigating this reporter sequence.

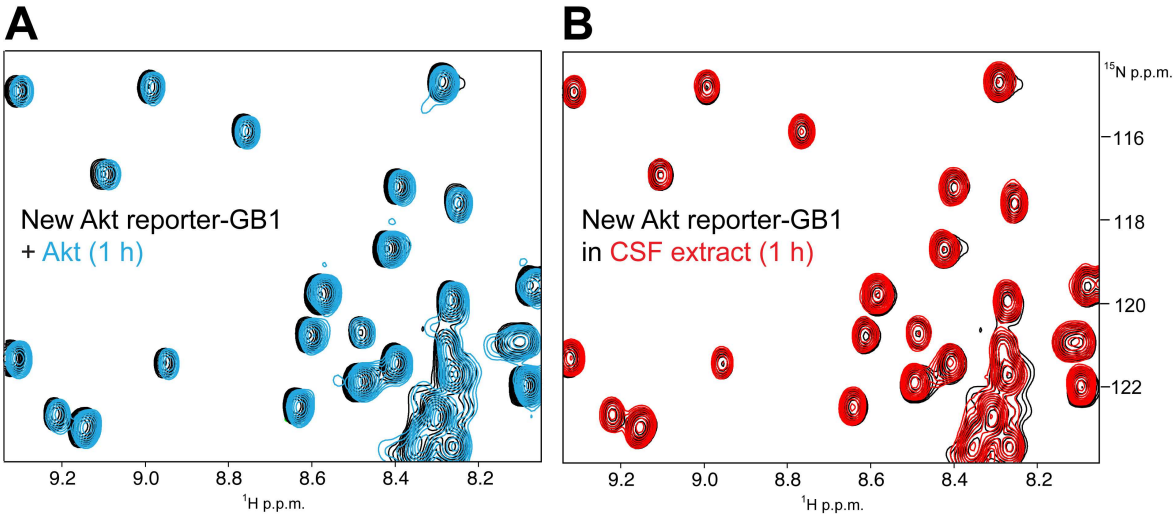

Figure 35. Phosphorylation of a new Akt KAR-GB1 construct. A) Overlay of 2D ^{1}H-^{15}N NMR spectra of uniformly ^{15}N-labeled Akt reporter-GB1 *in vitro* reacted with 500 U of Akt at t=0 (black) and at t=1 h (blue). B) Overlay of 2D ^{1}H-^{15}N NMR spectra of Akt reporter-GB1 in CSF extract, at t=0 (black) and at t=1 h (red). All reactions were performed at reporter concentrations of 50 µM at pH 7.5, 25°C.

2.4 Analyzing KAR cross-reactivity

After optimizing KAR sequences and identifying KAR phosphorylation sites, I set out to thoroughly investigate the range of KAR cross-reactivities, especially with kinases that share similar consensus site motifs. In the following, I outline three different examples for KAR cross-reactivity tests. I also demonstrate how substantial KAR cross-reactivity was eventually resolved in one particular case.

2.4.1 p42MAPK/Cdk1 KAR cross-reactivities

In a first instance, I focused on the cross-reactivities of proline-directed KARs that I designed for Cdk1 and p42MAPK readouts. The minimal consenus motifs for both kinases require an invariant proline at the position P+1. The Cdk1 reporter sequence (i.e. GQARTPPKKKRKV) was optimized as described in section **2.3.1**. The p42MAPK reporter sequence (i.e. YAPRSPAKLAKFQFPA) was based on a MAPK substrate study[66]. 50 U of Cdk1 phosphorylated the individual Cdk1 and p42MAPK TentaGel-PEGylated KARs with a T_{50} of 10.9 h and 12.0 h, respectively (**Fig. 36A**). In a mixed, competitive reaction setup with both KARs present in the same reaction, 50 U of Cdk1 preferentially phosphorylated the Cdk1 KAR, although modification of the p42MAPK KAR was detected as well (**Fig. 36B**). In this reaction mixture, phosphorylation of the Cdk1 reporter was about 2-fold more efficient than that of the p42MAPK reporter (**Fig. 36B**). Hence, strong cross-reactivity existed between Cdk1 and p42MAPK reporters. Arginine, or lysine residues at the P+3 position are critically required for Cdk1 recognition[123] (**2.3.1**). In the original KAR construct, the p42MAPK sequence also contained a lysine residue at this position (**Fig. 36D**). It therefore became evident that this residue significantly contributed to the cross-reactivity behavior. Upon mutation of Lys392 of the p42MAPK KAR to alanine (i.e. GYAPRSPAALAKFQFPA), cross-reactivity with Cdk1 was efficiently abolished (**Fig. 36C**). In addition, the optimized p42MAPK reporter (K392A) slightly improved its *in vitro* phosphorylation efficiency with p42MAPK (**Fig. 36E**). Therefore, the optimized p42MAPK KAR was now able to properly discriminate between cellular p42MAPK and Cdk1 activities.

In addition to the proline at the P+1 position, a second proline at the P-2 position is equally important for recognition by p42MAPK (P-X-S/T-P). Also p42MAPK additionally

requires a distal DEF site (F/Y-X-F/Y-P) at downstream of P-site for kinase-substrate specificity[66] (see **1.1.7**). Neither the second proline nor DEF site was present in the Cdk1 reporter. Consistently, the Cdk1 KAR was not phosphorylated by p42MAPK (**Fig. 36F**). Based on these results, I concluded that the Cdk1 and optimized p42MAPK KARs exclusively conveyed their respective cellular kinase activities.

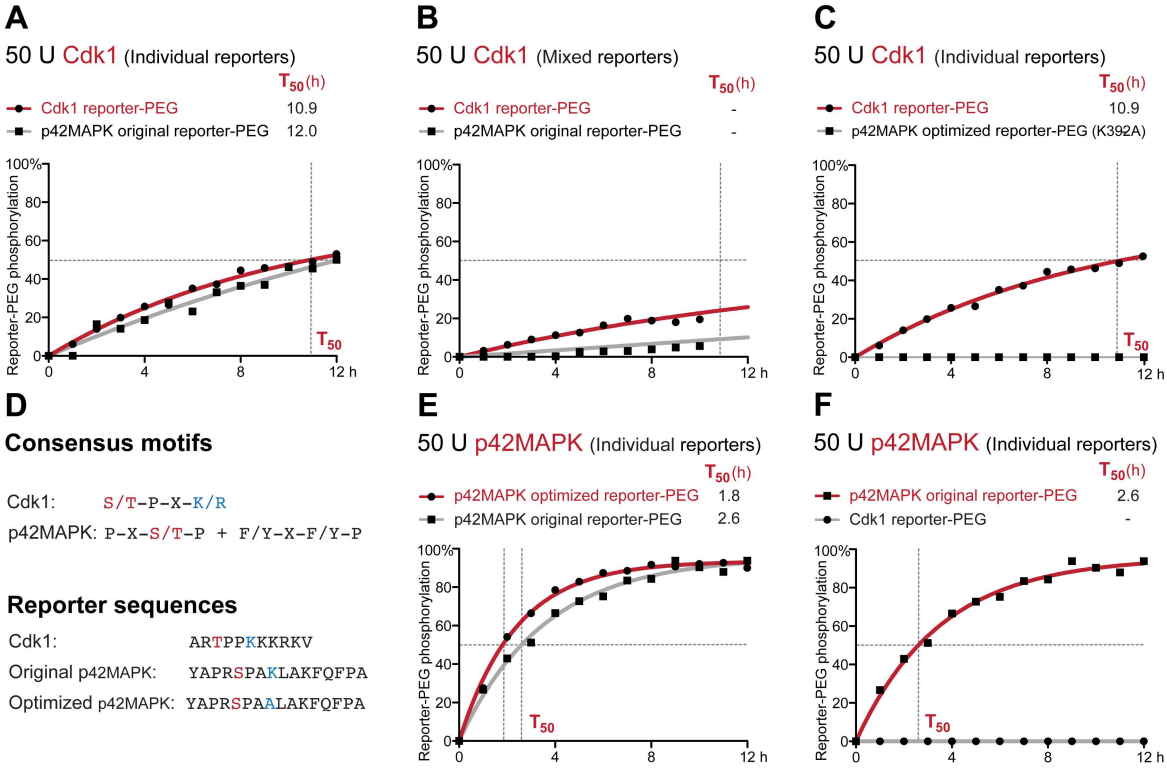

Figure 36. Cross-reactivities of proline-directed Cdk1 and p42MAPK reporters. A) Phosphorylation curves of individual Cdk1 (red) and p42MAPK reporters (grey) with 50 U of Cdk1. B) Build-up curves of a reaction mixture of Cdk1 (red) and p42MAPK reporters (grey) with 50 U of Cdk1. C) Phosphorylation curves of individual Cdk1 and the optimized p42MAPK KAR (K392A) with 50 U of Cdk1. D) Consensus sequences of Cdk1 and p42MAPK and reporter sequences. E) Phosphorylation curves of original (grey) and optimized (red) p42MAPK KARs with 50 U of p42MAPK. F) Modification curves of the Cdk1 (grey) and p42MAPK (red) reporters with 50 U of p42MAPK. All reactions were performed at reporter concentrations of 50 µM at pH 7.5, 25°C.

2.4.2 Arginine/lysine directed kinase cross-reactivities

2.4.2.1 PKA/PAK1 KAR cross-reactivities

In section **2.3.2**, I reported that the PKAtide-based PKA reporter (GRTGRRNSIGGGGG-GB1) was a better substrate than the Kemptide-based KAR (GLRRASLGGGGG-GB1) and that cellular PKA activity relied on endogenous pools of cAMP, which are not present in CSF extracts. Therefore, cellular PKA is not active in CSF extracts. Despite that notion, ~30% of both types of PKA KARs were efficiently phosphorylated in CSF extracts, in the absence of exogenous cAMP (**Fig. 37A-C**). These phosphorylation behaviors indicated substantial degrees of cross-reactivities of the PKA reporters with other kinases. Consequently, I assessed the *in vitro* phosphorylation behavior of the PKAtide-based KAR in Rsk2 and p21 activated kinase 1 (PAK1) reactions. Rsk2 and PAK1 share similar consensus sequences with PKA (**Fig. 38F**). Both kinases are further involved in *Xenopus* oocyte to egg maturation[29,158]. *In vitro* phosphorylation of the PKAtide-based reporter by PKA, Rsk2 and PAK1 resulted in T_{50} values of 4.9 h, 7.3 h and >12h, respectively (**Fig. 37D**). Hence, the PKA reporter exhibited substantial cross-reactivity with Rsk2 and PAK1.

These cross-reactivity results led to further investigations of the cross-phosphorylation behavior of the PAK1 reporter with Rsk2. The PAK1 KAR (i.e. RRRLSFAEP) was derived from the PAKtide substrate, as PAK1 has an identical consensus sequence as Rsk2 (i.e. R-R-X-S/T-θ)[159]. Cross-phosphorylation was investigated in mixed reaction setups. In a first instance, PAK1-, PKA- and Rsk2 reporters were simultaneously reacted with 500 U of Rsk2. Rsk2 phosphorylated all KARs but displayed a clear preference for the Rsk2 reporter with a T_{50} value of 19.6 min (**Fig. 37E**). The PAK1 reporter was the second most preferred Rsk2 substrate with a T_{50} value of 38.0 min, whereas the PKA KAR was modified with the lowest rate and a T_{50} value of 54.1 min. Thus, the phosphorylation rate of the Rsk2 KAR in a mixed reaction setup is roughly two-fold lower than the individual reaction conditions (T_{50}=8.5 min). These results establish that the PKA and PAK1 KARs are also phosphorylated by Rsk2. Cross-reactivities of that sort would lead to false quantifications of cellular PKA and PAK1 activities in cell extracts that also contain active Rsk2. As a consequence, I omitted PKA and PAK1 reporters in CSF extract kinase activity assays.

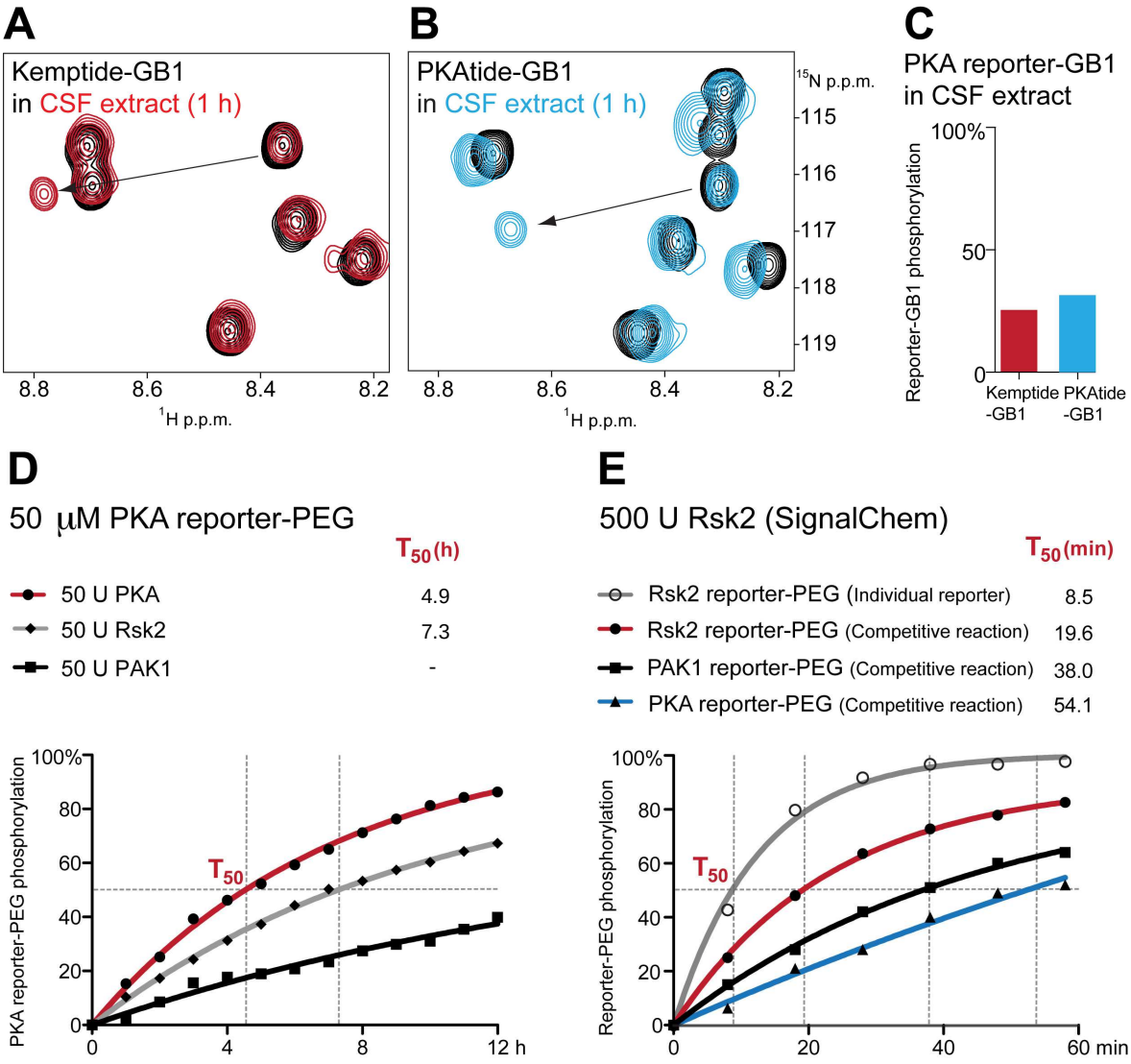

Figure 37. Cross-reactivities of reporters against arginine/lysine directed kinases. A) Overlay of 2D ^{1}H-^{15}N NMR spectra of the Kemptide-based PKA reporter-GB1 in CSF extract at t=0 (black) and at t=1 h (red). B) Overlay of 2D ^{1}H-^{15}N NMR spectra of the PKAtide-based PKA reporter-GB1 in CSF extract at t=0 (black) and at t=1 h (blue). C) Cross-reactivity quantifications of Kemptide- and PKAtide-based reporter-GB1 with other mitotic kinases in CSF extracts (red and blue, respectively). D) Phosphorylation curves of isolated reactions of the PKAtide-based PKA reporter with 50 U of Rsk2 (grey), 50 U of PKA (red) and 50 U of PAK1 (black). E) Cross-reactivities of PAK1 and PKA reporters with 500 U of Rsk2. Modification curves of a mixed reaction setup of Rsk2 (red), PAK1 (black) and PKA (blue) KARs and 500 U of Rsk2 and the modification curve of the Rsk2 KAR with 500 U of Rsk2 (grey) of the isolated reaction. All reactions were performed at reporter concentrations of 50 µM at pH 7.5, 25°C.

2.4.2.2 PKA/PAK1/Aurora B/PKB cross-reactivities with the Rsk2 KAR

Rsk2 belongs to the PKA, PKG and PKC (AGC) kinase family, which share a common consensus motif[14,59]. I had therefore investigated the range of Rsk2 reporter cross-reactivity with other known AGC kinases that play a role in meiotic cell cycle progression, such as PKA, PAK1 and PKB/Akt[26,158]. When I reacted the Rsk2 reporter-GB1 substrate with 1,000 U of PKA, NMR signals of Ser235 and Ser236 disappeared. Conversely, two new NMR signals appeared in 30 min at δ (^{1}H/^{15}N)=8.08/117.0 p.p.m. and δ (^{1}H/^{15}N)=8.95/117.1 p.p.m. and the latter signal indicated the phospho-serine (**Fig. 38A**, left panel). After 60 min, a new NMR signal appears at δ=8.85/115.6 ppm (^{1}H/^{15}N) (**Fig. 38A**, right panel). The results implied a stepwise modification of Rsk2 reporter by PKA in a manner that was highly reminiscent of the original Rsk2 kinase reaction (**Fig. 33A**). In contrast to Rsk2, PKA phosphorylated Ser235 before it modified Ser236, which constituted a different reaction mechanism than what had been observed for Rsk2. This mode of PKA action was further confirmed by *in vitro* experiments with the synthetic Rsk2 reporters (**Fig. 38B**). In contrast to PKA, PAK1, Aurora B and to a lesser extent also Akt/PKB, three other protein kinases with consensus motifs similar to Rsk2, only phosphorylated Ser235, but not S236, of the Rsk2 KAR (**Fig. 38C, D, E**).

Thus, AGC kinases and Aurora B phosphorylated the Rsk2 KAR in slightly different manners, despite having similar kinase consensus sequences (**Fig. 38F**). PKA and Rsk2 modified both substrate serines of the Rsk2 KAR, albeit in a different order. In contrast, PAK1, Aurora B and Akt phosphorylated only Ser235. Because the Rsk2 reporter was phosphorylated at Ser236 first in CSF extracts, and only later at Ser235, it is quite certain that cellular Rsk2 was causing these modifications.

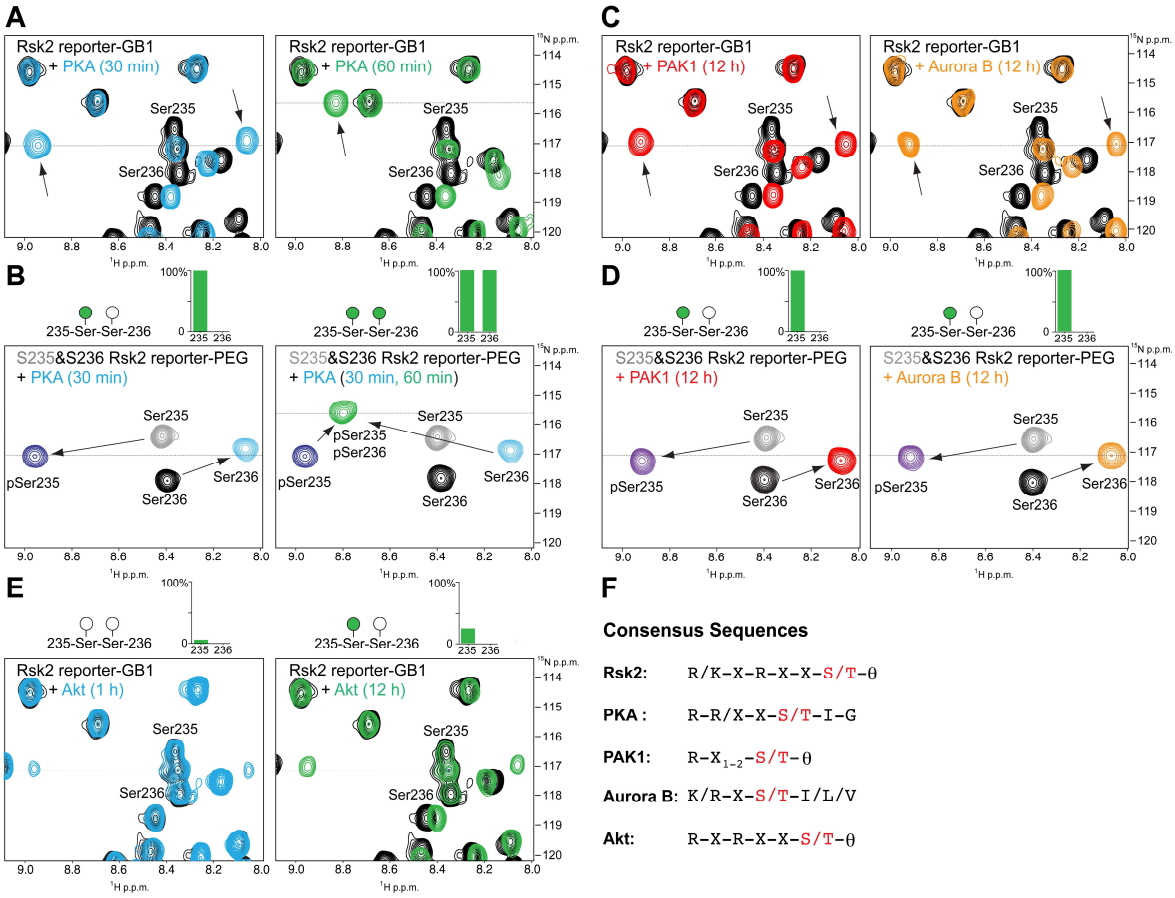

Figure 38. Cross-reactivities of the Rsk2 reporter with PKA, PAK, Aurora B and Akt/PKB. A) *In vitro* phosphorylation of uniformly ^{15}N isotope-labeled Rsk2 reporter-GB1 with 1,000 U of PKA at t=0 min (black), at t=30 min (blue) and at t=60 min (green). B) Step-wise phosphorylation of Rsk2 reporter by PKA. Overlay of 2D ^{1}H-^{15}N NMR spectra of the Rsk2 S235-reporter (grey, violet, green) and the S236-reporter (black, cyan, green) in *in vitro* reactions with 1,000 U of PKA at t=0 min, at t=30 min and at t=60 min, respectively. C) *In vitro* phosphorylation of recombinant Rsk2 reporter-GB1 with 500 U of PAK1 (left panel) and with 500 U of Aurora B (right panel), at t=0 (black) and at t=12 h (red, orange). D) *In vitro* phosphorylation of Rsk2 Ser235- and Ser236-reporter with 500 U of PAK1 (left panel) and 500 U of Aurora B (right panel). E) *In vitro* phosphorylation of recombinant Rsk2 KAR-GB1 with 500 U of Akt at t=0 min (black), at t=1 h (blue) and at t=12 h (green). All reactions were performed at reporter concentrations of 50 µM at pH 7.5, 25°C. F) Consensus sequences for arginine/lysine directed protein kinases.

2.4.2.3 Rsk2/Chk1 KAR cross-reactivities

Rsk2 KAR cross-reactivity tests were further extended to check point kinase 1 (Chk1). Chk1 has the consensus motif θ-X-R/K-X-X-S/T-θ, which is similar to Rsk2 (i.e. R/K-X-R-X-X-S/T-θ)[59]. When the Rsk2 Ser236 reporter was reacted with 50 U of Chk1, no phosphorylation was detected (**Fig. 39A**). Hence, the Rsk2 reporter did not cross-react with Chk1.

Furthermore, I tested cross-reactivity of the Chk1 reporter with Rsk2 kinase. The Chk1 reporter sequence was based on protein phosphatase Cdc25c (i.e. RLYRSPSM PEKLDR)[160]. Nonetheless, when the Chk1 KAR was phosphorylated with 50 U of Rsk2, minor level (~22%) of cross-phosphorylation was observed (**Fig. 39B**). In mixed reaction setups with both the Chk1 and Rsk2 KARs and 50 U of Rsk2, no phosphorylation of the Chk1 KAR was detected (**Fig. 39C**). In this reaction setup, Rsk2 phosphorylated its reporter with a rate (T_{50}=2.7 h) that was indistinguishable from the isolated reaction (T_{50}=2.5 h) (**Fig. 39B, C**). I therefore concluded that the Rsk2 reporter did not display cross-reactivity with Chk1 in mixed reaction setups. Thus, concurrent modifications of Chk1 and the Rsk2 KARs would clearly convey their respective kinase activities in multiplexed kinase activity profiling assays.

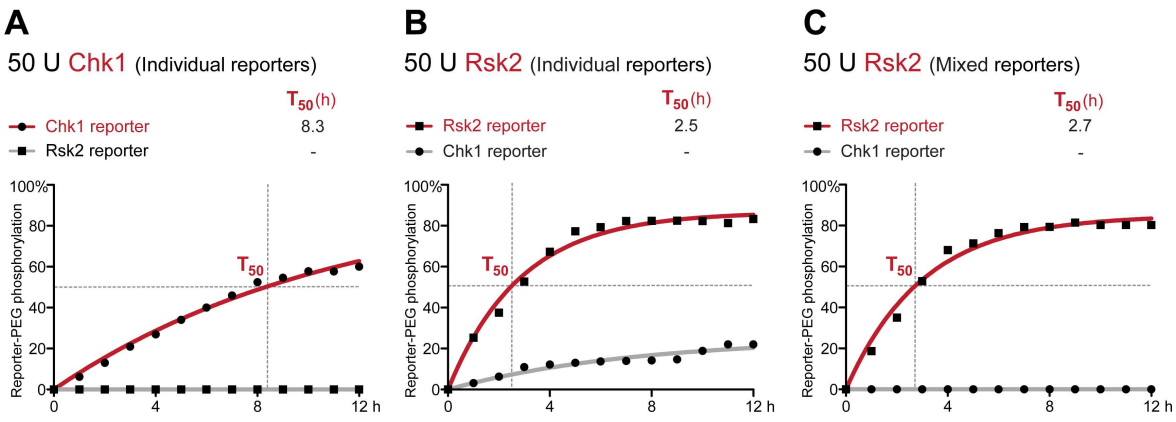

Figure 39. Cross-reactivities of Rsk2 and Chk1 reporters. A) *In vitro* phosphorylation curves of individual Chk1 (red) and Ser236-Rsk2 (grey) reporters with 50 U of Chk1. B) *In vitro* phosphorylation curves of individual Ser236-Rsk2 (red) and Chk1 (grey) KARs with 50 U of Rsk2. C) *In vitro* phosphorylation curves of mixed Ser236-Rsk2 (red) and Chk1 (grey) reporters with 50 U of Rsk2. All reactions were performed at reporter concentrations of 50 µM at pH 7.5, 25°C.

2.5 Summary of KAR sequences

In summary, I constructed and optimized KARs to obtain maximal phosphorylation efficiencies and minimal cross-reactivities. Individual reporter sequences that have been generated and tested are summarized in **Table 2**.

2.6 Phosphorylation and pH

The NMR signal intensities of backbone amide (^{1}H-^{15}N) resonances depend on water/amide proton exchange rates. In the range of physiological pH (i.e. 7-7.5), amide cross-peak volumes decrease linearly with the proton concentration of the solution. In many instances, better signal to noise ratios (S/N) in ^{1}H-^{15}N NMR spectra are thus obtained at pH 6.4. However, most kinases display their highest activities under physiological conditions and at pH values of 7.5. Therefore, I investigated changes in NMR signal intensities and individual KAR phosphorylation efficiencies both at pH 7.5 and pH 6.4, *in vitro* and in CSF extracts.

At pH 7.5, most of the phosphorylatable protein residues in the individual KARs gave rise to comparable NMR signal intensities (^{1}H-^{15}N), except for the unmodified serines in the PKA- and p42MAPK-GB1 reporters (**Fig. 40A,** reference spectra with arrows). In contrast, these NMR signals were clearly visible at pH 6.4 (**Fig. 40B**). These events were also similar to the unmodified threonine in the PDK1-GB1 reporter (**Fig. 40C, D**). At pH 7.5, all NMR signals of the phosphorylated serine, threonine residues of the individual KAR sequences were equally well detected. This behavior is in agreement with the notion that phosphorylated protein residues exhibit different chemical exchange behaviors than non-modified amino acids. On average, the presence of phosphate groups slows down water/amide proton exchange rates and phospho-residues usually display higher S/Ns. Notably, I am able to follow all the phosphorylation reactions at pH 7.5 by monitoring increases in signal intensities of the phosphorylated protein residues even in the case of PKA and p42MAPK reporters. Although I did not observe major changes in kinase efficiencies at pH 6.4, all phosphorylation reactions were performed under physiological conditions at pH 7.5.

Table 2. KAR sequences

Kinase	Full name	Consensus Motif	Protein Source	Reference	Original Sequence	Final
Plk1	Polo-like-kinase 1	D/E-X-S/T-Ø –X_{1-2}-D/E	Myt1	124	419-HLGESSFSSDWDDESLG-435	ALGESSFSSDWDDESLG
Chk1	Checkpoint 1 kinase	Ø-X-ß-X-X-S/T-Ø	Cdc25c	160	281-RLYRSPSMPEKLDR-293	RLYRSPSMPEKLDR
PKA	Protein kinase A or cAMP-dependent protein kinase	R-R-X-S/T- Ø	Kemptide PKAtide	60 138	LRRASLG RTGRRNSI	RTGRRNSI
p42MAPK	p42 Mitogen-activated protein kinase/ Extracellular-regulated kinase 2 (Erk2)	P-X-S/T-P	Elk1 (PKF)	66	YAPRSPAKLAKFQFPA	YAPRSPAALAKFQFPA
PAK1	p21-activated kinase	R-R-X-S/T- Ø	PAKtide	159	RRRLSFAEP	RRRLSFAEP
Rsk2	p90-ribosomal S6 kinase 2	R-R-X-S/T- Ø	40S Ribosomal protein	151	228-IAKRRRLSSLRA-239	IAKRRRLSSLRA
CK1δ	Casein kinase 1δ	DDDD-X-X-S/T	CK1 peptide	145	DDDDVASLPGLRRR	
				64	RRKDLHDDEEDEAMSITA	
		pS/pT-X-X-S/T	CK1 phospho-peptide	146	KRRRALpSVASLPGL	KRRRAIpSVASLPGL
CK2	Casein kinase 2	S/T-X-X-E/D	SV40	126	AMGEEMPSSDDEATAD	
			CK2 peptide	137	RRRADDSDDDDD	RRRADDSDDDDD
PDK1	Phosphoinositide-dependent protein kinase 1		Human Akt1	161	301-KDGATMKTFCGTPEY-315	
			PDKtide (Akt and PRK2)	65	KDGATMKTFCGTPEYLAPEVRREP RILSEEEQEMFRDFDYIADWC	KDGATMKTFCGTPEYLAPEVRREP RILSEEEQEMFRDFDYIADWC
Cdk1	Cyclin-dependent kinase 1	S/T-P-X-K/R	SV40	126	QHSTPPKKKRKV	QARTPPKKKRKV
PKB	Protein kinase B or Akt	R-X-R-X-X-S/T	c-Raf	122	252-SQRQRSTSTPNVH-264	-
			Akt peptide	152	RPRAATF	-

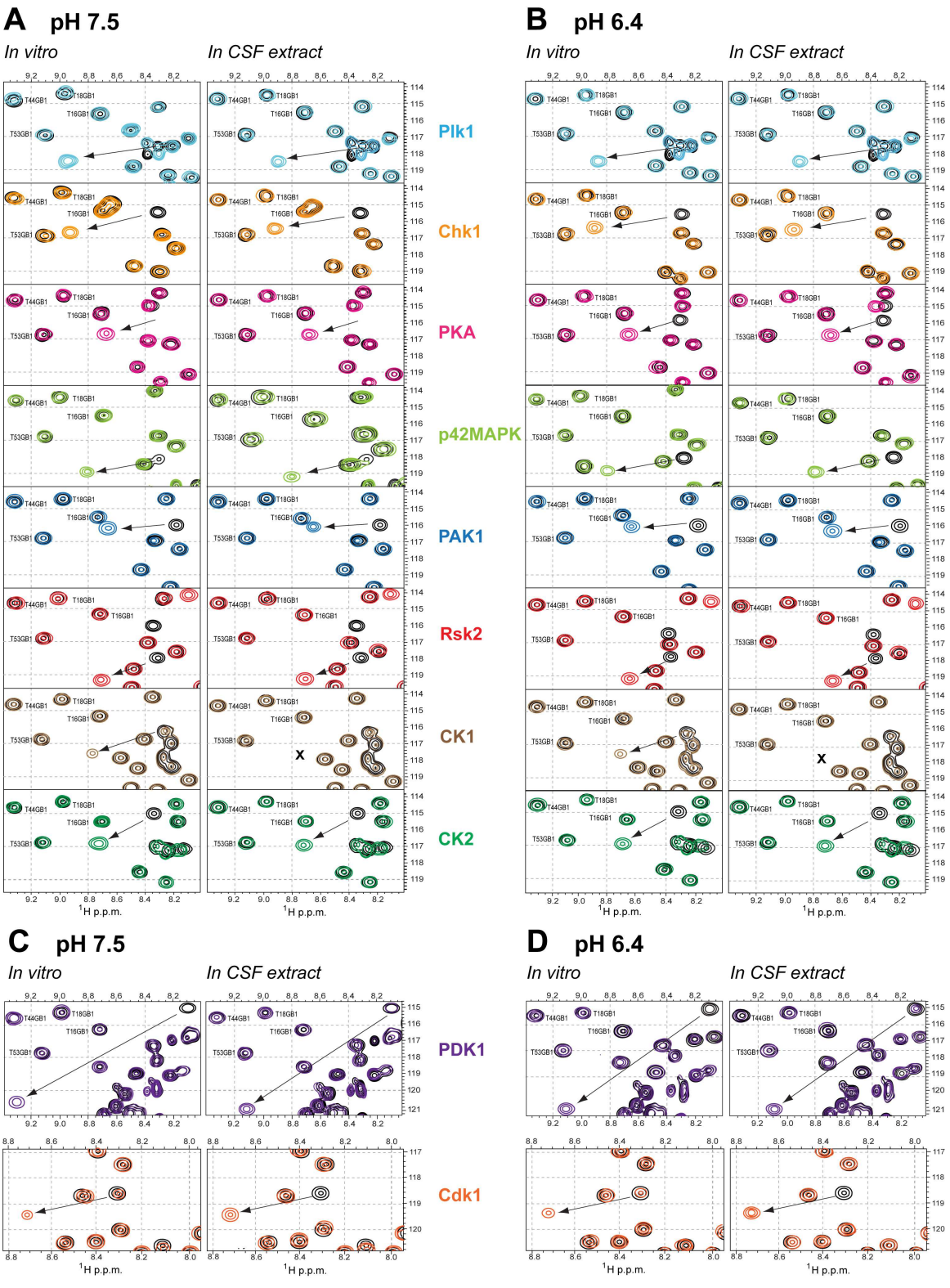

Figure 40. Comparison of NMR signal intensities and phosphorylation efficiencies of recombinant KAR-GB1 constructs at pH 7.5 and 6.4. A) Overlay of 2D ^{1}H-^{15}N NMR spectra of serine-KAR-GB1 constructs *in vitro* (left panel) and in CSF extracts (after 1 h, right panel) at pH 7.5. B) Overlay of 2D ^{1}H-^{15}N NMR spectra of serine KAR-GB1 at pH 6.4. C) Overlay of 2D ^{1}H-^{15}N NMR spectra of threonine-KAR-GB1 constructs *in vitro* (left panel) and in CSF extracts (after 1 h, right panel) at pH 7.5. D) Overlay of 2D ^{1}H-^{15}N NMR spectra

of threonine KAR-GB1 constructs *in vitro* (left panel) and in CSF extracts (after 1 h, right panel) pH 6.4. The reference spectra of each KAR are in black while the reaction samples are colored differently according to the different KARs. All reactions were performed at reporter concentrations of 50 µM at 25°C. All of *in vitro* reactions were performed with 500 U of commercial kinases for 1 h. Only the *in vitro* reactions for the Plk1, PAK1 and Cdk1 KAR-GB1 constructs were performed with 50 U of the respective kinases for 12 h, because these were supplied with lower unit-equivalents by the vendors

2.7 Quantitative kinase profiling

2.7.1 Quantification accuracy and detection limits

To determine the accuracy with which reporters can report differences in individual phosphorylation activities, I *in vitro* reacted CK2 and p42MAPK reporters with different amounts of the respective commercial enzymes. At 10 to 100 unit equivalents both kinases produced reaction trajectories (i.e. modification curves) that were reproducible and linear **(Fig. 41)**. The standard error between individual reaction runs was well below 5 U so that differences in kinase activities as low as 5 U equivalents could accurately be measured. In terms of sensitivity and experimental detection limits, enzymatic activities as low as 10 U equivalents could be determined with a high level of confidence.

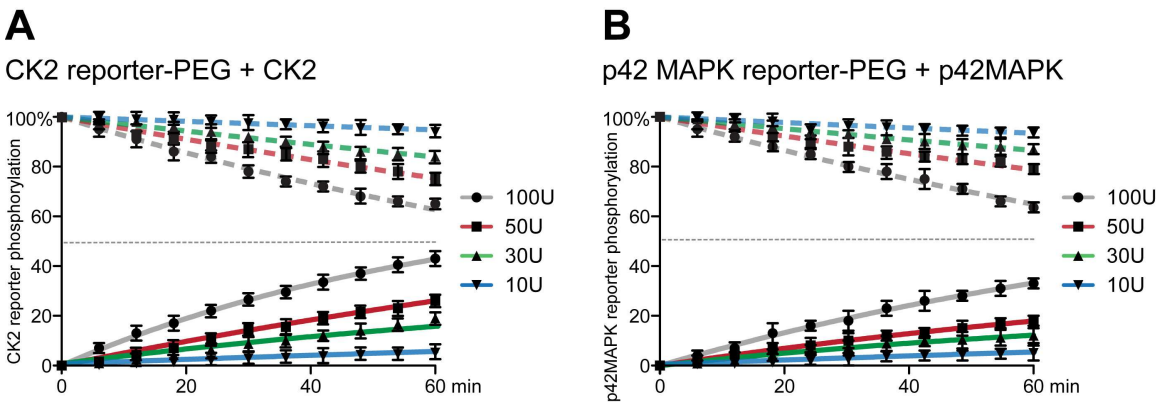

Figure 41. Quantification accuracy and detection limits. A) *In vitro* phosphorylation of the CK2 reporter with commercial CK2. Time-resolved modification curves with 10, 30, 50, and 100 U of CK2 are shown in blue, green, red and grey, respectively. Increase of NMR signals of the modified KAR is shown as solid lines. Decrease of the NMR signals of the unmodified KAR is shown as dashed lines. B) *In vitro* phosphorylation of the p42MAPK reporter with commercial p42MAPK. Time-resolved modification curves with 10, 30, 50, and 100 U of p42MAPK are shown in blue, green, red and grey, respectively. All of *in vitro* reactions were set up with KAR concentrations of 50 µM and at pH 7.5, 25°C.

2.7.2 Quantitative profiling of commercial kinases

One of the goals of this project was to measure relative kinase activities in a time-dependent manner by monitoring individual KAR phosphorylation states by time-resolved NMR spectroscopy. In principle, the rates of KAR modifications that I am to detect by time-resolved NMR spectroscopy depend on two main parameters: kinase/substrate/reporter affinities and kinase/substrate/reporter concentrations. Because most of my measurements are to be conducted in cellular environments, absolute concentrations of all available substrate entities, besides the added KARs, as well as endogenous levels of cellular kinases are not known. It is therefore important to carefully investigate and adjust a few reaction parameters that can be determined accurately. In a first instance, these are the individual kinase/KAR affinities. Since I did not actually measured individual kinase/KAR affinities, a reductionist's point of view would have to suffice: All KARs were designed based on kinase consensus sequences. One can therefore assume that all KAR sequences constitute 'optimal' kinase substrate sites that enable efficient modification reactions. To test the variation of KARs in their absolute kinase affinities, I devised the following test: Different companies selling recombinant kinases for enzymatic *in vitro* assays measure their kinase activities with different protocols and on different substrate molecules. As these kinase activities are provided to the customer in terms of enzymatic unit (U) equivalents, time-resolved *in vitro* kinase reactions with enzymes from different vendors adjusted to identical unit equivalents should, in principle, yield highly congruent modification trajectories for one the same KAR. Moreover, different KARs, and different kinases, reacted under identical activity conditions (i.e. same unit equivalents) should result in highly similar reactions behaviors. This will further indicate that individual KAR/kinase affinities are in a comparable range. To test this assumption, I purchased four different kinases from two independent sources; SignalChem and New England BioLabs (NEB). KAR phosphorylation reactions were set up with identical unit equivalent settings of all four kinases and time-resolved modification trajectories were recorded by NMR spectroscopy (**Fig. 42**). Surprisingly, neither the individual reaction profiles of kinases from the same company, nor the same kinase profiles of the different companies were similar. Comparable phosphorylation rates were only detected for CK2 (500 U), with T_{50} values of 13.2 min and 14.8 min for kinases from SignalChem and NEB, respectively. The moderate differences were observed for the phosphorylation reactions with PKA,

p42MAPK and CaMK2. In addition, the two companies did not use the same standard peptides for defining the enzymatic activities of PKA and CK2 (**Table 3**). This fact can possibly explain the differences in measured PKA activities. In other cases, both companies used the same standard peptide substrates and identical reaction temperatures (30°C) to assay p42MAPK and CaMK2 activities. Together, these results suggested that the differences in kinase qualities between individual companies were quite larger than the differences in kinase/KAR affinities that I set out to explore.

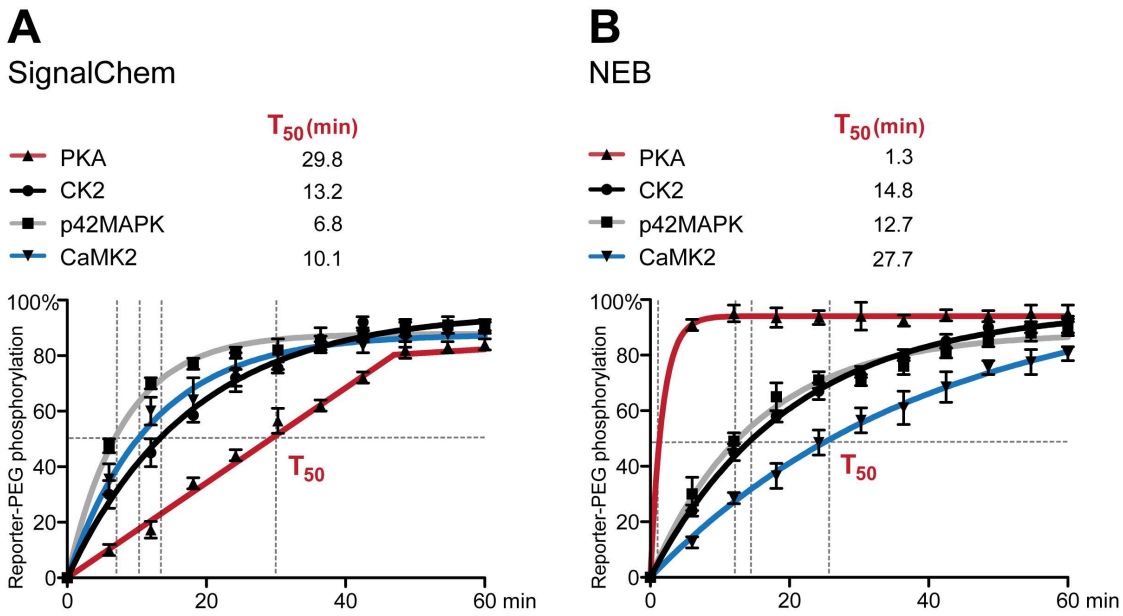

Figure 42. Time-resolved *in vitro* kinase activity profiling. A) *In vitro* phosphorylation curves of peptide-based KARs with 500 U of the SignalChem kinases. PKA (red), CK2 (black), p42MAPK (grey) and CaMK2 (blue). B) *In vitro* phosphorylation curves of peptide-based KARs with 500 U of NEB kinases. All reactions were performed at reporter concentrations of 50 µM at pH 7.5, 25°C.

Table 3. Kinase substrate comparison

Kinase	Kinase substrate for activity assay		
	NEB	SignalChem	KARs
PKA	Kemptide (LRRASLG)	CREBtide (KRREILSRRPSYR)	PKAtide (GRTGRRNSI)
CK2	CK2 peptide (RRRADDSDDDDD)	Casein substrate	CK2 peptide (same as NEB)
p42MAPK	Myelin basic protein	Myelin basic protein	Peptide coded from Elk1 protein (YAPRSPAALAKFQFPA)
CaMK2	Autocamtide-2 (KKALRRQETVDAL)	Autocamtide-2 (KKALRRQETVDAL)	Peptide coded from Cdc25c (RLYRSPSMPEKLDR)

2.8 Cellular kinase activity profiling

In the previous sections, I have outlined strategies to generate different KARs (**2.1, 2.2**), optimization routines to enhance their kinase activity reporting properties and specificities (**2.3**), elaborate cross-reactivity tests (**2.4**) and how to determine quantification accuracies and detection limits (**2.7.1**). In the following section, I will describe cellular applications of KARs to probe for endogenous kinase activities in complex environments such as CSF cell extracts, how to profile multiple cellular kinase activities in parallel and how to use KARs to study the properties of kinase inhibitors.

2.8.1 Quantitative profiling of cellular kinase activities

To exemplify this aspect of KAR usage, I outline two profiling studies to determine the endogenous activities of cellular CK2 and p42MAPK in CSF extracts and how to quantitatively correlate kinase activities measured directly in cell extracts to *in vitro* data. In a first step, reference modification trajectories of CK2 and p42MAPK were recorded with 500 U of the respective enzymes *in vitro* (**Fig. 43A** and **B**). These curves revealed T_{50} values of 14.8 min for CK2 and 12.7 min for p42MAPK. In CSF extract, I measured T_{50} values of 18.1 min for the CK2 reporter and 9.1 min for the p42MAPK reporter.

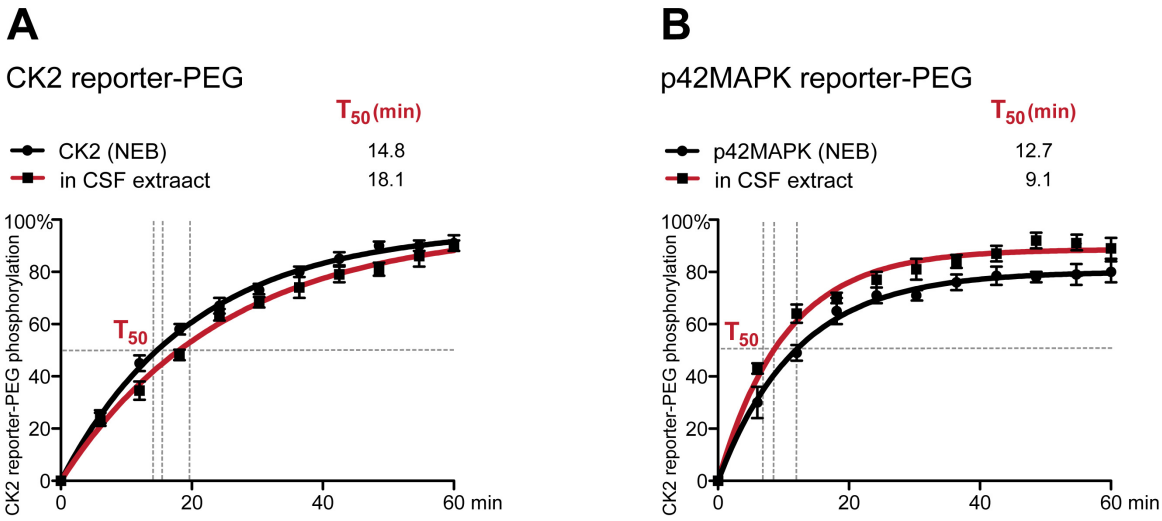

Figure 43. Quantitative NMR profiling of cellular CK2 and p42MAPK activities. A) Superpositions of *in vitro* (500 U CK2, black) and in CSF extract (red) phosphorylation curves of the CK2 reporter. B) Superpositions of *in vitro* (500 U p42MAPK, black) and in CSF extracts (red) phosphorylation curves of the p42MAPK reporter. All reactions were performed at KAR concentrations of 50 µM and at pH 7.5, 25°C.

Based on the differences in T_{50} values that I had determined for the 500 U *in vitro* reactions, I concluded that cellular CK2 activity in CSF extract corresponded to 409 unit equivalents (U_{equ}) of the respective *in vitro* reaction. For cellular p42MAPK in CSF extracts that number was 698 U_{equ}.

2.8.2 Multiplexed-profiling of cellular kinases activities

Probably the breakthrough of single-site, selective ^{15}N isotope-labeled, peptide-based KARs is the ability to use them in a combined, multiplexed fashion in one and the same reaction setup. Multiplexed kinase activity profiling of a number of cellular enzymes in parallel has thus become possible. In the following, I set out to investigate the quantitative reporting capabilities of 8 different KARs to be monitored simultaneously by time-resolved NMR spectroscopy in CSF extract. Initially, I determined the reference NMR peak pattern of a 'virtual' mixture of these 8 KARs by assembling their individual 2D ^{1}H-^{15}N resonance signals in one combined NMR spectrum (**Fig. 44A**). In a next step, I followed the same rationale and assembled a combined CSF extract NMR spectrum, using the NMR resonance positions that I had previously measured for the individual KARs in 'isolated' CSF experiments (**Fig. 44B**). Finally, I ran a CSF extract experiment, in which I jointly added all 8 KARs to the same 'reaction mixture' (**Fig. 44C**). Qualitative inspection of the consecutive 2D ^{1}H-^{15}N NMR spectra readily revealed efficient phosphorylation of all KARs by endogenous, cellular kinases. Moreover, all 2D NMR signals were sufficiently well set apart to enable quantitative, time-resolved deductions of the 8 individual phosphorylation trajectories in a reproducible fashion (**Fig. 44D**). With a degree of accuracy, 8 cellular kinase activities could be determined quantitatively in a single set of consecutive NMR experiments.

In fact, these results established that multiplexed, quantitative NMR profiling of cellular kinase activities was indeed possible. Kinase activities measured in CSF extract individually and in the multiplexed reaction setup were remarkably similar (**Table 4**). Thus, I ensured that no cross-reactivities affected the different kinase activities under those experimental conditions. Based on the results from the multiplexed CSF reaction, Cdk1 activity was determined to be the most active kinase in metaphase-arrested extracts, with a specific activity of 2,373 U_{equ}. Plk1 and Chk1 followed as the second most active kinases with 1,425 and 1,096 U_{equ}, respectively. Rsk2 and p42MAPK

exhibited similar activities of 874 and 648 U_{equ}, respectively. Activities of CK1δ and CK2 were 591 and 451 U_{equ}, respectively. Finally, cellular PDK1 was the least active kinase with 189 U_{equ} in this assay.

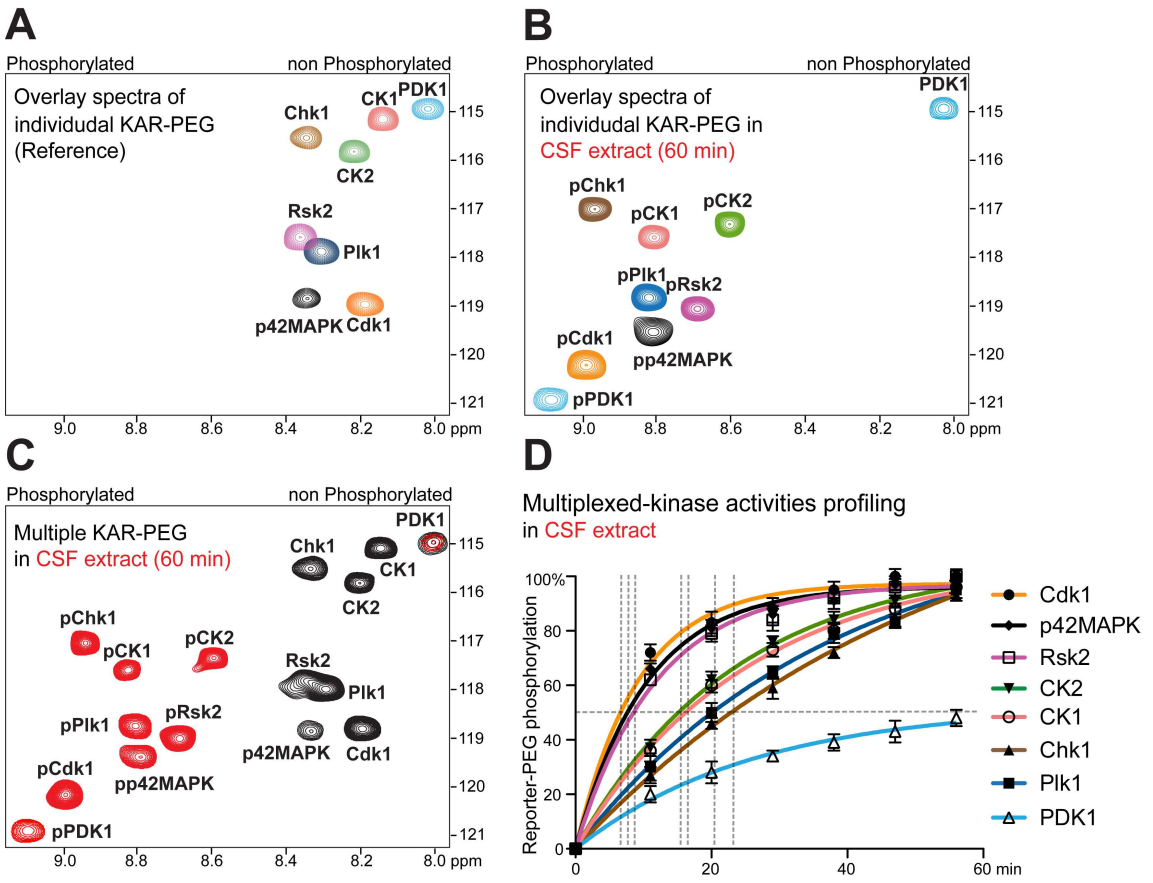

Figure 44. Multiplexed profiling of cellular kinase activities. A) Overlay of 2D ^{1}H-^{15}N NMR spectra of individual KARs in their reference (unmodified) states. B) Overlay of 2D ^{1}H-^{15}N NMR spectra of individual KARs in their phosphorylated states, as determined in individual KAR reactions in CSF extracts. NMR resonance signals are false colored according to the identities of the different KARs. C) 2D ^{1}H-^{15}N NMR spectra of the mixture of the 8 different KARs in the reference sample (black) and in CSF extracts (red). Each NMR signal reports on the activity of a different kinase. D) Phosphorylation curves of the 8 KARs in CSF extracts. All reactions were performed at KAR concentrations of 50 µM and at pH 7.5, 25°C.

Table 4. Cellular kinase activities in CSF extracts

Kinase	Individual KAR reaction		Multiple KAR reaction		Measured reference T_{50} of KARs with respective kinase (*in vitro*)	
	T_{50} (min)	Enzymatic activity (U)	T_{50} (min)	Enzymatic activity (U)		
Cdk1	9.8	1,656	6.7	2,373	5.3 h	(50 U NEB)
Rsk2	10.1	742	8.6	874	2.5 h	(50 U SignalChem)
p42MAPK	9.1	698	9.8	648	12.7 min	(500 U NEB)
Chk1	18.0	1,383	22.7	1,096	8.3 h	(50 U SignalChem)
CK2	18.1	409	16.4	451	14.8 min	(500 U NEB)
CK1	16.2	638	17.5	591	20.7 min	(500 U NEB)
Plk1	23.1	1,233	20.0	1,425	9.5 h	(50 U SignalChem)
PDK1	T_{25}=21.7	145	T_{25}=16.7	189	2.6 h (T_{25}=1.0 h)	(50 U SignalChem)

Enzymatic activity unit equivalents (U_{equ}) of each cellular kinase were calculated based on the measured reference T_{50} of KARs with respective kinases (*in vitro*). Phosphorylation of the PDK1 KAR was lower than 50% in CSF extracts (Fig. 44D) and, hence, its activity was alternatively determined according to its T_{25} value (i.e. 25% of substrate turnover).

2.8.3 Kinase inhibitor profiling

Kinase inhibitors are major targets in drug development[51,162-164]. Consequently, quantitative methods to directly determine kinase inhibitor efficiencies in cellular environments are of particular importance[165,166]. Multiplexed profiling of cellular kinase activities by NMR spectroscopy could potentially be very useful to quantitatively measure kinase inhibitor efficiencies under physiological conditions, as well as to determine the specificities of individual kinase inhibitors and their possible off target effects.

For the next couple of experiments, I set out to investigate the ability of the multiplexed kinase activity profiling approach to quantitatively report on the efficiencies and specificities of three different Cdk1 inhibitors. All three inhibitor compounds are based on chemical structures that function as ATP analogues and thereby compete for endogenous ATP binding to cellular Cdk1 (and possibly also other kinases). For the multiplexed reaction setup, I decided to initially monitor the basal activities of Cdk1, Chk1

and Plk1 in parallel, in CSF extract (**Fig. 45A**). The half maximal inhibitory concentration (IC_{50}) of the first Cdk1 inhibitor, which is a cell-permeable indolylmethylene-2-indolinone derivative or Cdk1 inhibitor 217695, was reported to be 5.8 µM, as determined in human HeLa cells[167]. Added to CSF extracts 15 min (final concentration 225 µM) prior to the addition of KARs and NMR monitoring, Cdk1 inhibitor 217695 decreased cellular Cdk1 activity 4-fold (**Fig. 45B**). However, Cdk1 inhibitor 217695 also reduced cellular Plk1 activity 1.5-fold, whereas Chk1 activity was slightly impeded. Thus, this Cdk1 inhibitor 217695 displayed a rather low inhibitory capacity and poor specificity with Plk1, which is a non-targeted cellular kinase.

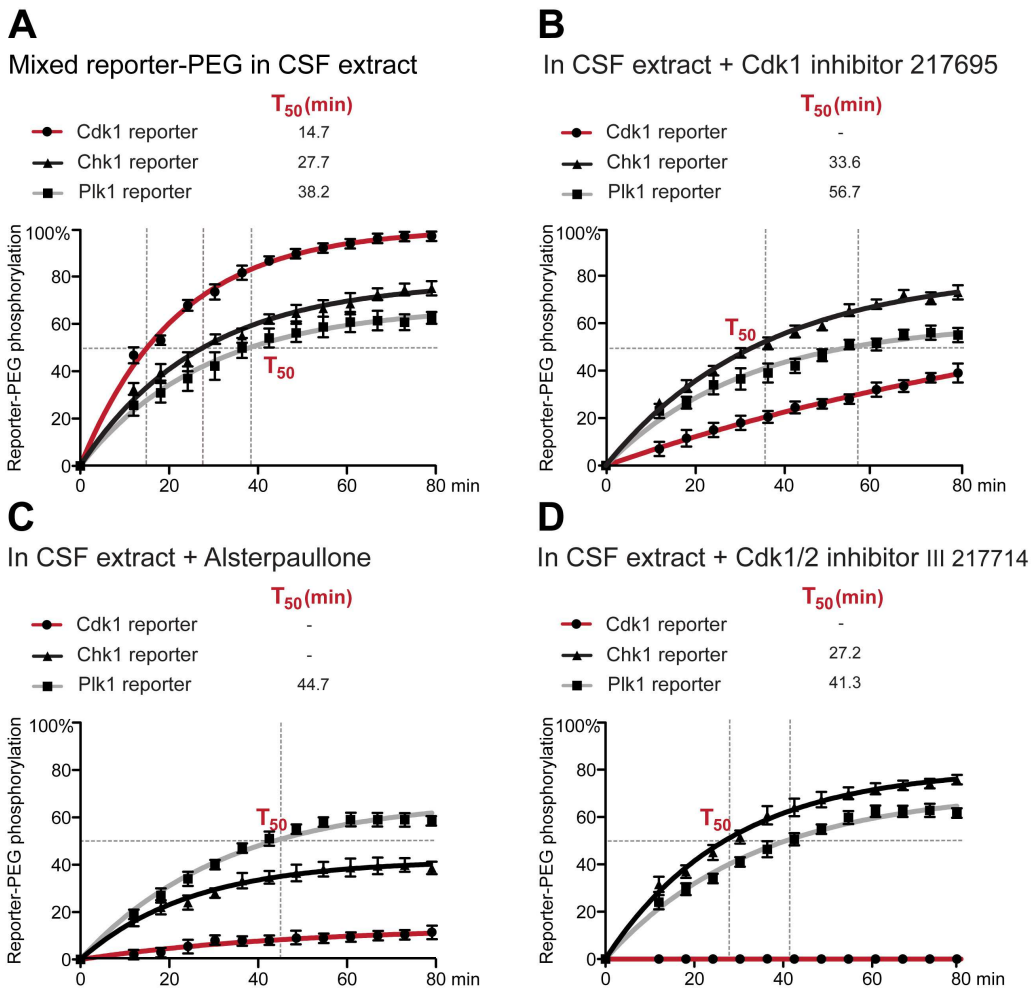

Figure 45. Kinase inhibitor profiling in CSF extract. A) Multiplexed NMR profiling of Cdk1 (red), Chk1 (black) and Plk1 (grey) activities in untreated CSF extracts. B) Multiplexed NMR profiling of Cdk1 (red), Chk1 (black) and Plk1 (grey) activities in Cdk1 inhibitor 217695-treated CSF extracts. C) Multiplexed NMR profiling of Cdk1 (red), Chk1 (black) and Plk1 (grey) activities in Alsterpaullone-treated CSF extracts. D) Multiplexed NMR profiling of Cdk1 (red), Chk1 (black) and Plk1 (grey) activities in Cdk1/2 inhibitor III 217714-treated CSF extracts. All reactions were performed at pH 7.5, 25°C.

The second Cdk1 inhibitor, Alsterpaullone (IC_{50} of 35 nM, as determined in human colon cancer HCT-116 cells)[168], which was added to the CSF extract with a final concentration of 225 µM, abolished 90% of the Cdk1 activity present in CSF extracts (**Fig. 45C**). Alsterpaullone slightly affected cellular Plk1 activity (from T_{50} value of 38.2 min to a T_{50} value of 44.7 min), but exhibited strong cross-reactivity with cellular Chk1 (~ 2-fold activity reduction). Finally, the third Cdk1 inhibitor, a cell-permeable triazolo-diamine compound (Cdk1/2 inhibitor III 217714, IC_{50} of 35 nM, as determined in HeLa cells)[169], displayed the highest Cdk1 inhibitory potential (final concentration 225 µM) (**Fig. 45C**). Cdk1/2 inhibitor III 217714 virtually eliminated cellular Cdk1 activity without showing any effect, cross-reactivity on cellular Chk1 and Plk1.

2.9 Profiling phosphatase activity

KARs were originally designed to report on cellular kinase activities. However, in the course of testing the cellular stabilities of the different KAR constructs, I noticed that some of KARs after being phosphorylated in a cell lysate, they exhibited dephosphorylation (i.e. reporting on the presence of cellular phosphatase activities). In this section, I will outline how KARs can also be used to probe for cellular phosphatase activities.

2.9.1 Reversible phosphorylation of the Plk1 KAR

In CSF extracts, the Plk1 reporter was efficiently phosphorylated to about 80% within the first 40 min of extract incubation. After this period, the Plk1 reporter was readily dephosphorylated until almost of the original NMR signal intensity was quantitatively recovered in its unmodified form (**Fig. 46A**). Conversely, time-resolved NMR monitoring reported the progressive decrease of the phospho-KAR signal. In the course of this reaction, subtle up-field chemical shift changes of the phospho-resonance NMR signals were noted, which were indicative of a slight acidification of the reaction mixture[170]. Dephosphorylation similarly occurred for the reporter-GB1 tagged version of the Plk1 reporter **(Fig. 46B)**. In analogy, initial phosphorylation followed by specific dephosphorylation after prolonged CSF extract exposure was also observed for the

Chk1, PDK1 and CK2 KARs (data not shown). These results implied that some KARs were targeted for specific phosphatase activities after extended periods of lysate incubation that reversibly removed their phosphorylation marks and reset their modification states. These events pointed to a tightly balanced interplay between cellular kinase and phosphatase activities in CSF extracts. At the same time, they also suggested the potential use of pre-phosphorylated KAR substrates (pKARs) as phosphatase activity reporters.

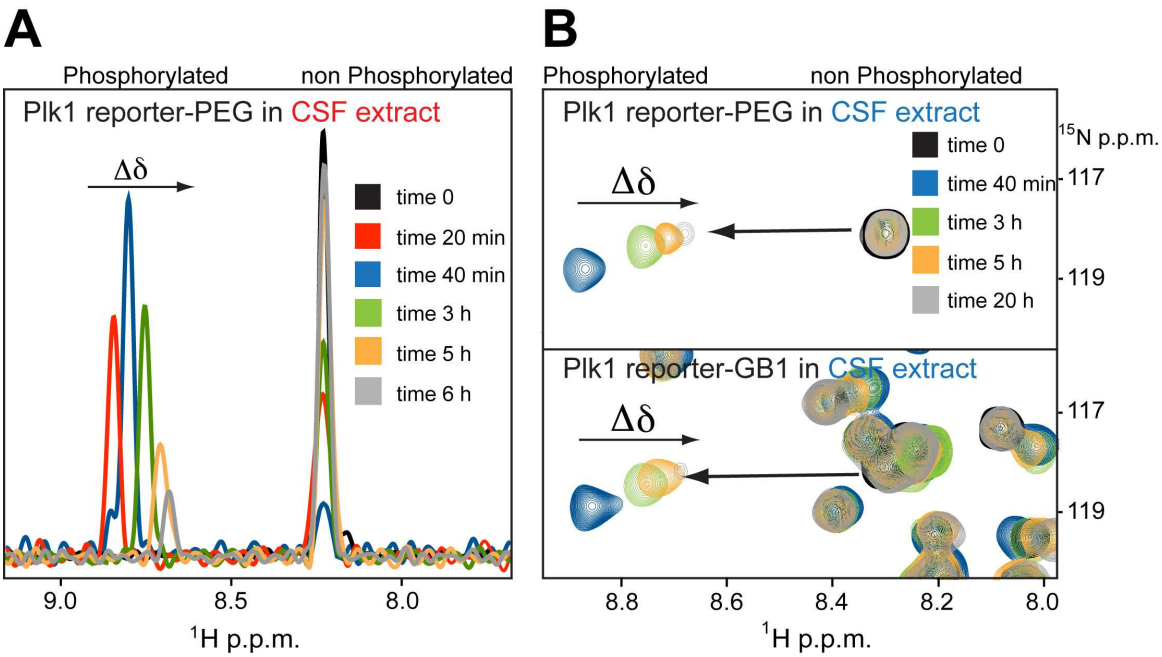

Figure 46. Reversible phosphorylation of the Plk1 reporter. A) Overlay of 1D ^{1}H NMR spectra (^{15}N edited) of the Plk1 reporter in CSF extract, at t=0 (black), at t=20 min (red), at t=40 min (blue), at t=3 h (green), at t=5 h (orange) and at t=6 h (grey). B) Overlay of 2D ^{1}H-^{15}N NMR spectra of the peptide-based Plk1 reporter (upper panel) and reporter-GB1 (lower panel) in CSF extracts. All reactions were performed at reporter concentrations of 50 µM at pH 7.5, 25°C.

The Plk1 reporter sequence was originally derived from the Myt1 protein (**2.3.5**), which is a membrane-associated kinase, containing a transmembrane segment between residues 373-392[94]. The Plk1 reporter may thus be susceptible to interact with cellular membranes, which could be enhancing dephosphorylation via membrane-bound phosphatases that are likely to be present in CSF extracts[171,172]. However, upon removal of the membrane fraction from CSF extracts via high-speed ultra-centrifugation, the Plk1 KAR displayed a similar dephosphorylation behavior (**Fig. 47A**). The results

demonstrated that the presence of cellular membranes was not the cause for dephosphorylation. Similarly, phosphorylation and subsequent dephosphorylation was also observed in nuclear extracts prepared from human HeLa cells, thus constituting a very different biological environment. Dephosphorylation in HeLa cell extracts was considerably slower than in CSF extracts and the subtle up-field chemical shift changes of the phospho-resonance NMR signals were not detected in the nuclear extract. (**Fig. 47B**). These results were from the low total protein concentration of the nuclear extract, which is 5 mg/mL (while that of the CSF extract is >100 mg/mL). Having low total protein concentration also indicates low metabolic activity and the proton release (causing acidification in the sample) in the HeLa nuclear extract, which can be used to explain in the case of no up-field chemical shift changes.

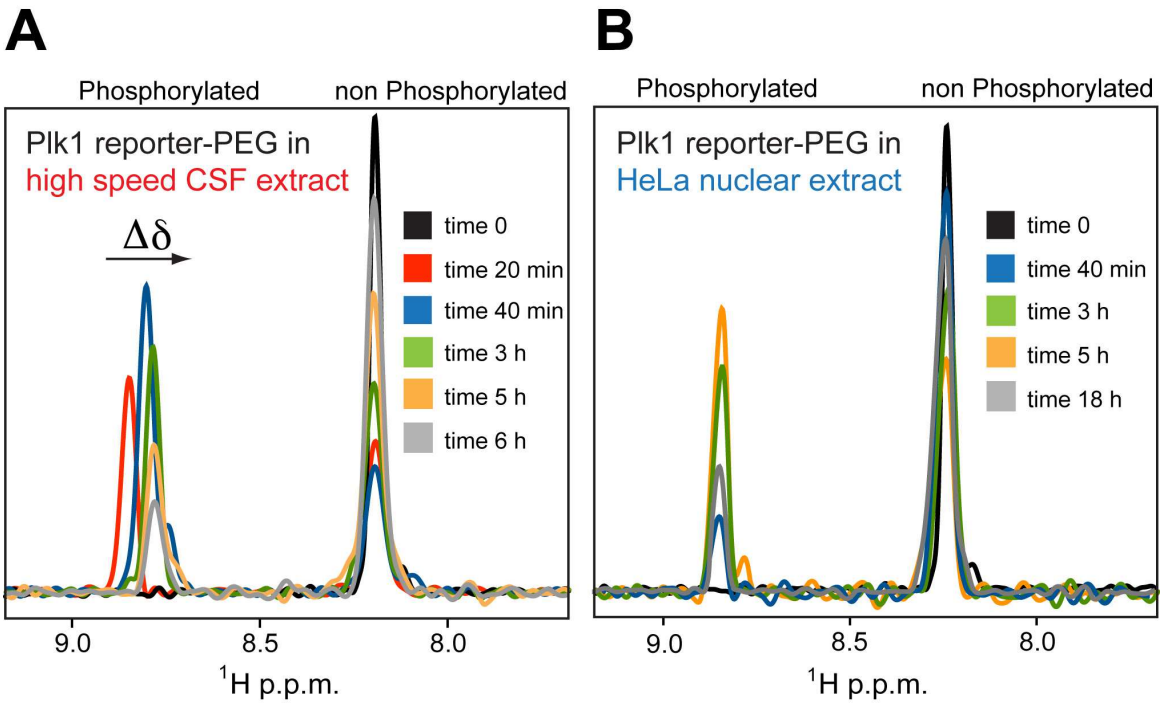

Figure 47. Reversible phosphorylation of the Plk1 reporter in cell extracts of different origins. A) Overlay of 1D ^{1}H NMR spectra (^{15}N edited) of the Plk1 reporter-PEG in membrane-removed (high-speed) CSF extracts, at t=0 (black), at t=20 min (red), at t=40 min (blue), at t=3 h (green), at t=5 h (orange) and at t=6 h (grey). B) Overlay of 1D ^{1}H NMR spectra (^{15}N edited) of the Plk1 reporter-PEG in HeLa nuclear extract, at t=0 (black), at t=40 min (blue), at t=3 h (green), at t=5 h (orange) and at t=18 h (grey). The nuclear extract with total protein concentration 5 mg/mL was a gift from Stamatios Liokatis. All reactions were performed at reporter concentrations of 50 µM at pH 7.5, 25°C.

2.9.2 Extract aging and reversible phosphorylation

Dephosphorylation of the Plk1 KAR suggested that a tightly controlled balance of kinase and phosphatase activities existed in cell extracts that was somehow modulated at longer times of extract storage at elevated temperatures (as NMR experiments are typically performed at 25º C). One possible explanation for this behavior was afforded by a decline in kinase activity over time, combined with the presence of cellular phosphatase activities. To experimentally address this hypothesis, I added Plk1 reporter-PEG to a fresh aliquot of CSF extract, whereas I stored a second CSF aliquot at 25º C for ~3 h to mimic extract aging. While the Plk1 profile of the fresh aliquot recapitulated the previously reported phosphorylation and dephosphorylation behavior, the aged extract display a vastly different modification curve (**Fig. 48A**). The total level of initially accumulated phospho-Plk1 substrate was much lower and rapid dephosphorylation set in earlier. I additionally monitored the activity of two different kinases in the same extract at different time points. In the beginning of a new experiment, I observed the Plk1 activity in CSF extract until 50% of the Plk1 reporter-PEG became dephosphorylated at 3 h. I then added 50 µM peptide Chk1 reporter-PEG to the same sample and detected its modification. The cellular Chk1 phosphorylated the Chk1 KAR to a level of 45% at the first hour, and then the Chk1 KAR reported a predominant phosphatase activity (**Fig. 48B**). Similar modification curves, which are observed in different KARs, demonstrate that a general decline in cellular kinase activities (regardless of the presence of KARs) was likely responsible for the observed dephosphorylation behaviors.

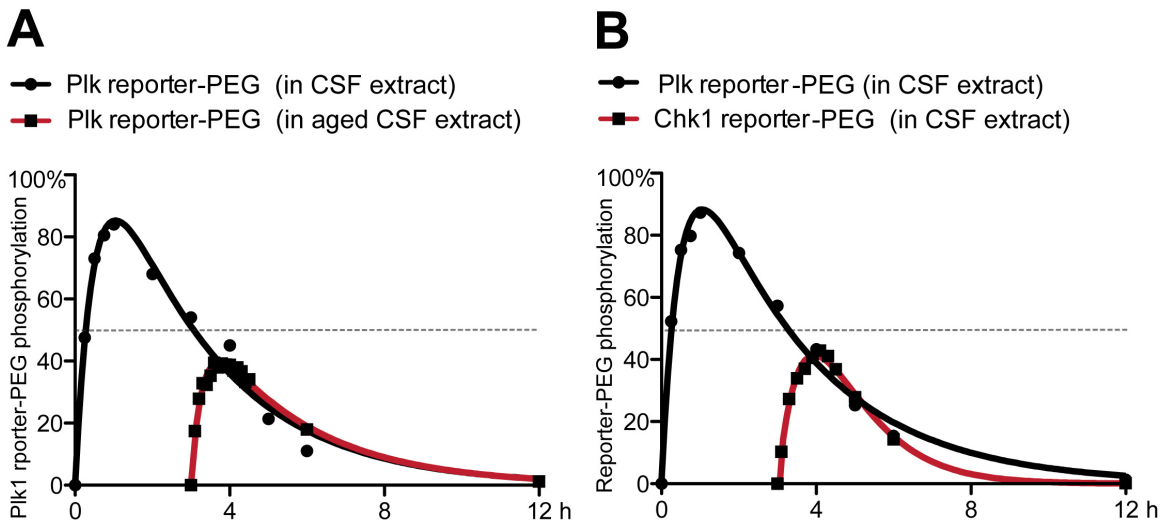

Figure 48. Cellular kinase activities in aged CSF extracts. A) Phosphorylation curves of the Plk1 reporter-PEG in fresh (black) and aged CSF extracts (red). B) Phosphorylation curves of the Plk1 reporter-PEG in fresh (black) and Chk1 reporter-PEG in the same extract (red) at 25ºC. The reactions were set with identical reporter concentration of 50 µM at pH 7.5.

2.9.3. Phosphatase inhibitor tests

As shown above, time-resolved kinase activity profiling in CSF extract established that some KARs were subjected to selective dephosphorylation, which was evidently modulated by time-dependent extract aging, a decline in certain cellular kinase activities. To confirm that cellular phosphatases were indeed causing the observed effects, I supplemented CSF extracts with increasing amounts of phosphatase inhibitors. While the onset of Chk1 reporter dephosphorylation was typically detected within the first two hour of CSF extract incubation (**Fig. 49A**), it was absent when the extract had been treated with 1.2 µM of okadaic acid, a well-known phosphatase inhibitor (**Fig. 49B**). Additionally, cellular Chk1 activity in okadaic acid-supplemented CSF extracts was measured to be twice as high as in extracts without phosphatase inhibitor (T_{50} values of 10.0 min and 17.3 min, respectively) **(Fig. 49C**). These results provided unbiased proof that endogenous phosphatase activities in CSF extracts selectively dephosphorylated certain KARs.

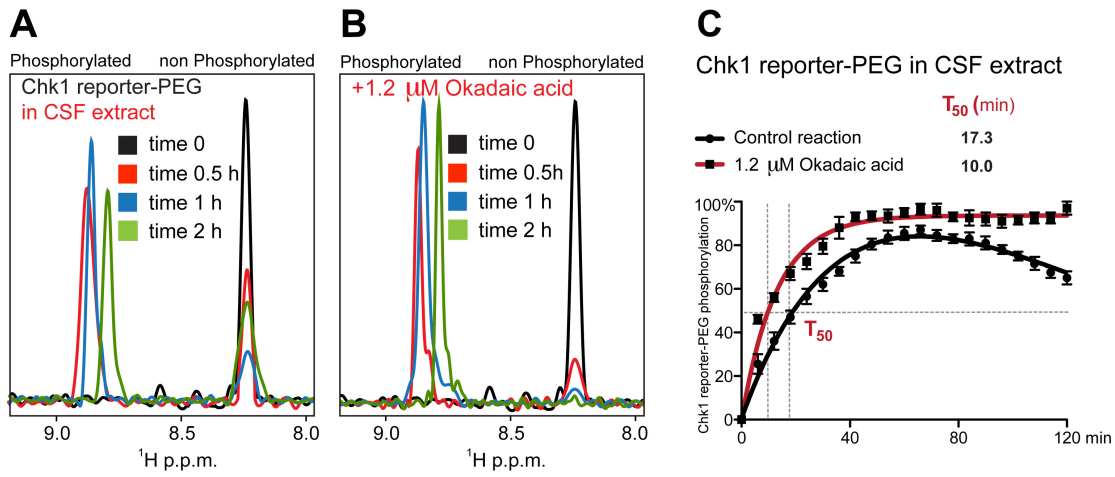

Figure 49. Inhibition of cellular phosphatase activities. A) Overlay of 1D ^{1}H NMR spectra (^{15}N edited) of the Chk1 reporter-PEG in untreated CSF extracts, at t=0 (black), at t=0.5 h (red), at t=1 h (blue) and at t=2 h (green). B) Overlay of 1D ^{1}H NMR spectra (^{15}N edited) of the peptide Chk1 reporter-PEG in 1.2 µM okadaic acid-treated CSF extracts, at t=0 (black), at t=0.5 h (red), at t=1 h (blue) and at t=2 h (green). C) Quantitative modification curves of the Chk1 reporter-PEG in untreated (black) and in 1.2 µM okadaic acid-treated (red) CSF extracts. All reactions were performed at KAR concentrations of 50 µM at pH 7.5, 25°C.

2.9.4. Quantification of cellular phosphatase activities

Having shown that KARs enable quantitative measurements of cellular kinase activities, I asked whether pre-phosphorylated versions of KARs (i.e. pKARs) could similarly report cellular phosphatase activities in a quantitative manner. To prove this, I initially prepared a pre-phosphorylated serine Chk1 KAR or pS Chk1 reporter-PEG by *in vitro* phosphorylation with commercial Chk1. The active recombinant Chk1 was subsequently removed from the fully phosphorylated sample. The resulting pS Chk1 KAR was then added to untreated CSF extracts and monitored dephosphorylation by endogenous phosphatases using time-resolved NMR spectroscopy (**Fig. 50A**). Similar to the KAR reaction, the pS Chk1 KAR was progressively modified and this time, the modification referred to a dephosphorylation event. While the concentration of the Chk1 phospho-KAR species continuously decreased, the concentration of the unmodified KAR species progressively increased. In complete analogy to the previously recorded kinase activity build-up curves, intersection of the complementary dephosphorylation curves yielded at T_{50} value, which quantitatively reported the endogenous phosphatase activities that selectively dephosphorylated pS Chk1 reporter in CSF extracts. Sustained phosphatase activity was detected and 60% of substrate molecules were dephosphorylated within 2 hours. Upon addition of 0.4 µM of okadaic acid, a 2-fold decrease in cellular phosphatase activities was monitored (**Fig. 50B**). 1.2 µM of inhibitor was sufficient to abolish the decrease of the substrate phosphorylation curve **(Fig. 50C)**. This does not mean that all of the phosphatase activity is eliminated, but that kinase activity is much more predominant in these conditions.

Furthermore, I proved the ability of pS Chk1 reporter to convey phosphatase activity *in vitro*. I found out that 70% of the peptide pS Chk1 reporter-PEG was dephosphorylated within 2 h by 2 U serine/threonine protein phosphatase type 2 A (PP2A) while there was no dephosphorylation in the control reaction (**Fig. 50D, E**). Therefore, the reporter is actually a substrate of PP2A and the constant activity of PP2A was comparable to the sustained activities of phosphatases in CSF extract. Together, these results established that phosphorylated versions of KARs (i.e. pKARs) quantitatively reported phosphatase activities in a reproducible manner.

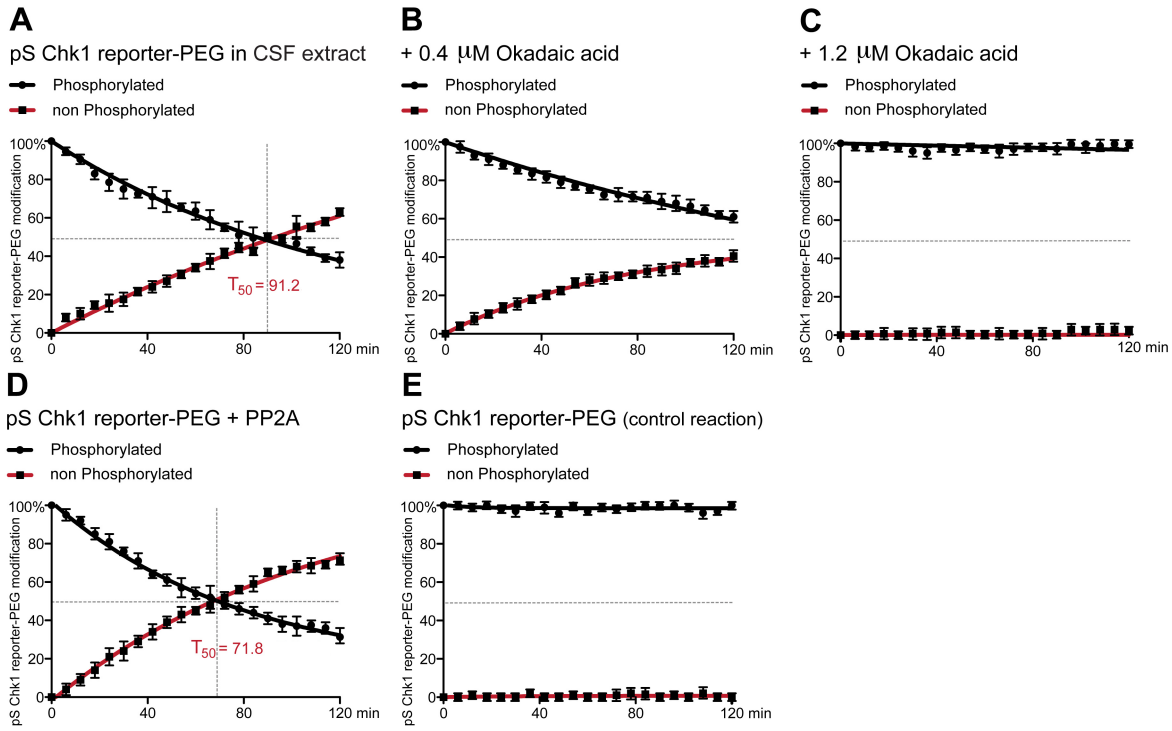

Figure 50. NMR profiling of cellular phosphatase activities. A) Dephosphorylation curves of the pS Chk1 reporter-PEG in untreated CSF extracts (T_{50}=91.2 min). B) Dephosphorylation curves of the pS Chk1 KAR in 0.4 µM okadaic acid-treated CSF extracts. C) Dephosphorylation curves of the pS Chk1 KAR in 1.2 µM okadaic acid-treated CSF extracts. D) Modification curves of the pS Chk1 reporter-PEG *in vitro* with 2 U PP2A. E) Modification curves of the pS Chk1 reporter-PEG in control reaction (*in vitro*). 1 U of the enzyme is defined as 1 nmole phosphate released per min from the 15 µM [^{32}P] labeled Phosphorylase A at 30°C. All reactions were performed at pKAR concentrations of 50 µM at pH 7.5, 25°C.

I further investigated the reactions of other reporters, which exhibited no dephosphorylation in CSF extract, for examples, the Cdk1 reporter-PEG and the Rsk2 reporter-PEG (**Fig. 51A, D**). The pre-phosphorylated threonine Cdk1 reporter (pT Cdk1 reporter-PEG) (Ac-GQARpTPPKKKRKV-PEG) exhibited no dephosphorylation in CSF extract and *in vitro* with 2 U PP2A (**Fig. 51B, C**). The comparable results were also obtained from the pS Rsk2 reporter-PEG (Ac-GIAKRRRLSSLRAGGG-PEG) (**Fig. 51E, F**) and the reactions observed in 2 h and 12 h provided similar outcomes (data not shown). The tested reporters thus do not function as PP2A substrate and their constant phosphorylation state in the CSF extract might come from the fact that they were not substrates of active cellular phosphatases.

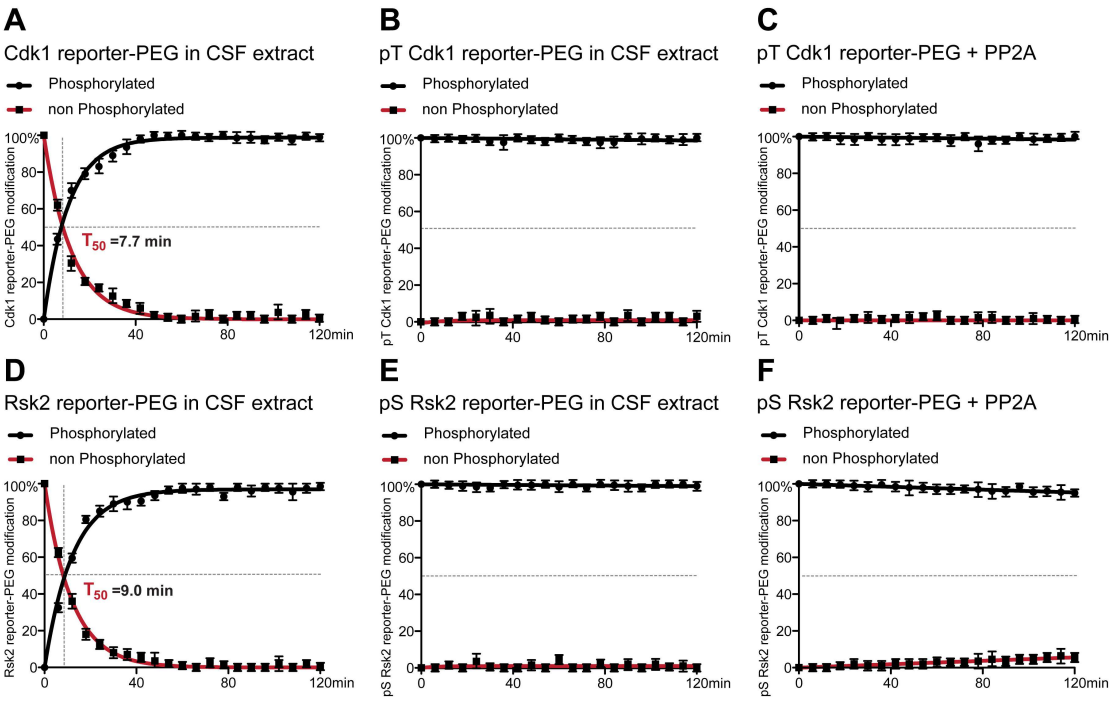

Figure 51. No dephosphorylation of the PEGylated Cdk1 and Rsk2 reporters. A) Modification curves of the peptide Cdk1 reporter-PEG in CSF extract. B) Modification curves of the pT Cdk1 reporter-PEG in CSF extract. C) Modification curves of the pT Cdk1 reporter-PEG *in vitro* with 2 U PP2A. D) Modification curves of the peptide Rsk2 reporter-PEG in CSF extract. E) Modification curves of the pS Rsk2 reporter-PEG (Ac-GIAKRRRLSpSLRAGGG-PEG) in CSF extract. F) Modification curves of the pS Rsk2 reporter-PEG *in vitro* with 2 U PP2A.

3. DISCUSSION

In this work, I have established the suitability of site-selective ^{15}N isotope-labeled serine/threonine kinase activity reporters (KARs), in combination with time-resolved, high-resolution NMR spectroscopy readouts, to simultaneously profile cellular kinase activities in cytostatic factor (CSF) arrested *Xenopus* egg extracts (**2.8.2**). The KAR sequences employed in this study were based on known kinase consensus motifs (**Table 2**) that were further optimized to provide maximal phosphorylation efficiencies (**2.3**) as well as high substrate specificities for the targeted kinases (**2.4**). Peptide-based KARs were generated and specifically ^{15}N isotope-labeled by solid phase peptide synthesis (SPPS) protocols (**2.2**) that included the selective addition of linear polyethylene-glycol (PEG) groups at the C-termini of the synthesized KARs in order to protect them from proteolytic degradation in CSF extracts (**2.2.4.2**). The high solubility of PEGylated KARs was particularly advantageous for the preparation of highly concentrated KAR stock solutions, which, in turn, permitted minimal dilutions of cell extracts in the course of preparing *in extract* NMR samples.

NMR has several distinctive features that facilitate this method for *in situ* protein phosphorylation studies in complex environments such as cell extracts[126,173]. Through advancements of this method and the implementation of novel concepts that selectively exploit some of these features and thereby further the applicability of time-resolved, high-resolution NMR measurements, I have generate sets of tools that enable investigations of cellular kinase and phosphatase activities with an unprecedented level of detail.

The purpose of this chapter is to outline the benefits of NMR-based readouts of cellular kinase and phosphatase activities and to discuss the biological discoveries that I have made with these novel tools.

3.1 Advantages/disadvantages of kinase activity profiling by NMR spectroscopy

Studying protein phosphorylation by NMR provides several advantages over other kinase activity assays. First, NMR enables direct, atomic-resolution observations of the actual phosphorylation events on the single amino acid level, without further sample manipulation, or purification steps. Due to this, individual phosphorylation reactions can be detected within a few minutes after addition of the site-selective ^{15}N isotope-labeled KAR to any reaction mixture, whether it is an *in vitro* reconstituted kinase assay, or an enzymatically active cell extract, or lysate. This enables instantaneous NMR measurements of individual kinase activities. In contrast, other methods require additional preparation and purification steps in order to transfer the samples to be analyzed into phospho-detection compatible forms and states. The peptide array screening method, for example, uses [γ-^{32}P] ATP and requires several additional steps (4-6 h) to eventually detect protein phosphorylation[36]. For radioisotope-incorporation assays, it was recommended to extend exposure times from 3 days to 1 week to improve signal-to-noise ratios for data analysis[35,36]. The integrated approach of using mass spectrometry (MS) and stable-isotope labeled substrate peptides (MS-KAYAK) takes at least 6 h (for the phosphopeptide enrichment step and liquid chromatography-MS quantification) to detect phosphorylation[40,41]. Lastly, the most common phospho-detection routine, Western blotting-based immunodetection requires at least 2-14 hours of experimental time before results are obtained[101,160].

Second, time-resolved NMR readouts permit continuous monitoring procedures, with which phosphorylation reactions of peptides, or proteins can be followed in real time. Initial rates of cellular kinase activities are quantitatively delineated by the analysis of individual modification curves of the different phosphorylation sites, or KAR NMR signals. In contrast to NMR, other mentioned methods often report kinase activities by end point measurements, via quantifications of reaction products rather than by examining the actual rates of kinase activities. Whenever quantitative readouts at multiple time points are desired, such reactions have to be set up with multiple samples that are quenched at individual time intervals and further processed for the respective analyses[36,41,160]. Therefore, most of these phospho-detection methods are not as convenient as NMR

spectroscopy, which continuously monitors actual phosphorylation reactions in single samples.

Third, the absolute amounts of substrate and phosphorylated product molecules are simultaneously detected by NMR spectroscopy. Using time-resolved NMR readouts, the intersections of the build-up curves of phospho-product accumulation and the decay curves of unmodified substrate depletion always relate to 50% of substrate turnover and thus function as reliability indices of the individual measurements. Absence of NMR signals of unmodified substrates indicates complete substrate turnover and completion of the phosphorylation reaction, which can accurately be determined. In contrast, most other kinase assays only detect the phosphorylated products and they require separate control reactions to quantify the actual amounts of product. For example, phospho-detection by immunoblotting necessitates loading of a defined amount of fully phosphorylated product in order to comparatively deduce the level of completion of the actual modification reaction. Similarly, MS-KAYAK requires the additional synthesis of stable isotope-labeled phosphopeptides to be used as internal standards[41]. Thus, quantitative monitoring of substrates and products in the same sample, as is afforded by NMR-based readouts, provides unique advantages over other methods.

Finally, the use of uniformly isotope-labeled peptide KARs offers an additional quality control measure, because peptide degradation during reaction processes in complex environments such as cell extracts is directly detected. Just as phosphorylation produces a different chemical environment for the modified protein/peptide residue, so too does protein/peptide cleavage result in new and unique chemical shift changes that can be monitored throughout the different reactions. Through this additional assessment, KARs can be further optimized for optimal stability in even the most concentrated cell extracts (with total protein concentration >100 mg/mL). In contrast to NMR, other techniques including [γ-^{32}P] ATP radionucleotide-incorporation experiments and immunoblotting only detect the phosphorylation state of the sample and not whether it is progressively degraded. Mass spectrometry is a powerful approach for the identification of post-translational protein modification states. However, even the MS-KAYAK technique does not detect sample degradation due to an additional phospho-peptide enrichment step[40,41].

Nonetheless, one of the major drawbacks of NMR spectroscopy is its poor overall sensitivity. High concentrations (typically in the micro-molar range in at least 100 µL sample) of NMR isotope-labeled proteins or peptides are typically required to detect NMR signals in the first place. For observing protein phosphorylation, a substantial degree of the NMR-active substrate turnover has to be accomplished before the modified species can be detected. Thus, low fidelity phosphorylation events remain invisible to NMR detection. In comparison, the highly sensitive MS-KAYAK technique requires femto-molar levels of substrate in only 20 µL of reaction volume[41]. Phospho-specific immunodetection methods that rely on affinities of product-antibody bindings can detect up to nanogram levels of phospho-products with 20-40 µL of sample required[32]. Peptide array technologies using [γ-^{32}P] ATP radionucleotide incorporation experiments[36] are able to detect phospho-proteins at quantities of only a few nanograms in 30 µL reactions. However, due to the small volume of the samples, problems related to evaporation may occur. For peptide arrays, concentrations of substrates and kinases may change during the long incubation periods, which may lead to experimental artifacts[36]. Therefore, large sample volumes as required for NMR-based measurements are advantageous, especially for monitoring reactions that require extended incubation times. In summary, the combination of NMR-based phospho-detection and peptide-base KARs provides several advantageous over other methods in kinase activity profiling approaches.

3.2 Insights into CSF biology and extract kinase activities

Having simultaneously probed 8 different kinase activities in CSF extracts by NMR spectroscopy (**2.8.2**), the results that I have obtained are in agreement with previous activity assays. First, I found that Cdk1, or Cdc2/cyclin B, which is also referred to as the maturation-promoting factor (MPF), was the most active kinase in these metaphase-arrested cell extracts. Cdk1 activity has previously been determined by a number of [γ-^{32}P] ATP radionucleotide incorporation assays, for which histone H1 was used as a reference substrate[102,174-176].

Second, I found that Plk1, another kinase of the Cdc2/cyclin B activation cascade, as well as Rsk2 and p42MAPK of the MAPK cascade (**Fig. 52**), were also highly active. Plk1 has been reported to be abundantly present in *Xenopus* egg extracts and to be an essential role in metaphase entry[97]. Phosphorylation of Cdc25c by Plk1 not only activates Cdc25c, but, in turn, also promotes nuclear localization of Cdc25c, which is required for MPF activation[177,178]. Moreover, microinjection experiments with Cdc25c promoted Plk1 activation, which suggested the positive feedback regulation[179,180] (**Fig. 52**). Rsk2 activity in CSF-arrest has been reported in several studies, including microinjection-[105] and immunodepletion experiments[104]. Rsk2 is known to phosphorylate and activate members of the exported repeated protein family (Emi/Erp)[181]. In consequence, active Emi/Erp inhibits the anaphase promoting complex/cyclosome (APC/C) and preserves CSF arrest[110,181]. Several immunologic studies revealed expression of p42MAPK in *Xenopus* oocytes and embryos[26,103,182,183].

Third, Chk1, an important regulator of the DNA damage response pathway is responsible for G2 checkpoint arrest[184-187]. Furthermore, Chk1 activity is essential for mitotic progression as its depletion leads to metaphase block[188]. It regulates the bipolar spindle formation and chromosome alignment during metaphase[188]. Based on this, metaphase-arrested extracts like CSF extract are expected to possess Chk1 activity. That indeed was the case, since the Chk1 activity was found to be abundantly present in CSF extracts and the calculated activity of Chk1 was even higher than that of Rsk2 and p42MAPK (**2.8.2, Table 4**).

The sequence of the Chk1 reporter was derived from the human phosphatase Cdc25c[160] and phosphorylation of the Chk1 reporter was extensively confirmed by *in vitro* assays using recombinant kinase (**2.4.2.2**). However, Ser216 of Cdc25c could also be phosphorylated by four additional kinases; Calmodulin/calcium-dependent protein kinase type 2 (CaMK2)[160], cAMP-dependent kinase or protein kinase A (PKA)[189], Cdc25c associated protein kinase 1 (c-TAK1)[190] and mitogen-activated protein kinase–activated protein kinase-2 (MAPKAPK 2 or MK2)[191]. The activity of the first kinase, CaMK2, is observed only in fertilized eggs and not in the CSF arrested-eggs[192] ruling out contributions of this kinase under my experimental conditions. In addition, CSF extract was supplemented with excess EGTA (a Ca^{2+} chelater[193]) during the extract preparation (**5.1.7**) and since Ca^{2+} is a CaMK2 activator, this kinase (even if present) is unlikely to be

active. Likewise, PKA activity has not been previously reported in CSF extract (its high activity is associated with interphase and in metaphase-anaphase transition only[139]). Furthermore, the regulation of PKA activity depends on the amount of cellular cAMP, which considerably decreases during metaphase entry (**1.1.5, 1.2.2**). As a result, the CaMK2 and PKA are inactive and do not phosphorylate the Chk1 reporter in CSF extract.

Additionally, the third kinase, c-TAK1, belongs to the CaMK2 subfamily[42] and is ubiquitously expressed in human tissues and different cell types[190]. Its activity has been reported to remain constant throughout the cell cycle and it was speculated to phosphorylate Ser216 *in vivo*[190]. Nonetheless, c-TAK1 has not been found in *Xenopus* oocytes, or eggs. Only *Xenopus* spleen appears to contain active c-TAK1 (*Xenopus* Gene Collection Database). Therefore, c-TAK1 is not likely to be responsible for phosphorylating the Chk1 KAR in CSF extracts. Also, the last kinase, MK2, is a cell cycle checkpoint kinase[191] and downstream of the stress-activated p38MAPK cascade[194]. The MK2 consensus sequence is X-X-θ-X-R/K-X-X-S/T-X-X motif, where θ is a hydrophobic residue[195]. Since the Chk1 KAR corresponds to the MK2 consensus sequence, it might constitute a substrate for MK2. MK2 has been reported to phosphorylate Cdc25c at Ser216 in G1, S and the G2/M checkpoint in response to UV-induced DNA damage[196]. Furthermore, recent work revealed a role for MK2 during meiotic cell-cycle progression through phosphorylation and activation of Plk1[197]. Mutating the Plk1 phosphorylation site targeted by MK2 blocked mitotic progression in HeLa cells. Additionally, depletion of MK2 resulted in spindle defects and a meiosis block in mouse oocytes[198]. Therefore, MK2 activity is present in metaphase. In *Xenopus* egg, MK2 has been reported to be relatively low abundant, especially compared to Chk1[199]. Together, these data suggested that phosphorylation of the Chk1 KAR in CSF extracts may partially also report MK2 activity. I have therefore renamed the KAR 'Chk1/MK2 reporter' (**Fig. 52**). Because Chk1 and MK2 have very similar consensus sequences, it will not be possible to construct a KAR that distinguishes between them. Optionally, the individual kinase activity can be further evaluated by using specific respective kinase inhibitors in the extract or by depletion either MK2 or Chk1.

Fourth, cellular PDK1, which is part of in the PI3K cascade (**Fig. 52**), exhibited low activity in CSF extracts. This result is not too surprising because high PDK1 activity is

usually observed early upon progesterone treatment. Residual PDK1 activity in CSF extracts may be required for Rsk2 activation, in addition to its phosphorylation by p42MAPK[88,200].

Finally, the constitutively active kinases CK1δ and CK2 were found to be present in CSF extracts. Previous experiments had suggested that CK1δ/ε acted as a mitotic kinase[199,201] that phosphorylated the early meiotic induction protein 2 (Emi2) at Ser644. This phosphorylation event was speculated to prevent Emi2 from binding to the anaphase-promoting complex/cyclosome and to thereby preserve metaphase[199]. Cellular CK1δ/ε levels were shown to significantly increase during spindle formation and CK1δ/ε inhibition prevented mitotic progression[201]. In case of CK2, activity of this highly abundant kinase had previously been detected in CSF extracts[202]. While these considerations might provide a rationale for active CK1δ in metaphase-arrested CSF extracts, they do not explain the presence of active CK2.

In summary, my results demonstrated the suitability of KARs in combination with time-resolved NMR readouts to determine cellular kinase activities in complex physiological environments such as CSF extracts. Using this novel tool, I simultaneously probed 8 different cellular kinase activities in parallel. Despite the impressive number (30-40) of different kinases that were analyzed by the MS-KAYAK approach using 90 different peptide substrates[41], this study did not specify the phosphorylation efficiencies of the different reporters. For example, the 'D1, D2, D3, and D4 peptides' were all used as protein kinase C (PKC) substrates, despite any information about their individual kinase 'affinities'. In addition, no information about cross-reactivity was provided. Therefore, quantifications based on KAYAK peptides have to be considered with caution.

Simultaneous profiling of multiple kinase activities in parallel also facilitates quantitative assessments of kinase inhibitor properties. Next, I will discuss the specific advantages of this method in identifying and characterizing kinase inhibitor efficiencies and specificities.

3.3 Insights into kinase inhibitor properties

Kinase are major drug targets in the pharmaceutical industries, especially for the treatment of cancer[51,203,204]. Numerous kinase inhibitors are based on ATP-analogues and compete with ATP in binding to kinases[51,52]. I tested kinase inhibitor specificities in multiplexed reaction setups (**2.8.3**) and found that 225 µM of Alsterpaullone for example, inhibited ~90% of the cellular Cdk1 activity in CSF extracts. This results is in good agreement with a previous study using [γ-^{32}P] ATP and a histone H1 reference peptide substrate[205]. Cellular inhibition of Cdk1 activity by Alsterpaullone, Cdk1 inhibitor 217695 and Cdk1/2 inhibitor III 217714 are consistent with *in vitro* assays, again using [γ-^{32}P] ATP-incorporation experiments, reported by Anastassiadis *et al*.,[163]. In this *in vitro,* activities of ~300 kinases and ~180 kinase inhibitors were annotated. Notably, the concentrations of kinase inhibitors used in CSF extract experiments were much higher than in other studies and the provided IC_{50} values. This is generally due to the fact that these inhibitor concentrations and IC_{50} values are usually determined in mammalian cell lysates, which are much less concentrated than CSF extracts (>100 mg/mL total protein).

KARs and NMR spectroscopy offer unique advantages for studying kinase inhibitors. Specifically, they enable accurate quantification of inhibitor specificities as shown in my example probing cellular Cdk1, Chk1 and Plk1 activities and cross-inhibition by the kinase inhibitors mentioned above. These tests required single NMR experiments only, whereas [γ-^{32}P] ATP-radionucleotide incorporation assays necessitate a much larger number of samples to obtain the comparable results[163,165]. Moreover, most kinase inhibitor studies are carried out *in vitro* and employ recombinant kinases, of which many are truncated versions of the respective enzymes. For developing a p70 ribosomal protein S6 kinase (p70S6K) inhibitor in one such study, only residues 1-421 of the catalytic kinase domain were employed. Therefore, interactions of this truncated kinase with the tested inhibitors may differ greatly from cellular, full-length kinase and false results may be obtained in consequence. The importance of investigating kinase activities in closely matching physiological environments and the most relevant biologically systems has increasingly been appreciated in the recent years. Especially in

this regard, KARs and NMR spectroscopy represent an important addition to the existing toolbox of phospho-detection and kinase activity profiling methods.

Besides quantifying cellular kinase activities and testing kinase inhibitors in physiological environments, NMR-base approaches can be further extended to analyze cellular phosphatase activity as well, which I will discuss in the following section.

3.4 Insights into kinase/phosphatase reactions

After being efficiently phosphorylated in CSF extracts, I monitored efficient dephosphorylation of Plk1, Chk1, PDK1 and CK2 KARs (**2.9.1**) (**Fig. 46, 47**). These results indicated the presence of active cellular serine/threonine phosphatases that appeared to specifically recognize this set of phospho-KARs and subsequently removed the individual phosphate moieties. Using the same concept as for cellular kinase activity profiling, I then quantified cellular phosphatase activities (**2.9.4**). Phosphatase assays were performed by pre-phosphorylating KARs in order to obtain pKARs. By time-resolved NMR, I simultaneously monitored NMR signal decrease of the phosphorylated residues and plotted individual dephosphorylation curves of pKARs. This demonstrated the suitability of NMR-based readouts of cellular phosphatase activities.

Most other phosphatase activity assays rely on the release of ortho-phosphate, which is subsequently measured in colorimetric detection experiments[206], or by radionucleotide release experiments[207]. Felix *et al.*, for example, employed ^{32}P-labeled skeletal muscle phosphorylase kinase and bovine casein to assess the activities of serine/threonine type 1 (PP1) and type 2A (PP2A) protein phosphatases. In their study, these authors found that both PP1 and PP2A were constantly active in 50% diluted CSF extracts. In my case, dephosphorylation of the pS Chk1 KAR was rather stable over 2 h in CSF extracts. Thus, cellular phosphatases appeared less prone to enzymatic fatigue than endogenous kinases. Additionally, the activity of PP2A *in vitro* with the pS Chk1 KAR was sustained. With these results, aging experiments in CSF extracts provided unbiased prove for the progressive reduction in cellular Chk1 activity while the cellular phosphatases were constant (**2.9.2**).

In a next step, I tested the effects of phosphatase inhibitors at different concentrations and found that 1.2 µM of okadaic acid, added to CSF extracts prior to KAR or pKAR measurements, greatly inhibited cellular phosphatase activities (**2.9.3**). The IC_{50} of okadaic acid is 0.1 nM and 10 nM for PP2A and PP1, respectively[208], which implied the presence of PP2A and PP1 activities in the CSF extract. It is interesting to note that the concentrations of okadaic acid used in the CSF extract NMR experiments were adjusted much to higher levels for full phosphatase inhibition. Again, this is likely due to greater overall protein concentrations in CSF extracts. Notably, the pS Chk1 reporter was proved to be a PP2A substrate *in vitro*. The results confirmed that cellular PP2A functioned on the dephosphorylation of the reporter in CSF extract, which corresponded to the fact that PP2A was abundant in the CSF extracts[209]. Moreover, previous studies had identified PP1 and PP2A as the cellular phosphatases that regulated dephosphorylation of Cdc25c Ser287 (numbering in *Xenopus*, in human the number is Ser216), which corresponds to the Chk1 KAR phospho-site[210-212]. Thus, dephosphorylation of the Chk1 KAR is accomplished by endogenous PP1 and PP2A activities in CSF extracts.

Although not every KAR was tested in okadaic acid-treated CSF extracts and *in vitro* with PP2A, data from several published works offer a basis for our understanding of the dephosphorylation behaviors of the Plk1 and PDK1 KARs. In the case of the Plk1 reporter, it is interesting to note that Plk1 itself is activated by phosphorylation of Thr210 by Aurora A and polo-like kinase kinase (Plkk)[213-215]. Plk1 deactivation is accomplished by dephosphorylation of Thr210 through PP2A[213] (**Fig. 52**). Thus, Plk1/Aurora A or Plkk activities may be higher at the beginning of the CSF extract experiment. As a result, Plk1 is activated and the phosphorylation of Plk1 reporter was detected. Progressive reductions in kinase activities in the 'aged' CSF extracts might possibly be met by unchanged PP2A activity, which eventually leads to KAR dephosphorylation.

For the second case, the PDK1 reporter sequence was generated based on activation-loop residues of the Akt protein kinase (**2.3.3**), whose own phosphorylation state is regulated via kinase and phosphatase actions. In Swiss 3T3 fibroblasts and rat adipocytes, dephosphorylation of full-length Akt by cellular PP2A has been reported[216,217]. Therefore, similar to the Plk1 KAR, cellular PP2A may also dephosphorylate the PDK1 KAR in CSF extracts (**Fig. 52**).

The function of CK2 in metaphase-arrest CSF extracts is unclear and dephosphorylation of the CK2 KAR equally enigmatic. CK2 regulation depends on autophosphorylation of the CK2 β-subunits[218,219]. Maybe, certain cellular phosphatases remove these activating CK2 signals over time in CSF extracts and thereby deactivate the kinase.

The constant phosphorylation state of the pT Cdk1 KAR and the pS Rsk2 KAR in CSF extract and *in vitro* with PP2A (**2.9.4**) suggested that the dephosphorylation of pKARs relied on the specificity of cellular phosphatases (i.e. PP2A) and the phospho-reporters. Unlike most serine/threonine kinases, most serine/threonine phosphatases are not thought to contain substrate consensus motifs. Phosphatases generally associate with a large number of possible substrates and many of their activities are controlled via intracellular localization[220]. In contrast to kinases, phosphatases specifically interact with a much larger variety of regulatory subunits, which, in most instances, determine substrate specificity[221,222]. These elaborate levels of regulating cellular phosphastase activities and specificities may well play into the differential modification and dephosphorylation behaviors that I had observed in CSF extracts.

In summary, the preliminary data from okadaic acid-treated CSF extracts and *in vitro* with PP2A, together with literature data suggest that phosphatases PP2A and/or PP1 may have been the acting activities to dephosphorylate the Chk1, Plk1, PDK1 and CK2 KARs. Besides, the constant phosphorylation state of some KARs such as Cdk1 and Rsk2 KARs indicate the specific recognition of phosphatases (i.e. PP2A) and their substrates. Roles for PP1 and PP2A in cell-cycle regulation are have been extremely investigated and both PP1 and PP2A have been implicated in the entry and exit of mitosis[210,211,213,223]. In this context, KARs and pKARs represent invaluable tools for future analyses.

Finally, during the cell extract preparation, the cells were disrupted either by spinning the whole eggs (*Xenopus* CSF egg extract) or by sonicating the cells (HeLa nuclear extract). This disruption step breaks cellular organelles, causing the release of phosphatases in the extract. The same KAR set probably exhibits a different degree of reversible phosphorylation in intact cell study.

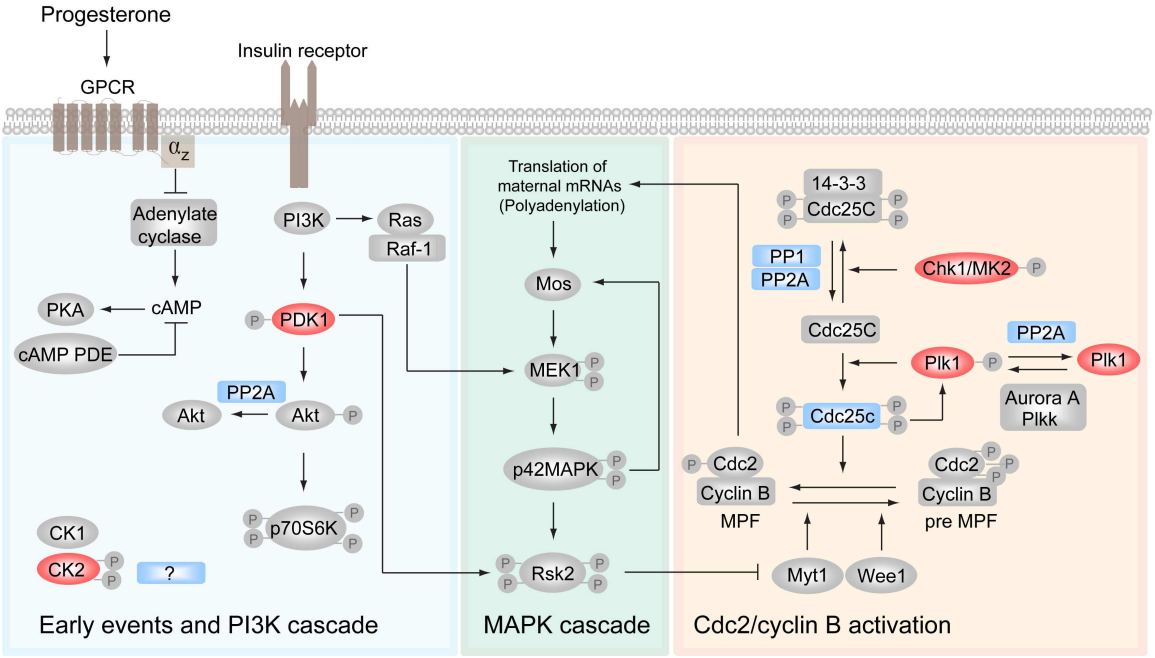

Figure 52. Cellular kinase and phosphatase activities in signaling pathways involved in meiotic cell cycle progression during *Xenopus* oocyte to egg maturation. Kinases for which KAR dephosphorylation has been established are shown in red. Active phosphatases are shown in blue.

4. PERSPECTIVES

This Ph.D. project has firmly established the combined use of time-resolved, quantitative NMR spectroscopy and site-selective ^{15}N isotope-labeled, peptide-based kinase activity reporters (KARs) as a suitable means to directly monitor multiple cellular kinase activities in parallel. Future studies will therefore include an expansion in the number of serine/threonine KARs and include KAR generation for tyrosine kinase profiling.

4.1 Expanding the existing KAR panel:

In this study, I have generated a first set of serine/threonine KARs, which I used to simultaneously examine 8 different kinases in *Xenopus* CSF egg extracts. As the maximum number of active kinases that can be simultaneously monitored is determined by the degree of spectral overlap of individual KAR NMR signals, future KARs will have to be designed with that in mind. Indeed with single residue-specific labeling, the spectral field is still largely open for new unique KARs. In the few cases where the spectra of two KARs overlap, one can probe the reaction using solely the increase in the relative phosphorylated species, as it is rare that both the unphosphorylated and phosphorylated peaks of different reporters overlap.

Similarly, future KARs will also target against tyrosine kinases. This particular avenue of investigations bears additional challenges, because the NMR characteristics of tyrosine phosphorylation are different to those of serine and threonine residues. Because tyrosine phosphorylation occurs at the distal phenyl moieties of the amino acids, phosphorylation-induced backbone-amide chemical shift changes of tyrosine residues are much less pronounced[170]. Rather than being at the tyrosine phosphorylation site, tyrosine phosphorylation events result in more significant backbone amide chemical shift changes in adjacent residues[224]. Site-selective labeling schemes of residues neighboring the actually modified tyrosines may indeed prove more suitable for tyrosine kinase activity reporters. Using residues neighboring profiling tyrosine kinase activities are actually advantageous because it increases the number of different amino acids (and therefore different unique chemical shifts) that can be ^{15}N-labled and mixed in a single NMR spectrum. Additionally, a tyrosine-KAR set could potentially be used to investigate

cellular kinase activities in pathological cell extracts, especially in cancer cell extracts because high activities of tyrosine kinases are often monitored in cancer cells[225,226].

4.2 In-cell NMR and KARs:

The *Xenopus* CSF extract model provides a well-characterized and reproducible standard system for profiling cellular kinase activities, but it only recapitulates a single stage of the eukaryotic cell-cycle, i.e. metaphase. Signaling during cell-cycle progression constitutes series of dynamic events and entails complex modification, cross-talks and multiple feedback loops. Those interested in cell signaling, ideally want to study kinase activities in living cells with temporal resolution, and it is this application of the NMR-KAR method that offers the most potential. One way to expand the CSF extract approach to whole cells is to microinject KARs into Stage VI *Xenopus* oocytes. Upon the addition of progesterone, oocyte maturation is triggered and the oocytes progress through meiosis I and II in a highly synchronized fashion. Cell-cycle regulated kinases become consecutively activated and repressed[72] and this could be monitored by time-resolved in-cell NMR spectroscopy. Furthermore, such *in vivo* NMR experiments could enhance our understanding of how individual layers of cross-talk between different kinase pathways execute regulated cell-cycle progression in eukaryotes.

4.3 Moving to mammalian systems:

As the Plk1 reporter conveyed Plk1 activity in HeLa nuclear extracts (**2.9.1**), the introduction of KARs into mammalian cells to determine multiple kinase activities *in vivo* would be another valuable and interesting application. Such experiments would rely on the development of reproducible and high-throughput approaches for protein/peptide delivery into mammalian cells. To this aim, cell-penetrating peptides[227,228], pore forming toxin Streptolysin[229,230] and protein/peptide electroporation (unpublished results) have been developed in the Selenko laboratory. The amount of KAR uptake and the remaining kinase activities inside the cells would have to be determined to further develop such a technique.

4.4 Screening phosphatase-substrate specificities with pKARs

I have demonstrated the possibility to use pre-phosphorylated KARs (pKARs) and NMR to quantify phosphatase activities in cell lysates and *in vitro*. This tool can also be applied to screen for phosphatase-substrate specificities and probably reveals the specific recognition elements.

4.5 Observing other PTMs:

The concept of KARs and NMR can also be extended to construct reporters for other post-translational protein modifications. For instance, generating acetyl-transferase activity reporters by selective isotope labeling of lysine residues has successfully been reported[231,232]. Similarly, methyltransferase activity reporters could be generated[233]. Additional sets of reporters, together with other diagnostic tools, can then be used to study entire protein signaling networks under both physiological and pathological conditions and inside whole cells.

5. MATERIALS AND METHODS

5.1 Materials

5.1.1 Vectors and primers

pET-DUET vectors were purchased from Novagen and primers were synthesized by Eurofins MWG Operon (Germany)

5.1.2 Chemicals

In general, chemicals from these companies were used: Roche (Mannheim), Amersham-Pharmacia (Freiburg), Sigma-Aldrich (Steinheim), AppliChem (Darmstadt), Roth Chemicals (Karlsruhe), Lucigen (USA).

5.1.3 Enzymes and cofactors

High fidelity Phusion polymerase	Finnzymes/Thermo Fisher Scientific
DpnI	New England Biolabs (Schwalbach)
Kinases	SignalChem (Canada)
	New England Biolabs (Schwalbach)
Adenosine triphosphate (ATP)	Fermentas/Thermo Fisher Scientific
Cyclic AMP	Sigmal-Aldrich (Steinheim)
$CaCl_2$ and calmodulin mixed solution	SignalChem (Canada)
L-α-Phosphatidyl-D-myo-inositol 3,4,5-triphosphate, dioctanoyl	Sigmal-Aldrich (Steinheim)
Okadaic acid	Applichem (Darmstadt)
Carboxypeptidase inhibitor from potato tuber mixture:	Sigma-Aldrich (Steinheim)
1,10 Phenanthroline HCl hydrate 97%	Sigma-Aldrich (Steinheim)
(2-Guanidinoethylmercapto) succinic acid	Fuka
Cdk1 inhibitor 217695	Calbiochem
Alsterpaullone	Calbiochem
Cdk1/2 inhibitor III 217714	Calbiochem
Serine/threonine protein phosphatase type 2A (PP2A)	Millipore (Schwalbach)

5.1.4 Kits and consumables

Qiagen Plasmid Extraction Kit	Qiagen (Hilden)
DNA ladder	New England Biolabs (Schwalbach)
ColorBrust protein marker	Sigmal-Aldrich (Steinheim)
ColorPlus Prestained protein marker	New England Biolabs (Schwalbach)
Dialysis membrane MWCO 3,500 Da	VWR Germany GmbH (Darmstadt)
Amicon Ultra MWCO 3,000 Da	Milipore (Schwalbach)

5.1.5 Microorganisms

E. coli BL21 (DE3) express	F^-*ompT hsdS*$_B$ (*r*$_B^-$*m*$_B^-$)*gal dcm* (Lucigen, USA)
E. coli BL21 (DE3) pLysS	F *ompT hsdS*$_B$ (*r*$_B$ *m*$_B$) *gal dcm* (Cm^R) (Lucigen, USA)

5.1.6 Media and antibiotics

Luria-Bertani (LB)		10 g/L Bactotryptone, 10 g/L NaCl, 5 mM NaOH, 5 g/L yeast extract (Sigma-Aldrich, Steinheim)
M9 minimum		6 g/L Na_2HPO_4, 3 g/L KH_2PO_4, 0.5 g/L NH_4Cl, 0.5 g/L NaCl, 4 g/L Glucose (AppliChem, Darmstadt)
Trace elements solution	(100X, 1 L)	5 g EDTA, 0.83 mg $FeCl_3$x $6H_2O$, 84 mg $ZnCl_2$, 13 mg $CuCl_2$x $2H_2O$, 10 mg $CoCl_2$x $6H_2O$, 10 mg H_3BO_3, 1.6 mg $MnCl_2$x $6H_2O$
O solution (500 mL)		28.8 g $MgCl_2$x $6H_2O$, 10 mL $FeCl_2$ stock solution
$FeCl_2$ stock solution (100 mL)		8 mL 37% HCl, 5 g $FeCl_2$, 184 mg $CaCl_2$x$2H_2O$, 64 mg H_3BO_3, 40 mg $MnCl_2$x

	$4H_2O$, 18 mg $CoCl_2x\ 6H_2O$, 4 mg $CuCl_2x\ 2H_2O$, 340 mg $ZnCl_2$, 605 mg $NaMoO_4x\ 2H_2O$
S solution (100 mL)	4.8 g K_2SO4
Vitamin solution (1 L)	50% (v/v) ethanol, 1.1 mg biotin, 1.1 mg folic acid, 110 mg para-aminobenzoic acid, 110 mg ribo flavin, 220 mg pantothenic acid, 220 mg pyridoxine HCl, 220 mg thiamine HCl, 220 mg niacinamide
^{15}N-NH_4Cl	Cambridge Isotope Laboratories (USA)
Kanamycin	Applichem (Darmstadt)
Ampicillin	Applichem (Darmstadt)
Chloramphenicol	Applichem (Darmstadt)

5.1.7 Metaphase-arrested *Xenopus laevis* egg extract preparation supplies

Cycloheximide	Sigmal-Aldrich (Steinheim)
Cytohalasin D	Sigmal-Aldrich (Steinheim)
Dithiotreitol	Sigmal-Aldrich (Steinheim)
Roche complete, EDTA-free-Protease inhibitor	Roche (Mannheim)
14X95-mm Ultraclear tubes	Beckman
MMR buffer	0.1 mM EDTA, 0.1 M NaCl, 2 mM KCl, 1 mM $MgCl_2$, 2 mM $CaCl_2$ and 5 mM Na-Hepes, adjust pH with NaOH to pH 7.8
Extract buffer (XB)	10 mM KCl, 0.1 mM $CaCl_2$, 1 mM $MgCl_2$, 50 mM Sucrose and 10 mM potassium HEPES, adjust pH with KOH to pH 7.7

Dejellying solution	XB buffer supplemented with 2% (w/v) Cystein
CSF-XB buffer	XB buffer supplemented with 2 mM $MgCl_2$ and 5 mM EGTA pH 7.7
CSF-XB-Protease inhibitor	200 mL CSF-XB buffer supplemented with 2 tablets of Roche complete, EDTA-free protease inhibitor

5.1.8 Solid phase peptide synthesis supplies

Fmoc-amino acid derivatives	GLS (China)
^{15}N-Serine-OH	Cambridge Isotope Laboratories (USA)
^{15}N-Threonine-OH	Cambridge Isotope Laboratories (USA)
2-(1H-benzotriazole-1-yl)-1,1,3,3-tetra methyluroniumhexafluorophosphate (HBTU)	Merck Novabiochem (Darmstadt)
N-(9-Fluorenylmethoxycarbonyloxy) succinimide	Sigma-Aldrich (Steinheim)
Tentagel PAP resin	Rapp Polymere (Tübingen)
Tentagel RRAM resin	Rapp Polymere (Tübingen)
2-unit and 10-unit PEG resins	Daniela Ponader and Dr. Laura Hartmann Max Planck Institute of Colloids and Interfaces, Potsdam
Other chemicals	Sigma-Aldrich (Steinheim)

5.1.9 NMR supplies

Deuteriumoxide 99.8%	Sigma-Aldrich (Steinheim)
Dimethylsulfoxide-D6	Deutero GmbH (Kastellaun)
Shigemi tubes	Deutero GmbH (Kastellaun)

5.2 Molecular biology methods

5.2.1 Restriction free cloning

5.2.1.1 Primer design

KAR construct was achieved by means of restriction-free (RF) cloning method[234]. KAR primers were typically designed based on pET-DUET vector (NOVAGEN). Nucleotide sequence of the forward primer of each KARs had a 24 base overlap with the vector at a Tobacco etch virus (TEV) protease cleavage site; 5' GAAAACCTGTATTT TCAGGGA 3'. The primers were elongated with nucleotide sequences of kinase substrate consensus sequences (30-45 bases). Finally, the forward primers were terminated with another 24 bases annealing to the vector to the 3' end of insertion point. The terminating sequence was based on N-terminal sequence of a soluble protein B1 domain of *Streptococcal* protein G (GB1): 5' CAGTACAAACTTATCCTGAACGG 3'. Reverse primers were complementary with the forward primer 3' → 5'.

5.2.1.2 Linear amplification reaction

Linear amplification reactions were performed in a total volume of 50 µL of 200 µM dNTP's, 1x reaction buffer, 25-50 ng pETDuet vector, 150 ng forward primer, 150 ng reverse primer and 2.5 unit PfuTurbo^{TM} (Stratagene). The mixture was heated for 30 s at 95 ºC, followed by 35 cycles of denaturation at 95 ºC (30 s), annealing at 58 ºC (1 min) and elongation at 72 ºC (8 min). PCR products were observed by agarose gel electrophoresis. The parental plasmid was digested by incubating the PCR products with 20 unit Dpn I at 37 ºC for 3 h.

5.2.2 Agarose gel electrophoresis

1% Agarose gels were prepared in 50 mL TE buffer (AppliChem) with 3 µL of 0.07% Ethidium Bromide (AppliChem). Electrophoresis experiments were carried out at 100 V for 30 min using Bromophenol Blue (AppliChem) as dye.

5.2.3 Electro-competent cells

According to a published protocol[235], *E. coli* BL21 (DE3) express pre-culture was inoculated in 5 mL LB medium and incubated overnight at 37 ºC. Next day, the pre-culture was transferred into 1 L LB medium and incubated at 37 ºC until an optical

density at 600 nm wavelength (OD_{600}) reached 0.5-0.6. After that, the culture was incubated on ice for 15 min prior to centrifuging at 4,000 g, 20 min, at 4 ºC. The resultant cell pellet was resuspended in 500 mL ice-cold sterile water and was subsequently centrifuged. The supernatant fraction was discarded and the pellet was resuspended with 500 mL ice-cold water. Then, the bacteria were pelleted at 600 g, 15 min, at 4 ºC. Eventually, the cell pellet was resuspended in 80 mL cold water supplemented with 10% glycerol and the cells were aliquoted, flash frozen and stored at -80 ºC.

5.2.4 Transformation

5 µL of DpnI digested PCR product was transformed into 50 µL electro competent *E. coli* BL21 (DE3) express cells by means of electroporation method[235]. The electroporation was performed with a 1 mm gap width-electroporation cuvette (Eppendorf, Hamburg) 1.8 kV and 200-400 ohms pulse. Next, 1 mL recovery medium (Lucigens) was immediately subjected into the cells. The cells were incubated at 37 ºC for 1 h prior being plated on a LB supplemented with 35 µg/mL kanamycin plate. The plate was incubated at 37 ºC for overnight.

5.2.5 Colony selection and DNA sequencing

Colonies from the transformation were tested their protein expression. Only the colonies with expected protein expression were selected and subjected to DNA sequencing. The DNA sequencing was performed by Invitek (Berlin).

5.2.6 Plasmid DNA extraction

DNA plasmids were extracted and purified by means of QIAprep Spin Miniprep Kit (Qiagen).

5.3 Biochemical methods

5.3.1 SDS-PAGE

All of electrophoresis experiments were performed with 18% SDS-PAGE unless specify. The gels were stained Coomassie brillant blue solution (Sigma Aldrich) and were de-stained with water.

5.3.2 Protein concentration determination

Accurate protein concentration was determined by absorption assays at 280 nm[236].

5.3.3 Protein overexpression and uniform isotope labeling

5.3.3.1 Recombinant KAR expression for colony selection

Each colony from the transformation was inoculated in 1 mL LB medium supplemented with 35 µg/mL kanamycin. When the culture reached OD_{600} approximately 0.5, the culture was induced protein expression by addition of 1 mM isopropyl β-D-thiogalactopyranoside (IPTG). After 4 h induction, the culture was pelleted and the protein expression of each colonies was detected by 18% SDS-PAGE.

5.3.3.2 Recombinant KARs expression and uniform isotope labeling

Transformed bacteria containing the KAR plasmid were inoculated in 10 mL M9 minimal medium using $^{15}NH_4Cl$ as a sole nitrogen source. Besides, the medium was supplemented with 1X Trace element, 1 µg/mL biotin, 1 µg/mL thiamin, 35 µg/mL kanamycin. Next day, the pre-culture were transferred into 500 mL M9 medium with mentioned additional substances. The protein induction was carried out by supplement of 0.4 mM IPTG when OD_{600} of the culture reached about 0.6. The cultivation was continued for an additional 4 h at 37 ºC. Cells were then harvested by centrifuging at 6,600 g for 15 min at 4 ºC. The pellet was flash frozen and stored at -80 ºC.

5.3.4 Purification of recombinant KAR

All recombinant proteins were expressed as fusion proteins of a N-terminal His-tag (6xH), followed by the protein domain GB1 and TEV protease cleavage site. At the C-

terminal side of the TEV site, the construct was fused with kinase substrate consensus sequences followed with a second protein domain GB1. The recombinant KAR cell pellet, which was collected from 500 mL culture (see above), was resuspended in 10 mL of 20 mM potassium phosphate at pH 8.0 containing 150 mM NaCl, 10 mM imidazole, 0.1% Triton-X, 1 mg/mL lysozyme and 1 tablet complete Protease inhibitors (Roche), 10 µg DNAse (AppliChem) and 100 µg RNase (AppliChem). The cells were disrupted by sonication on ice. The resultant cell lysate was spun at 30,000 g for 30 min at 4 ºC to remove insoluble materials. The supernatant protein was applied onto a Nickel column (Qiagen) equilibrated with the lysis buffer. The protein was eluted from the column with a buffer containing 20 mM potassium phosphate at pH 8.0, 150 mM NaCl and 300 mM imidazole. Fractions containing KARs were collected and the N-terminal tag was removed by TEV cleavage. The cleavage reaction was incubated for 1 h at room temperature before the protein was dialyzed against 20 mM potassium phosphate at pH 8.0 containing 150 mM NaCl at 4 ºC for overnight. The cleaved N-terminal tag was separated from the GB1-fused reporter by the second Nickel affinity chromatography. The recombinant KARs were further purified with size exclusion chromatography (Hi-load Superdex 30, GE Healthcare) equilibrated with 20 mM potassium phosphate at pH 7.5 containing 150 mM NaCl. The KARs were concentrated with 4,000 g (Amicon Ultra MWC 3000 Da) and protein concentration was determined from UV absorption using a cell with an optical path length of 1 cm.

The purified KARs were aliquoted, frozen in liquid nitrogen and stored at -80 ºC prior NMR experiments.

5.3.5 Production of tobacco etch virus (TEV) protease

The pTPSN plasmid containing the TEV protease gene was transformed into *E.coli* BL21(DE3) pLysS strain. The TEV culture in 1 L LB with 35 µg/mL kanamycin and 35 µg/mL chloramphenicol was incubated at 37 ºC. After reaching OD_{660nm} 0.5, the culture was cooled down to 22 ºC. The TEV protein induction was achieved by supplement of 1 mM IPTG to the culture. The culture was continually incubated at 22 ºC for overnight. The cell was harvested by centrifuging at 4,000 g for 15 min at 4 ºC. The cell pellet was resuspended with the lysis buffer (**see 5.3.4**) and the cells were disrupted by sonication on ice. After centrifugation, the protein in soluble part was subsequently applied to the

Nickel column. The elution fractions were analyzed by 18% SDS-PAGE. The TEV fractions were desalted using a PD-10 desalting column (GE Healthcare) and the protein was stored in 20 mM Tris-HCl buffer, 150 mM NaCl, 2 µM DTT and 10% glycerol. The protease was aliquoted and frozen in liquid nitrogen and stored at -80 ºC.

5.3.6 Cyclin B Δ90 production

I kindly obtained the cyclin B Δ90 ligated pET3b plasmid from Hideki Yokoyama, Mattaj Group, European Molecular Biology Laboratory, Heidelberg. The protein expression and purification protocols are briefly described here[101]. The plasmid was transformed into *E.coli* BL21(pLysS)-Expression strain. 1 L of cyclin B Δ90 culture in LB supplemented with 50 µg/mL ampicillin and 35 ug/mL chloramphenicol was incubated at 37 ºC until the culture reached OD_{660nm} 0.4. The cyclin B Δ90 expression was induced with 0.2 mM IPTG and the culture was subsequently incubated for 1 h at 37 ºC. Then, I harvested the cells by spinning the cell at 4,000 g for 15 min at 4 ºC. The cell pellets were washed with 0.9% NaCl solution before the second centrifugation. I then resuspended the pellet with 25 mL Buffer A (10 mM Tris, 50 mM NaCl, 1 mM EDTA pH 8.0) containing 5 mM DTT, 0.05% Nonidet P-40 and 1 tablet protease inhibitor and incubated the cells on ice for 15 min. Next, I disrupted the cells by sonication for 2 min on ice. The lysate was spun in a Sorvall SS-34 rotor at 20,000 g for 15 min at 4 ºC. The pellet was washed with 10 mL Buffer A supplemented with 0.5 M NaCl before being centrifuged again. I resuspended the pellet with 20 mL Buffer A containing 8 M Urea and 5 mM DTT. The protein was gradually diluted with 20 mL Buffer B (50 mM Tris, 100 mM KCl, 5 mM $MgCl_2$ and 5 mM DTT) before being centrifuged at 20,000 g for 5 min in a Sorcall HB-4 rotor at 4 ºC. The supernatant was dialyzed against 1 L Buffer B with 5 mM DTT for 4 h. It is recommended to renew the dialysis buffer 3 times during the process. The protein was aliquoted and frozen with liquid nitrogen before being stored at -80 ºC.

5.3.7 Metaphase-arrested *Xenopus* egg extract preparation

5.3.7.1 Primed frogs

Female *Xenopus* frogs were injected with 100 U pregnant mare serum gonadotropin (PMSG, Sigma-Aldrich) 3-14 days prior harvesting the eggs. The PMSG induces maturation of frog oocytes. 16-18 h before extract preparation, the primed frogs were induced to ovulate by injection with 500 U human chorionic gonadotropin (HCG, Sigma-Aldrich). Each primed frog was placed individually into a plastic bucket containing MMR buffer and was stored at 16 ºC for overnight.

5.3.7.2 Metaphase-arrested *Xenopus laevis* egg extract preparation

The cytostatic factor-arrested metaphase egg extracts were prepared as follow[70]. Next day, XB, CSF-XB, CSF-XB-Pi buffers and dejellying solution were freshly prepared. Laid *Xenopus* eggs from each frogs were collected with 600-mL beakers. The laid eggs were washed with MMR buffer until all of the debris was removed. Then, jelly surrounding the eggs was removed by gentle swirling the eggs in dejellying solution for 4-5 min. When the eggs are dejellied, the egg volume decreases. The eggs pack tightly and orient with their vegetal poles down. Next step, the eggs were washed several times with CSF-XB to remove the dejellying solution. After that, CSF-XB-Pi was rinsed into the eggs.

The eggs were transferred into 14x95-mm ultraclear tubes containing 1 mL CSF-XB-Pi and 20 µg/mL cytochalasin D. The eggs were slowly packed by spinning at 100 g for 30 sec and at 500 g for 1 min at 16 ºC. Excess buffer in the top layer of the ultraclear tubes was removed. Crashing the eggs was performed by spinning at 15,000 g for 20 min at 16 ºC. Three layers are obtained from the crashed eggs. The top yellow represented lipid droplets while the dark layer at the bottom of the tube contained pigment granules, nuclei and yolk proteins. The cytoplasmic layer, as *Xenopus* CSF extract, was located in the middle of the tubes. The CSF extract was collected and was supplemented with 10 µg/mL protease inhibitor, 20 µg/mL cytochalasin D and 1.7% (v/v) cyclin B Δ90. The extract was eventually aliquoted, frozen with liquid nitrogen and stored at -80 ºC.

5.3.7.3 Cytostatic factor (CSF)-arrested metaphase egg extracts test

To confirm stage of the CSF extract, 20 µL of the extract was mixed with 2,000-6,000 *Xenopus laevis* sperm nuclei and 0.5 µg tubulin labeled with tetramethyl rhodamine isothiocyanate rhodamine dye (Tebu Bio). The spindle assembly sample was incubated for 30-60 min at 20 ºC. The sample slide was prepared by placing 1 µL of the sample on a microscope slide, followed with 1 µL fixing solution on the top. The slide was covered gently with an 18X18-mm cover slip. The half spindle or spindle formation was observed by Fluorescence microscopy.

According to the previously published protocol[237], *Xenopus* sperm nuclei were prepared by Hideki Yokoyama.

5.3.7.4 High-speed CSF arrested egg extract preparation

High-speed CSF egg extract was achieved by additionally spinning the CSF extracts at 100,000 g for 1 h at 16 ºC (11x 34mm centrifuge tubes, TLS55 rotor). Pure cytoplasm at the top layer was collected.

5.4 Solid phase peptide synthesis

5.4.1 Generation of Fmoc-derivative amino acids

The coupling reaction of Fmoc-^{15}N-Ser-OH or Fmoc-^{15}N-Thr-OH was set up by adding in a dropwise fashion of 2 mmol N-(9-Fluorenylmethoxycarbonyloxy) succinimide (in 2 mL dioxane) into 2 mmol ^{15}N-Ser-OH/^{15}N-Thr-OH (in 2 mL of 10% Na_2CO_3). The reaction was incubated for overnight at room temperature (**Fig. 53**). Next day, the reaction pH was adjusted to 2.0 by 1 M HCl. The product was subsequently extracted from the reaction with ethylacetate and was washed with H_2O and with saturated NaCl, respectively. Ethylacetate was removed by evaporation and the crude product was dried under vacuum. Fmoc-^{15}N-Ser-OH/Fmoc-^{15}N-Thr-OH crude was purified by means of a preparative HPLC C18 column. The mass of the Fmoc-^{15}N-derivative was verified by ESI-MS analysis.

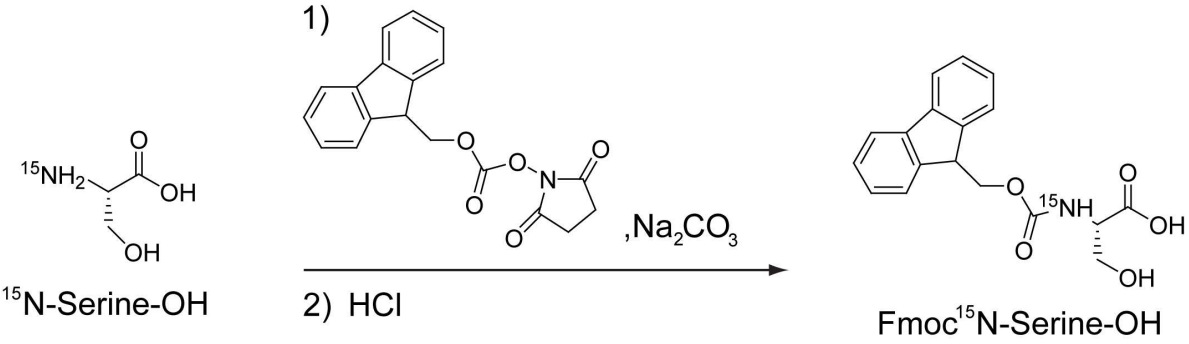

Figure 53. Fmoc ^{15}N-Serien-OH synthesis schematic.

5.4.2 Fmoc-based solid phase peptide synthesis (SPPS)

Peptide KARs were synthesized on a 25 µmol scale using standard Fmoc-based solid-phase chemistry on a Intavis Respep XL synthesizer. Tentagel RRAM resin (capacity: 0.19 mmol/g) was used as a solid support for peptides and D-amino acid containing peptides. The resins from Daniela Ponader and Dr. Laura Hartmann were used for synthesizing the peptides fused with 2-unit and 10-unit PEG (capacity: 0.15 mmol/g and 0.25 mmol/g, respectively). In order to conjugate the peptides with multiple PEG units, Tentagel PAP resin (capacity: 0.22 mmol/g) was used as a solid support. Side chains of Fmoc-amino acids were protected as follows: Glu(OtBu), Asn(Trt), Thr(tBu), Tyr(tBu),

Arg(Pbf), Asn(Trt), Asp(OtBu), His(Trt), Lys(Boc) and Ser(tBu). 250 µmol of Fmoc-amino acid stocks were prepared in dimethylformamide (DMF). Removal of the Fmoc group was carried out with 20% piperidine in DMF. Couplings were achieved using 225 µmol of HBTU (in DMF) as the activation agent and 0.6 mM of N-Methylmorpholine (NMM) in DMF/NMP. The automated peptide synthesis machine started coupling the C-terminal amino acid of peptide KAR with the resin. The synthesis continued until the sequence of the peptide reached the phosphorylatable amino acid residue.

In order to selective NMR isotope label the reporter, the resultant synthetic KAR was manually coupled with a mixture of 100 µmol Fmoc-protected isotope-labeled derivatives (Fmoc-^{15}N –Ser-OH or Fmoc-^{15}N-Thr-OH), 87.5 µmol HBTU and 0.6 mmol NMM in DMF. The reaction was incubated for 3 h under N_2 gas at room temperature. The side chain of Fmoc-^{15}N-Ser was protected by an additional transient protection. The protection reaction was incubated with 125 µmol triphenylchloromethane and 250 µmol N,N-Diisopropylethylamine (DIPEA) in DMF for 1 h.

The automated peptide synthesis machine completed the rest of peptide sequences. Every synthetic KAR was N-terminally capped with acetylglycine.

5.4.3 Peptide cleavage and precipitation

The peptides were detached from the resin, at the same time, with complete removal of the side-chain protection groups by a cleavage cocktail. The cocktail consisted of TFA/ Phenol/ Triisopropylsilane/ H_2O (85:5:5:5) and the cleavage reaction was incubated for 3.5 h at room temperature. The cleaved products were precipitated in cold diethyl ether before being centrifuged at 4,000 g for 10 min at 4 ºC. The peptide products were present in either precipitation form or in ether phase depending on their fusion groups. Eventually, the crude peptides were lyophilized for overnight.

5.4.4 Purification of peptide-based KARs

The peptide crudes were purified on a Varian ProStar 210 HPLC system equipped with a Dynamax C18 column (8 µm, 250x21.4 mm, Varian). The purifications were conducted with 0.1% TFA in water (Buffer A) and 80% acetonitrile, 0.1% TFA in water (Buffer B).

The peptides were eluted with gradient of buffer B (5-95%) for 60 min, flow rate 13 mL/min. The peptide mass was analyzed by either MALDI-MS or ESI-MS and the purity of the peptide products was confirmed by analytical RP-HPLC. The analytical HPLC was performed on a Varian ProStar 210 HPLC system with a Nucleosil C18 column (5 μm, 4.6x250 mm, Machery-Nagel). The analytical gradient was 5-95% buffer B for 60 min with a flow rate of 1 mL/min. The peptide-based KARs were lyophilized for overnight and were stored at 4 ºC.

5.4.5 Mass spectrometry analysis

ESI-MS analysis was conducted by Alexander Dose on a Mariner ESI-TOF (Applied Biosystems). The peptide mass was also analyzed by MALDI-MS on a MALDI-TOF-TOF, 4700 Proteomics Analyzer (Applied Biosystems) by using α-cyano-4-hydroxycinnamic acid as a matrix.

5.5 NMR experiments

5.5.1 Sample preparation

Reference samples contained 50 µM of ^{15}N-labeled recombinant or synthetic KARs and 10% (v/v) D_2O in 20 mM potassium phosphate buffer pH 7.5/ pH 6.4 with 150 mM NaCl in total volume of 300 µL. *In vitro* phosphorylation reactions were in the same buffer as reference samples supplemented with 0.3 mM ATP and 3.3 mM $MgCl_2$ and defined amounts of corresponding kinases and cofactors. *In extract* samples consisted of 50 µM ^{15}N-labeled KARs, 3.3 mM $MgCl_2$, 220 µLCSF-extract and 30 µL D_2O. All NMR samples were loaded in Shigemi NMR tubes (5 mm diameter) for the NMR measurements.

5.5.2 Data collection

All NMR measurements were operated at 298K with either 600MHz or 750MHz Bruker Advance Spectrometer equipped with a {^{1}H/^{13}C, ^{15}N} cryoprobe. 1D ^{15}N/^{1}H correlation NMR spectra were recorded with 1024 (^{1}H) and acquisition time per experiment was approximately 1.5 min. At the beginning of this project, I recorded 2D ^{15}N/^{1}H HSQC correlation spectra of uniformly ^{15}N labeled recombinant KARs with 64 transients and 1024 (^{1}H) x 256 (^{15}N) complex points (interscan delay=1.3 s, 48 min per acquisition time). Afterward, our laboratory succeeded in setting up 2D ^{15}N/^{1}H SOFAST-HMQC correlation spectra with 8 transients and 2048 (^{1}H) x 256 (^{15}N) complex points (interscan delay=60 ms, 6 min per acquisition time). This set up was used for the experiments with uniformly ^{15}N labeled recombinant KARs. Besides, we set up 2D ^{15}N/^{1}H SOFAST-HMQC correlation spectra with 32 transients and 1024 (^{1}H) x 256 (^{15}N) complex points (interscan delay=60 ms, 8 min per acquisition time) for multiple peptide-based KARs experiments. We have indeed shown that sofast-HMQC pulse sequence with short interscan delays provides around 10 times better signal-to-noise ratio for measurements an unfolded peptide at room temperature and at pH > 6.8[238].

Sample preparation required approximately 5 min before NMR data acquisition. In addition, time-resolved NMR data were recorded in the identical setup *in reference*, *in vitro* and *in extract* NMR experiments.

5.5.3 NMR spectra analysis

NMR spectra were processed by zero-filling (ZF) to 2 K and 256 points in the proton and nitrogen dimension, respectively. 90º (^{1}H) and 90 º bell-sine window functions were used for apodization. All data were processed with iNMR 3.3.9.

5.5.4 Analysis of phosphorylation kinetic

The peak intensities of ^{1}H/^{15}N resonance cross peaks at the individual time points were integrated with iNMR 3.3.9. The data were normalized and the kinetic plots were fitted with GraphPad Prism 5.0. In most cases, the reactions were performed in conditions where the substrate (KAR) concentration is lower than the K_m of the enzymes. I used thus a first-order rate exponential function to fit the evolution curves of substrate/product concentrations:

$$[S] = S_0 \exp(-t/T_{Phosphorylation})$$

$$[P] = P_0 (1-\exp(-t/T_{Phosphorylation}))$$

For a case where the substrate concentration is higher than the considered K_m, I used a linear function to fit the initial evolution curve (before the plateau due to complete reaction).

$$[S] = \frac{S_0}{T_{Phosphorylation}} \times (1- t)$$

$$[P] = \frac{P_0}{T_{Phosphorylation}} \times t$$

6. REFERENCES

1. Cohen, P. The role of protein phosphorylation in human health and disease. The Sir Hans Krebs Medal Lecture. Eur J Biochem 268, 5001-10 (2001).
2. Ubersax, J. A. & Ferrell, J. E., Jr. Mechanisms of specificity in protein phosphorylation. Nat Rev Mol Cell Biol 8, 530-41 (2007).
3. Manning, G., Plowman, G. D., Hunter, T. & Sudarsanam, S. Evolution of protein kinase signaling from yeast to man. Trends Biochem Sci 27, 514-20 (2002).
4. Manning, G., Whyte, D. B., Martinez, R., Hunter, T. & Sudarsanam, S. The protein kinase complement of the human genome. Science 298, 1912-34 (2002).
5. Johnson, L. N. & Barford, D. The effects of phosphorylation on the structure and function of proteins. Annu Rev Biophys Biomol Struct 22, 199-232 (1993).
6. Groban, E. S., Narayanan, A. & Jacobson, M. P. Conformational changes in protein loops and helices induced by post-translational phosphorylation. PLoS Comput Biol 2, e32 (2006).
7. Cheng, Y., Zhang, Y. & McCammon, J. A. How does activation loop phosphorylation modulate catalytic activity in the cAMP-dependent protein kinase: a theoretical study. Protein Sci 15, 672-83 (2006).
8. Cohen, P. The origins of protein phosphorylation. Nat Cell Biol 4, E127-30 (2002).
9. Wehr, M. C., Reinecke, L., Botvinnik, A. & Rossner, M. J. Analysis of transient phosphorylation-dependent protein-protein interactions in living mammalian cells using split-TEV. BMC Biotechnol 8, 55 (2008).
10. Nardozzi, J. D., Lott, K. & Cingolani, G. Phosphorylation meets nuclear import: a review. Cell Commun Signal 8, 32 (2010).
11. Giasson, B. I. & Mushynski, W. E. Aberrant stress-induced phosphorylation of perikaryal neurofilaments. J Biol Chem 271, 30404-9 (1996).
12. Krook, A. et al. Characterization of signal transduction and glucose transport in skeletal muscle from type 2 diabetic patients. Diabetes 49, 284-92 (2000).
13. Radivojac, P. et al. Gain and loss of phosphorylation sites in human cancer. Bioinformatics 24, i241-7 (2008).
14. Mora, A., Komander, D., van Aalten, D. M. & Alessi, D. R. PDK1, the master regulator of AGC kinase signal transduction. Semin Cell Dev Biol 15, 161-70 (2004).
15. Echols, N. et al. Comprehensive analysis of amino acid and nucleotide composition in eukaryotic genomes, comparing genes and pseudogenes. Nucleic Acids Res 30, 2515-23 (2002).
16. Thomason, P. & Kay, R. Eukaryotic signal transduction via histidine-aspartate phosphorelay. J Cell Sci 113 (Pt 18), 3141-50 (2000).

17. Klumpp, S. & Krieglstein, J. Reversible phosphorylation of histidine residues in vertebrate proteins. Biochim Biophys Acta 1754, 291-5 (2005).
18. Besant, P. G., Attwood, P. V. & Piggott, M. J. Focus on phosphoarginine and phospholysine. Curr Protein Pept Sci 10, 536-50 (2009).
19. Ciesla, J., Fraczyk, T. & Rode, W. Phosphorylation of basic amino acid residues in proteins: important but easily missed. Acta Biochim Pol 58, 137-48 (2011).
20. Besant, P. G. & Attwood, P. V. Mammalian histidine kinases. Biochim Biophys Acta 1754, 281-90 (2005).
21. Johnson, S. A. & Hunter, T. Kinomics: methods for deciphering the kinome. Nat Methods 2, 17-25 (2005).
22. Seger, R. & Krebs, E. G. The MAPK signaling cascade. Faseb J 9, 726-35 (1995).
23. Johnson, G. L. & Lapadat, R. Mitogen-activated protein kinase pathways mediated by ERK, JNK, and p38 protein kinases. Science 298, 1911-2 (2002).
24. Tardito, D. et al. Signaling pathways regulating gene expression, neuroplasticity, and neurotrophic mechanisms in the action of antidepressants: a critical overview. Pharmacol Rev 58, 115-34 (2006).
25. Parikh, J. R., Klinger, B., Xia, Y., Marto, J. A. & Bluthgen, N. Discovering causal signaling pathways through gene-expression patterns. Nucleic Acids Res 38, W109-17 (2010).
26. Ferrell, J. E., Jr. Xenopus oocyte maturation: new lessons from a good egg. Bioessays 21, 833-42 (1999).
27. Schmitt, A. & Nebreda, A. R. Signalling pathways in oocyte meiotic maturation. J Cell Sci 115, 2457-9 (2002).
28. Muslin, A. J., Klippel, A. & Williams, L. T. Phosphatidylinositol 3-kinase activity is important for progesterone-induced Xenopus oocyte maturation. Mol Cell Biol 13, 6661-6 (1993).
29. Palmer, A., Gavin, A. C. & Nebreda, A. R. A link between MAP kinase and p34(cdc2)/cyclin B during oocyte maturation: p90(rsk) phosphorylates and inactivates the p34(cdc2) inhibitory kinase Myt1. Embo J 17, 5037-47 (1998).
30. Pawson, T. & Linding, R. Network medicine. FEBS Lett 582, 1266-70 (2008).
31. Barabasi, A. L., Gulbahce, N. & Loscalzo, J. Network medicine: a network-based approach to human disease. Nat Rev Genet 12, 56-68 (2011).
32. Alegria-Schaffer, A., Lodge, A. & Vattem, K. Performing and optimizing Western blots with an emphasis on chemiluminescent detection. Methods Enzymol 463, 573-99 (2009).
33. Min, D. H. & Mrksich, M. Peptide arrays: towards routine implementation. Curr Opin Chem Biol 8, 554-8 (2004).
34. Martin, S. E. & Peterson, B. R. A colorimetric enzyme-linked on-bead assay for identification of synthetic substrates of protein tyrosine kinases. J Pept Sci 8, 227-33 (2002).

35. Hutti, J. E. et al. A rapid method for determining protein kinase phosphorylation specificity. Nat Methods 1, 27-9 (2004).
36. Chen, C. & Turk, B. E. Analysis of serine-threonine kinase specificity using arrayed positional scanning peptide libraries. Curr Protoc Mol Biol Chapter 18, Unit 18 14 (2010).
37. Hoogendijk, A. J., Diks, S. H., Peppelenbosch, M. P., Van Der Poll, T. & Wieland, C. W. Kinase activity profiling of gram-negative pneumonia. Mol Med 17, 741-7 (2011).
38. Mok, J. et al. Deciphering protein kinase specificity through large-scale analysis of yeast phosphorylation site motifs. Sci Signal 3, ra12 (2010).
39. Simons, P. C. et al. Duplexed, bead-based competitive assay for inhibitors of protein kinases. Cytometry A 71, 451-9 (2007).
40. Yu, Y. et al. A site-specific, multiplexed kinase activity assay using stable-isotope dilution and high-resolution mass spectrometry. Proc Natl Acad Sci U S A 106, 11606-11 (2009).
41. Kubota, K. et al. Sensitive multiplexed analysis of kinase activities and activity-based kinase identification. Nat Biotechnol 27, 933-40 (2009).
42. Hanks, S. K., Quinn, A. M. & Hunter, T. The protein kinase family: conserved features and deduced phylogeny of the catalytic domains. Science 241, 42-52 (1988).
43. Morgan, D. O. & De Bondt, H. L. Protein kinase regulation: insights from crystal structure analysis. Curr Opin Cell Biol 6, 239-46 (1994).
44. Hubbard, S. R., Mohammadi, M. & Schlessinger, J. Autoregulatory mechanisms in protein-tyrosine kinases. J Biol Chem 273, 11987-90 (1998).
45. Knighton, D. R. et al. Crystal structure of the catalytic subunit of cyclic adenosine monophosphate-dependent protein kinase. Science 253, 407-14 (1991).
46. Knighton, D. R. et al. Structure of a peptide inhibitor bound to the catalytic subunit of cyclic adenosine monophosphate-dependent protein kinase. Science 253, 414-20 (1991).
47. De Bondt, H. L. et al. Crystal structure of cyclin-dependent kinase 2. Nature 363, 595-602 (1993).
48. Hubbard, S. R., Wei, L., Ellis, L. & Hendrickson, W. A. Crystal structure of the tyrosine kinase domain of the human insulin receptor. Nature 372, 746-54 (1994).
49. Roskoski, R., Jr. MEK1/2 dual-specificity protein kinases: structure and regulation. Biochem Biophys Res Commun 417, 5-10 (2010).
50. Madhusudan et al. cAMP-dependent protein kinase: crystallographic insights into substrate recognition and phosphotransfer. Protein Sci 3, 176-87 (1994).
51. Zhang, J., Yang, P. L. & Gray, N. S. Targeting cancer with small molecule kinase inhibitors. Nat Rev Cancer 9, 28-39 (2009).
52. Dar, A. C. & Shokat, K. M. The evolution of protein kinase inhibitors from antagonists to agonists of cellular signaling. Annu Rev Biochem 80, 769-95 (2011).
53. Uhler, M. D. et al. Isolation of cDNA clones coding for the catalytic subunit of mouse cAMP-dependent protein kinase. Proc Natl Acad Sci U S A 83, 1300-4 (1986).

54. Lowery, D. M., Lim, D. & Yaffe, M. B. Structure and function of Polo-like kinases. Oncogene 24, 248-59 (2005).
55. Elia, A. E., Cantley, L. C. & Yaffe, M. B. Proteomic screen finds pSer/pThr-binding domain localizing Plk1 to mitotic substrates. Science 299, 1228-31 (2003).
56. Yuan, J. et al. Cooperative phosphorylation including the activity of polo-like kinase 1 regulates the subcellular localization of cyclin B1. Oncogene 21, 8282-92 (2002).
57. Yu, Z., Liu, Y. & Li, Z. Structure-function relationship of the Polo-like kinase in Trypanosoma brucei. J Cell Sci 125, 1519-30 (2012).
58. Lee, K. S., Grenfell, T. Z., Yarm, F. R. & Erikson, R. L. Mutation of the polo-box disrupts localization and mitotic functions of the mammalian polo kinase Plk. Proc Natl Acad Sci U S A 95, 9301-6 (1998).
59. Aitken, A. Protein consensus sequence motifs. Mol Biotechnol 12, 241-53 (1999).
60. Moore, M. J., Adams, J. A. & Taylor, S. S. Structural basis for peptide binding in protein kinase A. Role of glutamic acid 203 and tyrosine 204 in the peptide-positioning loop. J Biol Chem 278, 10613-8 (2003).
61. Zheng, J. et al. 2.2 A refined crystal structure of the catalytic subunit of cAMP-dependent protein kinase complexed with MnATP and a peptide inhibitor. Acta Crystallogr D Biol Crystallogr 49, 362-5 (1993).
62. Brown, N. R., Noble, M. E., Endicott, J. A. & Johnson, L. N. The structural basis for specificity of substrate and recruitment peptides for cyclin-dependent kinases. Nat Cell Biol 1, 438-43 (1999).
63. Davis, R. J. The mitogen-activated protein kinase signal transduction pathway. J Biol Chem 268, 14553-6 (1993).
64. Marin, O., Meggio, F. & Pinna, L. A. Design and synthesis of two new peptide substrates for the specific and sensitive monitoring of casein kinases-1 and -2. Biochem Biophys Res Commun 198, 898-905 (1994).
65. Biondi, R. M. et al. Identification of a pocket in the PDK1 kinase domain that interacts with PIF and the C-terminal residues of PKA. Embo J 19, 979-88 (2000).
66. Sheridan, D. L., Kong, Y., Parker, S. A., Dalby, K. N. & Turk, B. E. Substrate discrimination among mitogen-activated protein kinases through distinct docking sequence motifs. J Biol Chem 283, 19511-20 (2008).
67. Gupta, S., Campbell, D., Derijard, B. & Davis, R. J. Transcription factor ATF2 regulation by the JNK signal transduction pathway. Science 267, 389-93 (1995).
68. Yang, S. H., Galanis, A. & Sharrocks, A. D. Targeting of p38 mitogen-activated protein kinases to MEF2 transcription factors. Mol Cell Biol 19, 4028-38 (1999).
69. Nebreda, A. R. & Ferby, I. Regulation of the meiotic cell cycle in oocytes. Curr Opin Cell Biol 12, 666-75 (2000).
70. Murray, A. W. Cell cycle extracts. Methods Cell Biol 36, 581-605 (1991).

71. Castro, A., Vigneron, S., Bernis, C., Labbe, J. C. & Lorca, T. Ubiquitin-mediated protein degradation in Xenopus egg extracts. Methods Mol Biol 322, 223-34 (2006).
72. Kishimoto, T. Cell-cycle control during meiotic maturation. Curr Opin Cell Biol 15, 654-63 (2003).
73. Tripathi, A., Kumar, K. V. & Chaube, S. K. Meiotic cell cycle arrest in mammalian oocytes. J Cell Physiol 223, 592-600 (2010).
74. Philpott, A. & Yew, P. R. The Xenopus cell cycle: an overview. Mol Biotechnol 39, 9-19 (2008).
75. Sadler, S. E. & Maller, J. L. Progesterone inhibits adenylate cyclase in Xenopus oocytes. Action on the guanine nucleotide regulatory protein. J Biol Chem 256, 6368-73 (1981).
76. Maller, J. L. & Krebs, E. G. Progesterone-stimulated meiotic cell division in Xenopus oocytes. Induction by regulatory subunit and inhibition by catalytic subunit of adenosine 3':5'-monophosphate-dependent protein kinase. J Biol Chem 252, 1712-8 (1977).
77. Chan, T. O. et al. Resistance of Akt kinases to dephosphorylation through ATP-dependent conformational plasticity. Proc Natl Acad Sci U S A 108, E1120-7 (2011).
78. Fayard, E., Xue, G., Parcellier, A., Bozulic, L. & Hemmings, B. A. Protein kinase B (PKB/Akt), a key mediator of the PI3K signaling pathway. Curr Top Microbiol Immunol 346, 31-56 (2010).
79. Andersen, C. B., Roth, R. A. & Conti, M. Protein kinase B/Akt induces resumption of meiosis in Xenopus oocytes. J Biol Chem 273, 18705-8 (1998).
80. Morley, S. J. & Pain, V. M. Hormone-induced meiotic maturation in Xenopus oocytes occurs independently of p70s6k activation and is associated with enhanced initiation factor (eIF)-4F phosphorylation and complex formation. J Cell Sci 108 (Pt 4), 1751-60 (1995).
81. Brevini, T. A. et al. Evolution of mRNA polyadenylation between oocyte maturation and first embryonic cleavage in cattle and its relation with developmental competence. Mol Reprod Dev 63, 510-7 (2002).
82. Fox, C. A., Sheets, M. D., Wahle, E. & Wickens, M. Polyadenylation of maternal mRNA during oocyte maturation: poly(A) addition in vitro requires a regulated RNA binding activity and a poly(A) polymerase. Embo J 11, 5021-32 (1992).
83. Sagata, N., Oskarsson, M., Copeland, T., Brumbaugh, J. & Vande Woude, G. F. Function of c-mos proto-oncogene product in meiotic maturation in Xenopus oocytes. Nature 335, 519-25 (1988).
84. Alessi, D. R. et al. Identification of the sites in MAP kinase kinase-1 phosphorylated by p74raf-1. Embo J 13, 1610-9 (1994).
85. Payne, D. M. et al. Identification of the regulatory phosphorylation sites in pp42/mitogen-activated protein kinase (MAP kinase). Embo J 10, 885-92 (1991).

86. Matten, W. T., Copeland, T. D., Ahn, N. G. & Vande Woude, G. F. Positive feedback between MAP kinase and Mos during Xenopus oocyte maturation. Dev Biol 179, 485-92 (1996).
87. Nishizawa, M. et al. Degradation of Mos by the N-terminal proline (Pro2)-dependent ubiquitin pathway on fertilization of Xenopus eggs: possible significance of natural selection for Pro2 in Mos. Embo J 12, 4021-7 (1993).
88. Bhatt, R. R. & Ferrell, J. E., Jr. Cloning and characterization of Xenopus Rsk2, the predominant p90 Rsk isozyme in oocytes and eggs. J Biol Chem 275, 32983-90 (2000).
89. Frodin, M., Jensen, C. J., Merienne, K. & Gammeltoft, S. A phosphoserine-regulated docking site in the protein kinase RSK2 that recruits and activates PDK1. Embo J 19, 2924-34 (2000).
90. Chrestensen, C. A. & Sturgill, T. W. Characterization of the p90 ribosomal S6 kinase 2 carboxyl-terminal domain as a protein kinase. J Biol Chem 277, 27733-41 (2002).
91. Nurse, P. M. Nobel Lecture. Cyclin dependent kinases and cell cycle control. Biosci Rep 22, 487-99 (2002).
92. Fesquet, D. et al. The MO15 gene encodes the catalytic subunit of a protein kinase that activates cdc2 and other cyclin-dependent kinases (CDKs) through phosphorylation of Thr161 and its homologues. Embo J 12, 3111-21 (1993).
93. Katula, K. S. et al. Cyclin-dependent kinase activation and S-phase induction of the cyclin B1 gene are linked through the CCAAT elements. Cell Growth Differ 8, 811-20 (1997).
94. Mueller, P. R., Coleman, T. R., Kumagai, A. & Dunphy, W. G. Myt1: a membrane-associated inhibitory kinase that phosphorylates Cdc2 on both threonine-14 and tyrosine-15. Science 270, 86-90 (1995).
95. Wells, N. J. et al. The C-terminal domain of the Cdc2 inhibitory kinase Myt1 interacts with Cdc2 complexes and is required for inhibition of G(2)/M progression. J Cell Sci 112 (Pt 19), 3361-71 (1999).
96. Owens, L. et al. Activation domain-dependent degradation of somatic Wee1 kinase. J Biol Chem 285, 6761-9 (2010).
97. Kumagai, A. & Dunphy, W. G. Purification and molecular cloning of Plx1, a Cdc25-regulatory kinase from Xenopus egg extracts. Science 273, 1377-80 (1996).
98. Li, J., Meyer, A. N. & Donoghue, D. J. Nuclear localization of cyclin B1 mediates its biological activity and is regulated by phosphorylation. Proc Natl Acad Sci U S A 94, 502-7 (1997).
99. Hagting, A., Karlsson, C., Clute, P., Jackman, M. & Pines, J. MPF localization is controlled by nuclear export. Embo J 17, 4127-38 (1998).
100. Yamano, H., Gannon, J., Mahbubani, H. & Hunt, T. Cell cycle-regulated recognition of the destruction box of cyclin B by the APC/C in Xenopus egg extracts. Mol Cell 13, 137-47 (2004).

101. Glotzer, M., Murray, A. W. & Kirschner, M. W. Cyclin is degraded by the ubiquitin pathway. Nature 349, 132-8 (1991).
102. Masui, Y. & Markert, C. L. Cytoplasmic control of nuclear behavior during meiotic maturation of frog oocytes. J Exp Zool 177, 129-45 (1971).
103. Sagata, N., Watanabe, N., Vande Woude, G. F. & Ikawa, Y. The c-mos proto-oncogene product is a cytostatic factor responsible for meiotic arrest in vertebrate eggs. Nature 342, 512-8 (1989).
104. Bhatt, R. R. & Ferrell, J. E., Jr. The protein kinase p90 rsk as an essential mediator of cytostatic factor activity. Science 286, 1362-5 (1999).
105. Gross, S. D., Schwab, M. S., Lewellyn, A. L. & Maller, J. L. Induction of metaphase arrest in cleaving Xenopus embryos by the protein kinase p90Rsk. Science 286, 1365-7 (1999).
106. Haccard, O. et al. Induction of metaphase arrest in cleaving Xenopus embryos by MAP kinase. Science 262, 1262-5 (1993).
107. Tunquist, B. J., Schwab, M. S., Chen, L. G. & Maller, J. L. The spindle checkpoint kinase bub1 and cyclin e/cdk2 both contribute to the establishment of meiotic metaphase arrest by cytostatic factor. Curr Biol 12, 1027-33 (2002).
108. Musacchio, A. & Hardwick, K. G. The spindle checkpoint: structural insights into dynamic signalling. Nat Rev Mol Cell Biol 3, 731-41 (2002).
109. Reimann, J. D. et al. Emi1 is a mitotic regulator that interacts with Cdc20 and inhibits the anaphase promoting complex. Cell 105, 645-55 (2001).
110. Reimann, J. D. & Jackson, P. K. Emi1 is required for cytostatic factor arrest in vertebrate eggs. Nature 416, 850-4 (2002).
111. Serber, Z., Corsini, L., Durst, F. & Dotsch, V. In-cell NMR spectroscopy. Methods Enzymol 394, 17-41 (2005).
112. Cavadini, S., Antonijevic, S., Lupulescu, A. & Bodenhausen, G. Indirect detection of nitrogen-14 in solid-state NMR spectroscopy. Chemphyschem 8, 1363-74 (2007).
113. Muchmore, D. C., McIntosh, L. P., Russell, C. B., Anderson, D. E. & Dahlquist, F. W. Expression and nitrogen-15 labeling of proteins for proton and nitrogen-15 nuclear magnetic resonance. Methods Enzymol 177, 44-73 (1989).
114. Selenko, P. & Wagner, G. Looking into live cells with in-cell NMR spectroscopy. J Struct Biol 158, 244-53 (2007).
115. Theillet, F. X. et al. Cell signaling, post-translational protein modifications and NMR spectroscopy. J Biomol NMR (*in press*).
116. Ramelot, T. A. & Nicholson, L. K. Phosphorylation-induced structural changes in the amyloid precursor protein cytoplasmic tail detected by NMR. J Mol Biol 307, 871-84 (2001).
117. Du, J. T. et al. Low-barrier hydrogen bond between phosphate and the amide group in phosphopeptide. J Am Chem Soc 127, 16350-1 (2005).

118. Zhou, P., Lugovskoy, A. A. & Wagner, G. A solubility-enhancement tag (SET) for NMR studies of poorly behaving proteins. J Biomol NMR 20, 11-4 (2001).
119. Okazaki, T., Sakoh, M., Nagaoka, Y. & Asami, K. Ion channels of alamethicin dimer N-terminally linked by disulfide bond. Biophys J 85, 267-73 (2003).
120. Han, Y., Albericio, F. & Barany, G. Occurrence and Minimization of Cysteine Racemization during Stepwise Solid-Phase Peptide Synthesis(1)(,)(2). J Org Chem 62, 4307-4312 (1997).
121. Van den Nest, W., Yuval, S. & Albericio, F. Cu(OBt)2 and Cu(OAt)2, copper(II)-based racemization suppressors ready for use in fully automated solid-phase peptide synthesis. J Pept Sci 7, 115-20 (2001).
122. Morrison, D. K., Heidecker, G., Rapp, U. R. & Copeland, T. D. Identification of the major phosphorylation sites of the Raf-1 kinase. J Biol Chem 268, 17309-16 (1993).
123. Songyang, Z. et al. Use of an oriented peptide library to determine the optimal substrates of protein kinases. Curr Biol 4, 973-82 (1994).
124. Nakajima, H., Toyoshima-Morimoto, F., Taniguchi, E. & Nishida, E. Identification of a consensus motif for Plk (Polo-like kinase) phosphorylation reveals Myt1 as a Plk1 substrate. J Biol Chem 278, 25277-80 (2003).
125. Cantin, G. T. et al. Combining protein-based IMAC, peptide-based IMAC, and MudPIT for efficient phosphoproteomic analysis. J Proteome Res 7, 1346-51 (2008).
126. Selenko, P. et al. In situ observation of protein phosphorylation by high-resolution NMR spectroscopy. Nat Struct Mol Biol 15, 321-9 (2008).
127. Powell, M. F. et al. Peptide stability in drug development. II. Effect of single amino acid substitution and glycosylation on peptide reactivity in human serum. Pharm Res 10, 1268-73 (1993).
128. Hamamoto, K., Kida, Y., Zhang, Y., Shimizu, T. & Kuwano, K. Antimicrobial activity and stability to proteolysis of small linear cationic peptides with D-amino acid substitutions. Microbiol Immunol 46, 741-9 (2002).
129. Galati, R., Verdina, A., Falasca, G. & Chersi, A. Increased resistance of peptides to serum proteases by modification of their amino groups. Z Naturforsch C 58, 558-61 (2003).
130. Tugyi, R. et al. Partial D-amino acid substitution: Improved enzymatic stability and preserved Ab recognition of a MUC2 epitope peptide. Proc Natl Acad Sci U S A 102, 413-8 (2005).
131. Xiao, Q. & Pei, D. High-throughput synthesis and screening of cyclic peptide antibiotics. J Med Chem 50, 3132-7 (2007).
132. Veronese, F. M. Peptide and protein PEGylation: a review of problems and solutions. Biomaterials 22, 405-17 (2001).

133. Roberts, M. J., Bentley, M. D. & Harris, J. M. Chemistry for peptide and protein PEGylation. Adv Drug Deliv Rev 54, 459-76 (2002).
134. Morris, C. J. et al. Pegylation of antimicrobial peptides maintains the active peptide conformation, model membrane interactions, and antimicrobial activity while improving lung tissue biocompatibility following airway delivery. Antimicrob Agents Chemother 56, 3298-308 (2012).
135. Polson, A. A theory for the displacement of proteins and viruses with polyethylene glycol. Prep Biochem 7, 129-54 (1977).
136. Remington, S. J. Serine carboxypeptidases: a new and versatile family of enzymes. Curr Opin Biotechnol 4, 462-8 (1993).
137. Kuenzel, E. A., Mulligan, J. A., Sommercorn, J. & Krebs, E. G. Substrate specificity determinants for casein kinase II as deduced from studies with synthetic peptides. J Biol Chem 262, 9136-40 (1987).
138. Glass, D. B., Cheng, H. C., Mende-Mueller, L., Reed, J. & Walsh, D. A. Primary structural determinants essential for potent inhibition of cAMP-dependent protein kinase by inhibitory peptides corresponding to the active portion of the heat-stable inhibitor protein. J Biol Chem 264, 8802-10 (1989).
139. Grieco, D., Avvedimento, E. V. & Gottesman, M. E. A role for cAMP-dependent protein kinase in early embryonic divisions. Proc Natl Acad Sci U S A 91, 9896-900 (1994).
140. Alessi, D. R. et al. Mechanism of activation of protein kinase B by insulin and IGF-1. Embo J 15, 6541-51 (1996).
141. Walker, K. S. et al. Activation of protein kinase B beta and gamma isoforms by insulin in vivo and by 3-phosphoinositide-dependent protein kinase-1 in vitro: comparison with protein kinase B alpha. Biochem J 331 (Pt 1), 299-308 (1998).
142. Sarbassov, D. D., Guertin, D. A., Ali, S. M. & Sabatini, D. M. Phosphorylation and regulation of Akt/PKB by the rictor-mTOR complex. Science 307, 1098-101 (2005).
143. Mahajan, K. et al. Ack1 mediated AKT/PKB tyrosine 176 phosphorylation regulates its activation. PLoS One 5, e9646 (2010).
144. West, D. W. Structure and function of the phosphorylated residues of casein. J Dairy Res 53, 333-52 (1986).
145. Flotow, H. & Roach, P. J. Role of acidic residues as substrate determinants for casein kinase I. J Biol Chem 266, 3724-7 (1991).
146. Flotow, H. et al. Phosphate groups as substrate determinants for casein kinase I action. J Biol Chem 265, 14264-9 (1990).
147. Santamaria, A. et al. The Plk1-dependent phosphoproteome of the early mitotic spindle. Mol Cell Proteomics 10, M110 004457 (2011).
148. Martin-Perez, J. & Thomas, G. Ordered phosphorylation of 40S ribosomal protein S6 after serum stimulation of quiescent 3T3 cells. Proc Natl Acad Sci U S A 80, 926-30 (1983).

149. Ruvinsky, I. & Meyuhas, O. Ribosomal protein S6 phosphorylation: from protein synthesis to cell size. Trends Biochem Sci 31, 342-8 (2006).
150. Wettenhall, R. E., Erikson, E. & Maller, J. L. Ordered multisite phosphorylation of Xenopus ribosomal protein S6 by S6 kinase II. J Biol Chem 267, 9021-7 (1992).
151. Brandon, S. D. & Masaracchia, R. A. Multisite phosphorylation of a synthetic peptide derived from the carboxyl terminus of the ribosomal protein S6. J Biol Chem 266, 380-5 (1991).
152. Alessi, D. R., Caudwell, F. B., Andjelkovic, M., Hemmings, B. A. & Cohen, P. Molecular basis for the substrate specificity of protein kinase B; comparison with MAPKAP kinase-1 and p70 S6 kinase. FEBS Lett 399, 333-8 (1996).
153. Lawlor, M. A. & Alessi, D. R. PKB/Akt: a key mediator of cell proliferation, survival and insulin responses? J Cell Sci 114, 2903-10 (2001).
154. Powell, D. W., Rane, M. J., Chen, Q., Singh, S. & McLeish, K. R. Identification of 14-3-3zeta as a protein kinase B/Akt substrate. J Biol Chem 277, 21639-42 (2002).
155. Kovacina, K. S. et al. Identification of a proline-rich Akt substrate as a 14-3-3 binding partner. J Biol Chem 278, 10189-94 (2003).
156. Konishi, H. et al. Identification of peripherin as a Akt substrate in neurons. J Biol Chem 282, 23491-9 (2007).
157. Zhou, Q. L. et al. Akt substrate TBC1D1 regulates GLUT1 expression through the mTOR pathway in 3T3-L1 adipocytes. Biochem J 411, 647-55 (2008).
158. Cau, J. et al. Regulation of Xenopus p21-activated kinase (X-PAK2) by Cdc42 and maturation-promoting factor controls Xenopus oocyte maturation. J Biol Chem 275, 2367-75 (2000).
159. Ross, H., Armstrong, C. G. & Cohen, P. A non-radioactive method for the assay of many serine/threonine-specific protein kinases. Biochem J 366, 977-81 (2002).
160. Hutchins, J. R., Dikovskaya, D. & Clarke, P. R. Regulation of Cdc2/cyclin B activation in Xenopus egg extracts via inhibitory phosphorylation of Cdc25C phosphatase by Ca(2+)/calmodulin-dependent protein [corrected] kinase II. Mol Biol Cell 14, 4003-14 (2003).
161. Alessi, D. R. et al. Characterization of a 3-phosphoinositide-dependent protein kinase which phosphorylates and activates protein kinase Balpha. Curr Biol 7, 261-9 (1997).
162. Arora, A. & Scholar, E. M. Role of tyrosine kinase inhibitors in cancer therapy. J Pharmacol Exp Ther 315, 971-9 (2005).
163. Anastassiadis, T., Deacon, S. W., Devarajan, K., Ma, H. & Peterson, J. R. Comprehensive assay of kinase catalytic activity reveals features of kinase inhibitor selectivity. Nat Biotechnol 29, 1039-45.
164. Kim, D. H. & Sim, T. Novel small molecule Raf kinase inhibitors for targeted cancer therapeutics. Arch Pharm Res 35, 605-15.

165. Davis, M. I. et al. Comprehensive analysis of kinase inhibitor selectivity. Nat Biotechnol 29, 1046-51.
166. Jecklin, M. C. et al. Affinity classification of kinase inhibitors by mass spectrometric methods and validation using standard IC(50) measurements. Anal Chem 81, 408-19 (2009).
167. Andreani, A. et al. Imidazo[2,1 -b]thiazolylmethylene- and indolylmethylene-2-indolinones: a new class of cyclin-dependent kinase inhibitors. Design, synthesis, and CDK1/cyclin B inhibition. Anticancer Drug Des 15, 447-52 (2000).
168. Leost, M. et al. Paullones are potent inhibitors of glycogen synthase kinase-3beta and cyclin-dependent kinase 5/p25. Eur J Biochem 267, 5983-94 (2000).
169. Lin, R. et al. 1-Acyl-1H-[1,2,4]triazole-3,5-diamine analogues as novel and potent anticancer cyclin-dependent kinase inhibitors: synthesis and evaluation of biological activities. J Med Chem 48, 4208-11 (2005).
170. Bienkiewicz, E. A. & Lumb, K. J. Random-coil chemical shifts of phosphorylated amino acids. J Biomol NMR 15, 203-6 (1999).
171. Jacob, G., Allende, C. C. & Allende, J. E. The hydrolysis of phosphatidylinositol 4-phosphate in membranes of Xenopus laevis oocytes: characteristics of a phosphomonoesterase. Comp Biochem Physiol B 100, 809-16 (1991).
172. Le Goascogne, C., Sananes, N., Gouezou, M. & Baulieu, E. E. Alkaline phosphatase activity in the membrane of Xenopus laevis oocytes: effects of steroids, insulin, and inhibitors during meiosis reinitiation. Dev Biol 119, 511-9 (1987).
173. Landrieu, I. et al. NMR analysis of a Tau phosphorylation pattern. J Am Chem Soc 128, 3575-83 (2006).
174. Gautier, J. et al. Cyclin is a component of maturation-promoting factor from Xenopus. Cell 60, 487-94 (1990).
175. Lohka, M. J., Hayes, M. K. & Maller, J. L. Purification of maturation-promoting factor, an intracellular regulator of early mitotic events. Proc Natl Acad Sci U S A 85, 3009-13 (1988).
176. Enserink, J. M. & Kolodner, R. D. An overview of Cdk1-controlled targets and processes. Cell Div 5, 11.
177. Toyoshima-Morimoto, F., Taniguchi, E. & Nishida, E. Plk1 promotes nuclear translocation of human Cdc25C during prophase. EMBO Rep 3, 341-8 (2002).
178. Karaiskou, A. et al. Polo-like kinase confers MPF autoamplification competence to growing Xenopus oocytes. Development 131, 1543-52 (2004).
179. Abrieu, A. et al. The Polo-like kinase Plx1 is a component of the MPF amplification loop at the G2/M-phase transition of the cell cycle in Xenopus eggs. J Cell Sci 111 (Pt 12), 1751-7 (1998).

180. Qian, Y. W., Erikson, E., Li, C. & Maller, J. L. Activated polo-like kinase Plx1 is required at multiple points during mitosis in Xenopus laevis. Mol Cell Biol 18, 4262-71 (1998).
181. Nishiyama, T., Ohsumi, K. & Kishimoto, T. Phosphorylation of Erp1 by p90rsk is required for cytostatic factor arrest in Xenopus laevis eggs. Nature 446, 1096-9 (2007).
182. Gotoh, Y. et al. In vitro effects on microtubule dynamics of purified Xenopus M phase-activated MAP kinase. Nature 349, 251-4 (1991).
183. Jessus, C. et al. Tyrosine phosphorylation of p34cdc2 and p42 during meiotic maturation of Xenopus oocyte. Antagonistic action of okadaic acid and 6-DMAP. Development 111, 813-20 (1991).
184. Walworth, N., Davey, S. & Beach, D. Fission yeast chk1 protein kinase links the rad checkpoint pathway to cdc2. Nature 363, 368-71 (1993).
185. Furnari, B., Rhind, N. & Russell, P. Cdc25 mitotic inducer targeted by chk1 DNA damage checkpoint kinase. Science 277, 1495-7 (1997).
186. Despras, E., Daboussi, F., Hyrien, O., Marheineke, K. & Kannouche, P. L. ATR/Chk1 pathway is essential for resumption of DNA synthesis and cell survival in UV-irradiated XP variant cells. Hum Mol Genet 19, 1690-701 (2010).
187. Ikegami, Y. et al. Chk1 phosphorylation at Ser286 and Ser301 occurs with both stalled DNA replication and damage checkpoint stimulation. Biochem Biophys Res Commun 377, 1227-31 (2008).
188. Tang, J., Erikson, R. L. & Liu, X. Checkpoint kinase 1 (Chk1) is required for mitotic progression through negative regulation of polo-like kinase 1 (Plk1). Proc Natl Acad Sci U S A 103, 11964-9 (2006).
189. Duckworth, B. C., Weaver, J. S. & Ruderman, J. V. G2 arrest in Xenopus oocytes depends on phosphorylation of cdc25 by protein kinase A. Proc Natl Acad Sci U S A 99, 16794-9 (2002).
190. Peng, C. Y. et al. C-TAK1 protein kinase phosphorylates human Cdc25C on serine 216 and promotes 14-3-3 protein binding. Cell Growth Differ 9, 197-208 (1998).
191. Manke, I. A. et al. MAPKAP kinase-2 is a cell cycle checkpoint kinase that regulates the G2/M transition and S phase progression in response to UV irradiation. Mol Cell 17, 37-48 (2005).
192. Lorca, T. et al. Calmodulin-dependent protein kinase II mediates inactivation of MPF and CSF upon fertilization of Xenopus eggs. Nature 366, 270-3 (1993).
193. Swulius, M. T. & Waxham, M. N. Ca(2+)/calmodulin-dependent protein kinases. Cell Mol Life Sci 65, 2637-57 (2008).
194. Kotlyarov, A. et al. Distinct cellular functions of MK2. Mol Cell Biol 22, 4827-35 (2002).
195. Stokoe, D., Caudwell, B., Cohen, P. T. & Cohen, P. The substrate specificity and structure of mitogen-activated protein (MAP) kinase-activated protein kinase-2. Biochem J 296 (Pt 3), 843-9 (1993).

196. Vician, L. J. et al. MAPKAP kinase-2 is a primary response gene induced by depolarization in PC12 cells and in brain. J Neurosci Res 78, 315-28 (2004).
197. Tang, J., Yang, X. & Liu, X. Phosphorylation of Plk1 at Ser326 regulates its functions during mitotic progression. Oncogene 27, 6635-45 (2008).
198. Yuan, J. et al. MAPK-activated protein kinase 2 is required for mouse meiotic spindle assembly and kinetochore-microtubule attachment. PLoS One 5, e11247 (2010).
199. Isoda, M. et al. Dynamic regulation of Emi2 by Emi2-bound Cdk1/Plk1/CK1 and PP2A-B56 in meiotic arrest of Xenopus eggs. Dev Cell 21, 506-19 (2011).
200. Jensen, C. J. et al. 90-kDa ribosomal S6 kinase is phosphorylated and activated by 3-phosphoinositide-dependent protein kinase-1. J Biol Chem 274, 27168-76 (1999).
201. Stoter, M. et al. Inhibition of casein kinase I delta alters mitotic spindle formation and induces apoptosis in trophoblast cells. Oncogene 24, 7964-75 (2005).
202. Wilhelm, V., Rojas, P., Gatica, M., Allende, C. C. & Allende, J. E. Expression of the subunits of protein kinase CK2 during oogenesis in Xenopus laevis. Eur J Biochem 232, 671-6 (1995).
203. Dancey, J. & Sausville, E. A. Issues and progress with protein kinase inhibitors for cancer treatment. Nat Rev Drug Discov 2, 296-313 (2003).
204. Georghiou, G., Kleiner, R. E., Pulkoski-Gross, M., Liu, D. R. & Seeliger, M. A. Highly specific, bisubstrate-competitive Src inhibitors from DNA-templated macrocycles. Nat Chem Biol 8, 366-74 (2012).
205. Muhlhausser, P. & Kutay, U. An in vitro nuclear disassembly system reveals a role for the RanGTPase system and microtubule-dependent steps in nuclear envelope breakdown. J Cell Biol 178, 595-610 (2007).
206. Geladopoulos, T. P., Sotiroudis, T. G. & Evangelopoulos, A. E. A malachite green colorimetric assay for protein phosphatase activity. Anal Biochem 192, 112-6 (1991).
207. Felix, M. A., Cohen, P. & Karsenti, E. Cdc2 H1 kinase is negatively regulated by a type 2A phosphatase in the Xenopus early embryonic cell cycle: evidence from the effects of okadaic acid. Embo J 9, 675-83 (1990).
208. Ishihara, H. et al. Calyculin A and okadaic acid: inhibitors of protein phosphatase activity. Biochem Biophys Res Commun 159, 871-7 (1989).
209. Mochida, S., Ikeo, S., Gannon, J. & Hunt, T. Regulated activity of PP2A-B55 delta is crucial for controlling entry into and exit from mitosis in Xenopus egg extracts. Embo J 28, 2777-85 (2009).
210. Margolis, S. S. et al. PP1 control of M phase entry exerted through 14-3-3-regulated Cdc25 dephosphorylation. Embo J 22, 5734-45 (2003).
211. Margolis, S. S. et al. A role for PP1 in the Cdc2/Cyclin B-mediated positive feedback activation of Cdc25. Mol Biol Cell 17, 1779-89 (2006).

212. Hutchins, J. R., Dikovskaya, D. & Clarke, P. R. Dephosphorylation of the inhibitory phosphorylation site S287 in Xenopus Cdc25C by protein phosphatase-2A is inhibited by 14-3-3 binding. FEBS Lett 528, 267-71 (2002).
213. Jang, Y. J., Ji, J. H., Choi, Y. C., Ryu, C. J. & Ko, S. Y. Regulation of Polo-like kinase 1 by DNA damage in mitosis. Inhibition of mitotic PLK-1 by protein phosphatase 2A. J Biol Chem 282, 2473-82 (2007).
214. Macurek, L. et al. Polo-like kinase-1 is activated by aurora A to promote checkpoint recovery. Nature 455, 119-23 (2008).
215. Seki, A., Coppinger, J. A., Jang, C. Y., Yates, J. R. & Fang, G. Bora and the kinase Aurora a cooperatively activate the kinase Plk1 and control mitotic entry. Science 320, 1655-8 (2008).
216. Andjelkovic, M. et al. Activation and phosphorylation of a pleckstrin homology domain containing protein kinase (RAC-PK/PKB) promoted by serum and protein phosphatase inhibitors. Proc Natl Acad Sci U S A 93, 5699-704 (1996).
217. Resjo, S. et al. Protein phosphatase 2A is the main phosphatase involved in the regulation of protein kinase B in rat adipocytes. Cell Signal 14, 231-8 (2002).
218. Chester, N., Yu, I. J. & Marshak, D. R. Identification and characterization of protein kinase CKII isoforms in HeLa cells. Isoform-specific differences in rates of assembly from catalytic and regulatory subunits. J Biol Chem 270, 7501-14 (1995).
219. Donella-Deana, A. et al. Autocatalytic tyrosine-phosphorylation of protein kinase CK2 alpha and alpha' subunits: implication of Tyr182. Biochem J 357, 563-7 (2001).
220. Shi, Y. Serine/threonine phosphatases: mechanism through structure. Cell 139, 468-84 (2009).
221. Lechward, K., Awotunde, O. S., Swiatek, W. & Muszynska, G. Protein phosphatase 2A: variety of forms and diversity of functions. Acta Biochim Pol 48, 921-33 (2001).
222. Xu, Y., Chen, Y., Zhang, P., Jeffrey, P. D. & Shi, Y. Structure of a protein phosphatase 2A holoenzyme: insights into B55-mediated Tau dephosphorylation. Mol Cell 31, 873-85 (2008).
223. Wurzenberger, C. & Gerlich, D. W. Phosphatases: providing safe passage through mitotic exit. Nat Rev Mol Cell Biol 12, 469-82 (2011).
224. Deshmukh, L., Meller, N., Alder, N., Byzova, T. & Vinogradova, O. Tyrosine phosphorylation as a conformational switch: a case study of integrin beta3 cytoplasmic tail. J Biol Chem 286, 40943-53 (2011).
225. Gschwind, A., Fischer, O. M. & Ullrich, A. The discovery of receptor tyrosine kinases: targets for cancer therapy. Nat Rev Cancer 4, 361-70 (2004).
226. Baselga, J. Targeting tyrosine kinases in cancer: the second wave. Science 312, 1175-8 (2006).

227. Inomata, K. et al. High-resolution multi-dimensional NMR spectroscopy of proteins in human cells. Nature 458, 106-9 (2009).
228. Bekei, B. et al. In-cell NMR in mammalian cells: part 1. Methods Mol Biol 895, 43-54 (2012).
229. Ogino, S. et al. Observation of NMR signals from proteins introduced into living mammalian cells by reversible membrane permeabilization using a pore-forming toxin, streptolysin O. J Am Chem Soc 131, 10834-5 (2009).
230. Bekei, B., Rose, H. M., Herzig, M. & Selenko, P. In-cell NMR in mammalian cells: part 2. Methods Mol Biol 895, 55-66 (2012).
231. Liokatis, S., Dose, A., Schwarzer, D. & Selenko, P. Simultaneous detection of protein phosphorylation and acetylation by high-resolution NMR spectroscopy. J Am Chem Soc 132, 14704-5 (2010).
232. Dose, A., Liokatis, S., Theillet, F. X., Selenko, P. & Schwarzer, D. NMR profiling of histone deacetylase and acetyl-transferase activities in real time. ACS Chem Biol 6, 419-24 (2011).
233. Theillet, F. X. et al. Site-Specific Mapping and Time-Resolved Monitoring of Lysine Methylation by High-Resolution NMR Spectroscopy. J Am Chem Soc (2012).
234. van den Ent, F. & Lowe, J. RF cloning: a restriction-free method for inserting target genes into plasmids. J Biochem Biophys Methods 67, 67-74 (2006).
235 Ausubel, F. M., Brent, R., Kingston, R. E., Moore, D. D., Seidman, J. G., Smith, J. A., & Struhl, K. Short protocols in molecular biology, fifth edition, 1-30, 1-31 (2002).
236. Stoscheck, C. M. Quantitation of protein. Methods Enzymol 182, 50-68 (1990).
237. Chong, J. P., Thommes, P., Rowles, A., Mahbubani, H. M. & Blow, J. J. Characterization of the Xenopus replication licensing system. Methods Enzymol 283, 549-64 (1997).
238. Theillet, F. X., Binolfi, A., Liokatis, S., Verzini, S. & Selenko, P. Paramagnetic relaxation enhancement to improve sensitivity of fast NMR methods: application to intrinsically disordered proteins. J Biomol NMR 51, 487-95 (2011).

7. ABBREVIATION

%	percent
δ	Chemical shift
2D	2-dimension
3D	3-dimension
ADP	Adenosine-5'-diphosphate
AGC	Protein kinase A, protein kinase G and protein kinase C family
APC	Anaphase promoting complex/cyclosome
ATP	Adenosine-5'-triphosphate
PBD	Polo box domain
Bub1	Budding uninhibited by benzimidazole protein 1
C	Celcius degree
cAMP	Cyclic adenosine monophosphate
CaMK2	Calcium-calmodulin dependent protein kinase 2
Cdc	Cell division cycle
Cdk	Cyclin dependent kinase
Chk1	Checkpoint 1 kinase
CK1	Casein kinase 1
CK2	Casein kinase 2
CRS	Cytoplasmic retention signal
CSF	Cytostatic factor
c-TAK1	Cdc25c associated protein kinase
DBRP	Destruction box recognition protein
DSK	Dual specificity kinase
Emi2	Early meiotic induction protein 2
Erp	Exported repeated protein family
Erk	Extracellular related protein kinase
ESI-MS	Electrospray ionization mass spectrometry
GB1	B1 domain of *streptococcal* protein G
GVBD	Germinal vesicle breakdown
h	Hour
IC50	Half maximal inhibitory concentration
IRK	Insulin receptor kinase

KARs	Kinase activity reporters
KAYAK	Kinase ActivitY Assay for Kinome profiling
MAPK	Mitogen activated protein kinase
MAPKK	Mitogen activated protein kinase kinase
MAPKKK	Mitogen activated protein kinase kinase kinase
min	minute
MPF	Maturation promotion factor
MALDI-TOF	Matrix-assisted laser desorption/ionization time of flight
MK2	MAP kinase-activated protein kinase
MS	Mass spectrometry
Myt1	Membrane-associated tyrosine and threonine specific Cdk1-inhibitory kinase 1
NLS	Nuclear localization sequence
NMR	Nuclear magnetic resonance
PBD	Polo box domain
PDE	Phosphodiesterase
PDK1	3-Phosphoinositide dependent protein kinase 1
PEG	Poly ethylene glycol
PG	Progesterone
PIF	PDK1-interacting fragments
PI3K	Phosphatidylinositol 3-kinase
PKA	Protein kinase A
PKB	Protein kinase B
PKC	Protein kinase C
Plk1	Polo-like kinase 1
PP	Protein phosphatase
p.p.m	part per million
PRK2	protein kinase C-related kinase 2
RNA	Ribonucleic acid
RP-HPLC	Reverse phase-high performance liquid chromatography
Rsk	Ribosomal S6 kinase
SDS-PAGE	Sodium dodecyl sulfate polyacrylamide gel electrophoresis
SPPS	Solid-phase peptide synthesis
STK	Serine/threonine kinase

T_{50}	Reaction half-time
TEV	Tobacco Etch Virus protease
TK	Tyrosine kinase
t_r	Retention time
U	Unit

ZUSAMMENFASSUNG

Protein Kinasen steuern biologische Signaltransduktionsprozesse in einer integrativen Art und Weise, während zelluläre Antworten auf solche Signaltransduktionsprozesse wichtige Schritte des Zellzyklus wie zum Beispiel die Übergänge in einzelne Zellzyklusstadien regulieren. Um die Aktivitäten einzelner Kinasen in diesen Prozessen verstehen zu lernen ist es wichtig die funktionellen Abhänigkeiten untereinander zu studieren. Dafür sind neue Methoden der integrativen Kinasen Analyse notwendig. Gleichzeitig, erlauben uns solche neuartigen, quantitativen Methoden auch die Wirkungsweise von Kinasen Inhibitoren zu studieren, welche vor allem in der Krebstherapie eine wichtige pharmakologische Rolle spielen. Hierbei ist es vor allem wichtig neue Herangehensweisen zur parallelen Charakterisierung mehrer Kinasen Aktivitäten zu entwickeln. In diesem Hinblick hat sich die hochauflösende Kernresonanz (NMR) Spektroskopie als hervorragend geeignetes, analytisches Instrument bestätigt. Einzelne Aminosäurereste von Proteinen haben charakteristische Kernresonanzfrequenzen und sobald Proteinreste von Kinasen in phosphorylierte Zustände überführt werden, führt dies zu spezifischen Veränderungen ihrer Resonanzfrequenzen, welche mittels der NMR Spektroskopie leicht auszulesen sind.

Ziel der Doktorarbeit war es neue Wege zur Charakterisierung von zellulaeren Kinase Aktivitäten zu erschließen. Im speziellen wurde darauf hingearbeitet auf Peptiden basierende Kinasen Reporter herzustellen die es uns erlauben würden mehrere dieser enzymatischen Aktivitäten gleichzeitig mittels NMR Spektroskopie direkt in der zellulären Umgebungen auszulesen. Im Zuge dieser Doktorarbeit ist es mir gelungen diese Idee umzusetzen und solche neuartigen Instrumente herzustellen. Diese fanden direkte Anwendungen in einem zellulären Modelsystem, den so genannten cytostatic-factor arrested (CSF) *Xenopus laevis* Ei Extrakten. Mittels zeitaufgelöster NMR Spektroskopie ist es mir gelungen in diesen Extrakten 8 Kinase Aktivitäten gleichzeitig, quantitativ und in einem einzigen NMR Experiment zu bestimmen. Des Weiteren wurden Anwendungen zur Charakterisierung von Kinase Inhibitoren erfolgreich umgesetzt.

Grundsätzlich ergibt sich durch diese neue Methodik eine Vielzahl an Anwendungen, vor allem in der Charakterisierung zellulärer Kinase Aktivitäten, aber auch in der Entwicklung neuartiger Wirkstoffe in der Krebstherapie.

ACKNOWLEDGEMENTS

I would like to express my gratitude to Philipp Selenko for the supervision through my Ph.D. study and all members of in-cell NMR group for their great support. Especially, I would like to thank to; Stamatios Liokatis for all of advices and for the HeLa nuclear extract, Francois Xavier Theillet for NMR assistance and enzymatic kinetic instruction, and to Marleen Rossum for laboratory management.

I am really grateful to the kind supervision from Prof. Dirk Schwarzer and the whole protein chemistry group (present address: Interfaculty Institute of Biochemistry, University of Tübingen). I would like to specially thank to Alexander Dose for all of his assistance/intruction for peptide-based reporter synthesis. Furthermore, I would like to extend my thank to Rebecca Klingberg, Till Teschke, Jan Oliver Jost and Bernhard Geltinger for their kind helps.

Moreover, I would like to thank to Iain Mattaj and the whole Mattaj group (European Molecular Biology Laboratory, Heidelberg), especially from Birgit Koch and Hideki Yokoyama for the kind supports during my stay in Heidelberg for *Xenopus* CSF extract preparation.

Besides, I am thankful to Laura Hartmann and Daniela Ponader (Department of Biomolecular Systems, Max Planck Institute of Colloids and Interfaces) for synthesizing 2 unit and 10 unit PEG resins.

Last but not least, I would like to thank to all of the supports from my family and my friends. Particularly, I appreciate the kind helps of Thomas Schendel and Gao Song for the thesis writing.

PUBLICATIONS

Thongwichian, R., and Selenko, P. In-cell NMR in *Xenopus laevis* oocytes. Methods Mol Biol 895, 33-41 (2012).

Theillet, F. X., Smet-Nocca, C., Liokatis, S., Thongwichian, R., Kosten, J., Yoon, M. K., Kriwacki, R. W., Landrieu, I., Leppens, G., and Selenko, P. Cell Signalling, post-translational protein modifications and NMR spectroscopy. J Biomol NMR (*in press*).

Rose, H. M*., Stuiver, M*., Thongwichian, R*., Theillet, F. X., Feller, S. M., and Selenko, P. Quantitative NMR analysis of Erk kinase activity and inhibition by U0126 in a panel of patient-derived colorectal cancer cell lines. Biochim Biophys Acta (*accepted*); where * indicates equal contribution.

Theillet, F. X*., Rose, H. M*., Liokatis, S., Binofil, A., Thongwichian, R., Stuiver, M., Selenko, P. Residue-resolved NMR monitoring of serine/threonine phosphorylation reactions in vitro and in mammalian cell extracts (*submitted*); where * indicates equal contribution.

Thongwichian R., Theillet, F. X., Dose, A., Schwarzer, D., and Selenko, P. Multiplexed *in situ* profiling of cellular kinase activities by time-resolved NMR spectroscopy (*in prep*).

ERKLÄRUNG

Ich verstehere, daß ich die von mir vorgelegte Dissertation selbständig angefertigt, die benutzten Quellen und Hilfsmittel vollständig angegeben und die Stellen der Arbeit einschließlich Tabellen, Karten und Abbildungen, die anderen Werken im Wortlaut oder dem Sinn nach entnommen sind, in jedem Einzelfall als Entlehnung kenntlich gemacht habe; daß diese Dissertation noch keiner anderen Fakultät oder Universität zur Prüfung vorgelegen hat. Die Bestimmungen dieser Promotionsordnung sind mir bekannt. Die von mir vorgelegte Dissertation ist von Dr. Philipp Selenko und Prof. Dr. Dik Schwarzer betreut werden.

Berlin, Oktober 2012

Rossukon Thongwichian

For reasons of data protection, the curriculum vitae is not included in the online version